# Cosmological Density Fluctuations and Their Effects in the Early Universe

To be submitted in the partial fulfilment for the degree of **DOCTOR OF PHILOSOPHY IN PHYSICS** 

BY

Sovan Sau 17PHPH16



Under the supervision of **Dr. Soma Sanyal** 

School of Physics
University of Hyderabad
Hyderabad 500 046, INDIA

October 2021

## **DECLARATION**

I hereby declare that, this thesis titled Cosmological Density Fluctuations and Their Effects in the Early Universe submitted by me, under the guidance and supervision of Dr. Soma Sanyal, is a bonafide research work and is free from plagiarism. I also declare that it has not been submitted previously, in part or in full to this University or any other University or Institution, for the award of any degree or diploma. I hereby agree that my thesis can be deposited in Shodhganga/INFLIBNET.

A report on plagiarism statistics from the University Librarian is enclosed.

Hyderabad

Date: 29.09.21

Sovan Sau

(Sovan Sau)

Reg. No.: 17PHPH16



#### **CERTIFICATE**

This is to certify that the thesis entitled **Cosmological Density Fluctuations and Their Effects in the Early Universe** submitted by Sovan Sau bearing registration number 17PHPH16 in partial fulfilment of the requirements for award of Doctor of Philosophy in the School of Physics is a bonafide work carried out by him under my supervision and guidance.

This thesis is free from plagiarism and has not been submitted previously in part or in full to this or any other University or Institution for award of any degree or diploma.

Further, the student has the following publications before the submission of the thesis for adjudication.

- "Diffusion coefficients and constraints on hadronic inhomogeneities in the early universe", Sovan Sau, Sayantan Bhattacharya and Soma Sanyal, Eur. Phys. J. C 79, 439 (2019), Chapter 4.
- "Decay of baryon inhomogeneities in an expanding universe", Pratik K. Das, Sovan Sau, Abhisek Saha, Soma Sanyal, Eur. Phys. J. C 81, 816 (2021), Chapter
   5.
- 3. "Neutrino currents in wakes of cosmic strings", **Sovan Sau** and Soma Sanyal, Eur. Phys. J. C **80**, 152 (2020), Chapter 6.
- 4. "Quark cores in extensions of the MIT Bag model", Salil Joshi, **Sovan Sau** and Soma Sanyal, J. High Energy Astrophys. **30**, 16-23 (2021), Chapter 7.

Further, the student has passed the following courses towards fulfilment of coursework requirement for Ph.D:

Course Code	Name	Credits	Pass/Fail
PY801	Research Methodology	4	Pass
PY802	Advanced Quantum Mechanics	4	Pass
PY803	Advanced Experimental Techniques	4	Pass
PY804	Advanced Condensed Matter Physics	4	Pass

Dr. Soma Sanyal

Thesis Supervisor

School of Physics

University of Hyderabad

Date: 29.09.21

Dr. SOMA SANYAL
Asst. Professor
School of Physics
University of Hyderabad
Hyderabad-500 046.

Prof. Ashok Chatterjee

Dean

School of Physics

University of Hyderabad

DEAN

School of Physics University of Myderabad HYDERABAD - 500 646

# Acknowledgements

It is a great pleasure for me to thank those people who have played very important roles in various ways and made this thesis possible.

I will start by thanking my supervisor Dr. Soma Sanyal. It is impossible to summarize her immense role in a few words. Her constant encouragement, comments and criticism have always been a source of inspiration throughout this journey of PhD. Besides all the physics discussions, she has supported me at different times. It is a pleasure recalling all the visits to her place and her cooking. Truly, she was a friend, philosopher and guide to me.

My sincere thanks to all the faculty members of the School of Physics, University of Hyderabad, especially to my doctoral committee members Dr. Rukmani Mohanta, Dr. P. K. Suresh for their guidance and to the dean Dr. Ashok Chatterjee. I would also like to thank Dr. E. Harikumar for his useful advice.

A special thanks to my collaborators Salil and Pratik and my group members Abhisek and Soumen; it was nice spending time and working with them. I have benefited from discussions with Suman (Panja), Susmita, Debika, Nurul, Jaydeb, Pabitra Da, Avishek Da and Vishnu. I have enjoyed the time in the university with them. I want to thank Suman (Mandal) for the needful conversation at times.

I would like to express my gratitude to the University of Hyderabad for the financial support throughout the tenure. I have to thank all the school of physics office staff, library staff and the administrative staffs of the university. It is my pleasure to thank all the people who though not directly involved with my thesis are nevertheless instrumental in making it happen.

I would like to thank Sucharita for the support, encouragement and trust that she has shown throughout this term. Lastly, though 'thanking' is a very small phrase to convey my gratitude. But, the most important thanks goes to my parents who have been the strength and support throughout my life.

### Abstract

Cosmological density fluctuations play an important role in the evolution of the universe. They have important implications for the phase transitions that occur in the early universe. These density fluctuations are often generated in the early universe from topological defects. These defects are generated in symmetry breaking phase transitions. Once generated, they survive in the early universe and generate different kinds of density fluctuations. Since many of the particles in the early universe have a specific baryon number, density fluctuations will mean fluctuations in the baryon number density too. These are called baryon inhomogeneities and once generated they have strong consequences on the evolution of the universe, specially for the big bang nucleosynthesis calculations. Baryon overdensities in the early universe plasma gradually diffuse out to reach a state of equilibrium. The diffusion of these inhomogeneities are important. If all the inhomogeneities diffuse out, then the big bang nucleosynthesis will occur in a homogeneous way across the universe, but if there are inhomogeneities present in the plasma we will end up with an inhomogeneous big bang nucleosynthesis. So, we study the diffusion of baryon inhomogeneities generated from topological defects in both an expanding and a non-expanding universe. We obtain the size and amplitude of the density inhomogeneities generated at the electroweak and quark hadron phase transition which can affect the nucleosynthesis results. We find that the electroweak inhomogeneities do not have any effect on the nucleosynthesis epoch but large inhomogeneities generated at the quark hadron transition will affect the nucleosynthesis results.

Apart from the nucleosynthesis calculations, density fluctuations can also lead to the generation of seed magnetic fields in the early universe. We study the overdensities generated by long cosmic strings as they move through the early universe plasma. Neutrinos moving around such strings can generate a neutral current close to the string. The interaction of the neutrinos and the electrons would further generate an electric charge separation in the overdensity behind the moving string. The non-alignment of the temperature gradient and the charge gradient would then generate a primordial magnetic field through the Biermann mechanism. We also make an estimate of the magnitude of the generated magnetic field. Finally, we also study the dense compact stars which can have a phase transition occurring in its core. The current observational data indicates the presence of massive neutron stars which may have a quark core inside it. We have discussed a model based on the extended bag model which leads to an isentropic phase transition in the core of a hybrid star. We have made the bag constant dependent on the chemical potential and the temperature. We then match the phase boundaries for a hybrid star with quark gluon plasma in the core covered by a thin crust of hadron and study the resultant parameter space to obtain stable compact objects. We find

that the model satisfies all the conditions of stability of a compact object for certain ranges of the bag constant in the presence of a massive strange quark. We calculate the gravitational redshifts from the masses and the radii of these stable compact objects. There are several observational candidates whose redshift values are in agreement with the ones obtained from our model. Thus our model shows that it is possible to model massive compact objects using extensions of the bag model with no exotic phases in its core.

# Contents

D	eclar	ation	iii
$\mathbf{C}_{0}$	ertifi	cate	v
$\mathbf{A}$	ckno	wledgements	iii
$\mathbf{A}$	bstra	act	x
Li	st of	Figures	ΧV
1	Intr	$\operatorname{roduction}$	1
	1.1	Introduction	1
		1.1.1 Historical overview	3
		1.1.2 The Pillars of the Big Bang Model	3
		1.1.3 The Thermodynamic History of the Universe	4
	1.2	Primordial fluctuations	6
	1.3	The Primordial magnetic field	8
	1.4	Plan of the thesis	9
<b>2</b>	Pha	ase Transitions in the Early Universe	13
	2.1	Phase Transition	13
		2.1.1 Order of Phase transition and order parameter	15
		2.1.2 Spontaneous symmetry breaking	17
	2.2	Topological Defects	20
	2.3	The QCD Phase transition	21
		2.3.1 The MIT Bag Model	21
		2.3.2 Consequence of the Quark-Hadron Phase Transition	23
3	Der	nsity inhomogeneities in early universe	25
	3.1	Density Inhomogeneities	25
	3.2	Density inhomogeneities due to cosmic string wake	26
		3.2.1 Cosmic string	26
			28
	3.3	Generation and evolution of baryon inhomogeneities	29

Contents

4	Dec	cay of hadronic inhomogeneities in an non-expanding universe	<b>35</b>
	4.1	Baryon inhomogeneities	35
	4.2	Diffusion Coefficients of nucleons	38
	4.3	Diffusion Coefficients after the Quark-Hadron phase transition	42
	4.4	Decay of inhomogeneities	46
	4.5	Neutrino degeneracy parameters	48
	4.6	Summary	51
<b>5</b>	Dec	cay of baryon inhomogeneities in an expanding universe	<b>55</b>
	5.1	Introduction	55
	5.2	The diffusion equation in the FLRW metric	56
	5.3	Diffusion in the electroweak scale	58
		5.3.1 Quark-electron scattering	59
		5.3.2 Quark-neutrino scattering	59
		5.3.3 Quark-muon scattering	60
	5.4	Decay of inhomogeneities in the quark gluon plasma phase	60
	5.5	Decay of inhomogeneities in the hadronic phase	66
	5.6	Summary	69
6	Cor	neration of magnetic field in cosmic string wake	73
U	6.1	Neutrino current density around cosmic strings	75
	6.2	Neutrino currents in moving cosmic string wakes	78
	0.2	6.2.1 Ponderomotive force	
			78
	<i>c</i> o	6.2.2 Magnetic field generation	
	6.3	Summary	84
7	$\mathbf{Q}\mathbf{u}$	ark cores in modified MIT Bag model	87
	7.1	Introduction	87
	7.2	The extended bag model	90
		7.2.1 Case 1: Two massless flavors (up and down)	92
		7.2.2 Case 2: Three massless flavors (up, down and strange)	93
		7.2.3 Case 3: Massless up, down and massive strange quarks	95
	7.3	The Tolman - Oppenheimer - Volkoff equations	97
	7.4	Results	98
		7.4.1 Mass-radius ratios with three massless flavors (up, down and strange)	98
		7.4.2 Mass-radius ratios for the massive strange quark	
	7.5	Summary	
8	Sun	nmary and Conclusion 1	L <b>07</b>
г.		,	
Bi	bliog	graphy 1	113

# List of Figures

1.1	Thermodynamic history of the universe	Ę
2.1 2.2	Phase diagram of water (Ref.[26])	
3.1 3.2 3.3	Defect generated from Mexican hat potential. (Ref.[52]) Deficit angle in cosmic string space time. (Credit-Smoot Group) Motion of two particle moving in parallel line in cosmic string space time.	26 27
3.4	(Ref.[52])	28 29
4.1	Diffusion coefficient of neutrons in the electron, neutron and muon plasma. The (black) dashed line denotes $x_e < x_{\mu}$ and the (red) dot- dashed line denotes $x_e \approx x_{\mu}$	44
4.2	Diffusion coefficient of protons in the electron, neutron and muon plasma. The (black) dashed line denotes $x_e < x_{\mu}$ and the (red) dot- dashed line denotes $x_e \approx x_{\mu}$	45
4.3	Diffusion coefficient of neutrons in the electron, neutron, proton, and neutrino plasma at temperatures below 10 MeV. The (red) dotted line denotes the presence of muons in the plasma. The (blue) solid line denotes the plasma without the presence of muons.	46
4.4	The decay of the inhomogeneity in a plasma with equal number of elec-	47
4.5	The decay of the baryon inhomogeneity in a muon rich plasma.	48
4.6	Comparison of abundances in the presence and absence of inhomogeneities for muon degeneracy greater than the electron degeneracy Plot of the abundances in the presence and absence of inhomogeneities for electron neutrino degeneracy greater than the muon neutrino degeneracy	50
	$included. \dots \dots$	51
5.1 5.2	The initial fluctuation at 200 GeV in the linear scale	62
5.3	decreases	63
	temperature decreases	64

List of Figures xvi

5.4	The decay of the fluctuation is shown in log scale between 1 $\mathrm{GeV}$ - 236 $\mathrm{MeV}$ for a plasma where a quark is moving through a sea of electrons		65
5.5	The decay of the fluctuation is shown in log scale between 1 GeV - 236 MeV for a plasma where a quark is moving through muons		66
5.6	The decay of the fluctuation is shown in log scale between 1 GeV - 236 MeV for a plasma where a quark is moving through neutrinos. Since the inhomogeneity decays faster here, as the magnitude goes down, the radial distance increases. The full curve at 236 MeV is not given, it is cut off at some point where baryon inhomogeneity is close to 0.01. Compared to the initial fluctuation which had an amplitude of 10 <sup>3</sup> , this can be taken to be zero		67
5.7	The decay of the initial fluctuation is shown in logscale between 200 MeV - 100 MeV		69
5.8	The decay of the initial fluctuation is shown in logscale between 100 MeV - 1 MeV		70
6.1	A plot of the neutrino current as a function of $r$ (distance from the cosmic string). Here $\alpha r$ is dimensionless. The current is oscillatory in nature and decreases with increase of distance from the string		78
6.2	An illustration to show the generation of magnetic field in the wakes of cosmic strings due to the non uniform neutrino overdensities		82
7.1	The graph shows the core pressure for stable masses at different bag constants for different values of the neutron radius. Beyond 0.66 fm all		05
7.2	the curves overlap		95
7.3	potential of the $u$ quark		<ul><li>97</li><li>99</li></ul>
7.4	at different bag constants for massless quarks		.00
7.5	Graph of mass $M$ (in solar masses) vs radius $R$ ( in kms) of stars at different bag constants for $m_s=100~{\rm MeV},\mu_u=100~{\rm MeV}$ for a core with		
7.6	u-d-s massive plasma	1	.01
7.7	massive plasma		
7.8	strange quark of mass $m_s = 100 \text{ MeV}$		
	strange quark of mass $m_s = 150 \text{ MeV}$	1	02

To my family

## Chapter 1

## Introduction

#### 1.1 Introduction

Density inhomogeneities are one of the fundamental building blocks of the early universe. Initially, the universe plasma is considered to be homogeneous and isotropic. Due to the various mechanisms, density inhomogeneities can be generated at different time scales in the plasma. Phase transitions, evolution of topological defects like cosmic strings, domain walls, etc. usually lead to the generation of inhomogeneities in the plasma. These density inhomogeneities might have several effects in the early universe.

In modern cosmology, the understanding of structure formation, and the generation and evolution of primordial magnetic fields in the early universe is still an important subject that needs to be understood. These inhomogeneities are one of the possible reasons for the generation of the large scale structures in the universe. They can also help to generate the seed magnetic field in the early universe. Apart from these, density inhomogeneities play an important role in nucleosynthesis calculations. In this thesis, we have studied the consequences of density fluctuations in the early universe.

Density inhomogeneities can be generated any time in the early universe. The most discussed inhomogeneities are either formed in electroweak scale or quark hadron scale [1, 2]. There might be various reasons or mechanism behind the generation of these fluctuations like, inflation, collapsing Z(3) domain wall or bubble nucleation etc. Inflation generates super horizon fluctuations which has larger length scales than the horizon size. Fluctuation generated by Z(3) domain walls have length scales smaller than the horizon size. These are sub horizon fluctuations. If inhomogeneities generated in the early universe survive up to the next phase transition then they may have a significant effect on the phase transition dynamics. This will depend on the nature of their decay. It has

been discussed that inhomogeneities generated in the electroweak scale generally do not survive up to the nucleosynthesis epoch. However the inhomogeneities generated in the quark hadron epoch may survive up to the nucleosynthesis. Dense inhomogeneities may form metastable quark nuggets. Possibility of metastable H dibaryons are also there due to the presence of strange quarks during the time of this transition.

In electroweak scale, the most abundant particles of these inhomogeneities are mostly the quarks, the electrons, the muons and the neutrinos etc. Baryon number is carried by the quarks in the electroweak scale. In the QCD scale, after hadronization, the neutrons, the protons, the electrons and in some places the muons are the most abundant particles. Baryon numbers are carried by the neutron and the proton in the QCD phase. Baryon numbers from these overdensities gradually diffuse to the underdense regions to try and attain an equilibrium state. The diffusion of the neutrons and the protons have been discussed in many articles. These diffusions through the overdensities can change the n/p ratio in various places in the plasma, which means they can modify the light element abundances like lithium, helium etc.

Cosmic strings are example of one dimensional topological defects, formed due to the axial or cylindrical symmetry breaking. Mathematically, strings are the solutions of certain field theories, whose energy is concentrated along an infinite line. We have got signatures of them from the recent data of the Cosmic Microwave Background Radiation (CMBR). Cosmic strings induce inconsistencies in the cosmic microwave background power spectrum [3, 4]. The evolution of these strings have also been simulated. Moving cosmic strings will generate wake like structure behind them. Those wake regions will have higher particle density than the background. Due to the CP violating decay mechanisms, happening in the early universe, there will be an inherent lepton asymmetry in the early universe plasma. Density inhomogeneities produced by these comic string wakes can help to generate seed magnetic field in the early universe.

Density inhomogeneities not only affect the evolution of structure formation and nucleosynthesis in the early universe, they can be found in compact structures like hybrid stars. The baryon density in an hybrid star is characterized by the chemical potential in the Bag model. Observational data says there are possibilities of having massive hybrid stars in the galaxies. Theoretical models are still trying to model those stars and match the corresponding data. In this thesis we have discussed a model, where we have modified the bag constant with a finite chemical potential and temperature dependence. This modified model can generate the higher mass radius limit to match the observational data of these massive compact objects. In the next part of the introduction we will give a historical overview of the early universe, then discusses about the density inhomogeneities and the primordial magnetic field generation in the early universe.

#### 1.1.1 Historical overview

The Standard Model of cosmology tells us that the origin and the evolution of the universe is based on the Big Bang Model, proposed by Friedman and Lemaitre [5]. 'Big bang', the term was first introduced by F. Hoyle. This theory is consistent with Hubble's law. The Universe began about ten to fifteen billion years ago. In 1929, Edwin Hubble found that since the birth of the universe, it is expanding and the recessional velocities of the galaxies from an astronomical object holds a proportional relation with the distance from that particular astronomical object [6]. According to the Big Bang model, initially the universe was an isotropic ball of radiation, having extremely high temperature and density. It started out as a hot compressed, higher density state and gradually started to cool and expand. The Big bang Model is developed within the frame work of two basic assumptions: the principle of equivalence and the cosmological principle. Based on these two principles, the universe evolved through different stages.

However this theory had some serious competitors (like the steady state theory by Hoyle and Narlikar) up to 1960. This model also satisfies the Hubble's law. Steady state model says that at large scales the universe is completely homogeneous and evolves with constant density in spite of the expansion of the universe [7, 8]. According to this model the rate of the creation of new matter is equal to the rate of expansion. This continuous creation is keeping the density of matter unchanged. But the Cosmic Microwave Background Radiation (CMBR) data acts as a major evidence in support of the Big Bang model and scientists accepted it as the most favorable model to describe the origin and evolution of the universe. There are some key evidences that play a pivotal role to support the Big Bang Model. These evidences for the Big Bang model are called "The Pillars of the Big Bang Model" [9]. We will discuss those in the next section.

#### 1.1.2 The Pillars of the Big Bang Model

• The first and the most important evidence is the expanding universe. The expansion of the universe is measured by the redshift of light coming from the galactic objects. In 1929 Edwin Hubble measured the observational data of redshifts from the galaxies [6]. Redshift is the shift of spectra towards longer wavelength for distant objects, which describes that all the galactic objects are moving away from

each other with some acceleration. So our universe is expanding gradually. This phenomena is consistent with the Big Bang Model.

- In 1965, Penzias and Wilson have discovered the Cosmic Microwave Background Radiation (CMBR) which is a strong land mark of the Big Bang Model [10, 11]. The Cosmic Microwave Background Radiation(CMBR) is the electromagnetic radiation which is considered to be the remnant part from the Big Bang. The temperature of this radiation is around 2.73K. At the recombination epoch radiation is decoupled from matter. This radiation is the oldest radiation in the universe. The photons become free streaming and do not interact with matter any more. This gives rise to the CMBR. In 1992 COBE experiment first verified this radiation.
- With the expansion of the universe, the temperature goes down and some of these nucleons are synthesized into the light elements such as hydrogen, helium, and deuterium etc. The most abundant atom in the universe is hydrogen atoms. It covers nearly 90 % of the atoms in the universe. Theoretical calculations from the Big bang nucleosynthesis predicts the abundance of these light elements, This prediction match with current measurements of the primordial elements. So this works as an evidence for the Big Bang Model.
- The standard Big Bang model also provides a framework for understanding the separation of matter from radiation to form galaxies. At about 10,000 years after the Big Bang, the universe temperature had fallen to such an extant that matter got detached from radiation. Big Bang model has the framework for the clustering of the matter particles to form the large scale structure of the universe.

#### 1.1.3 The Thermodynamic History of the Universe

According to the Big Bang model the universe started expanding at a very early stage [5]. As the universe expanded and gradually cooled down from a very dense state it gave rise to the universe as we see it today.

At the initial stage the universe consisted of a plasma of the relativistic elementary particles. This initial stage is called the Planck era. At this stage the order of the universe age is around  $10^{-43}$  sec. This time scale is called the Planck time scale. The universe was radiation dominated during this period. At this stage the energy and the temperature of the universe were so high that all the four fundamental force were speculated to be unified to form one force. It had a temperature of the order of  $10^{19}$  GeV.

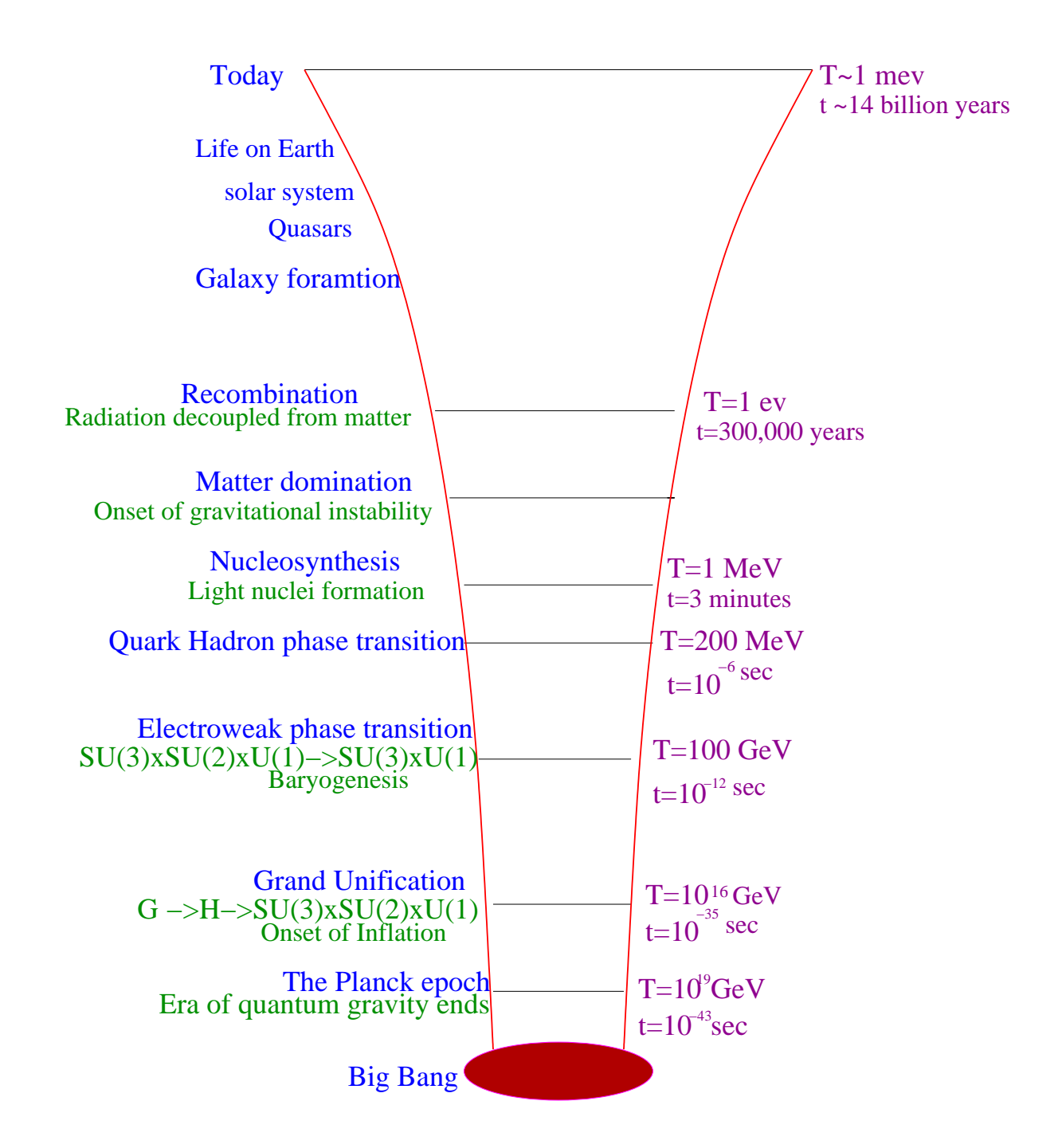


FIGURE 1.1: Thermodynamic history of the universe

The earliest phase transition is believed to be the GUT (Grand Unified Theory) Phase Transition at the energy scale of  $10^{15}$ - $10^{16}$  GeV [12]. At this time, the universe was  $10^{-35}$  sec old. The inflationary stage follows the GUT stage. This stage undergoes a stage of accelerated expansion. This stage terminates with the reheating of the universe.

The next is the Electroweak Phase Transition at the energy scale of 100 GeV. This is a

symmetry breaking phase transition which resulted in the separation of the electromagnetic and the weak force. In our universe, the number of particles, is greater than the number of anti particles. This particle-antiparticle asymmetry might have been generated in this time. Magnetic fields are also present in our current universe. It is quite possible that the seeds of these fields were generated in this period.

Following this, the next predicted phase transition is the Quark-Hadron Phase Transition which takes place around 200 MeV. During this epoch, hadrons were formed. After hadronization, three quarks form the baryon and a quark and an anti-quark form the meson. This phase transition may have generated baryon inhomogeneities in the plasma [2]. Density inhomogeneities generated during this epoch will survive up to the nucleosynthesis era [13]. The most abundant baryons in the universe after this phase transition were the protons and the neutrons. The neutron proton ratio in the universe determines the ratio of the light elements formed during nucleosynthesis.

After this comes the nucleosynthesis era. At this time the proton and the neutron form the nuclei. These nuclei come together and form the light elements like hydrogen, helium etc. This era happened around 0.1 MeV. Following this, matter decoupled from the radiation and the radiation epoch ended. This was followed by the matter dominated epoch. The matter dominated epoch saw the formation of the stars and galaxies. It is the epoch in which we currently reside.

#### 1.2 Primordial fluctuations

The theory of cosmological fluctuations has become an important part of modern cosmology as it is the framework which links the early universe with the recent data. The theory was initially developed by Lifshitz [14] and a significant work to understand the physics of cosmological fluctuations was done by Bardeen [15]. Primordial fluctuations are considered to be the seeds of all the large scale structures. These fluctuations generated in the early universe are mostly in the form of metric perturbations or density perturbations. The fluctuation can be of two types depending upon the Hubble scale: super-horizon and sub-horizon fluctuations. Primordial fluctuations are scale-invariant and adiabatic in nature. Adiabatic fluctuations tells that the local state of matter (determined by the energy density  $\rho$  and the pressure P) at some space time of the perturbed universe is the same as in the background universe at some slightly different time.

The Friedmann-Robertson-Lemaitre-Walker (FLRW) metric describes the homogeneous and isotropic universe. The FLRW metric stress-energy tensor requires energy and momentum transfer over a considerable scale to produce spatially dependent density

perturbations. The radiation pressure plays a pivotal role by creating some fluctuations and determining their characteristic scales. Besides, it modifies the pre-existing primordial fluctuations. Primordial fluctuations can be decomposed into scalar, vector and tensor modes. Vector fluctuations decay faster in the expanding universe, hence these are not so important for the cosmological background. On the other hand, the scalar metric fluctuations are indeed important. They are the key factor behind the large scale structure of the universe. To show this we have to describe the evolution of the spacetime by the first Friedmann equation for a homogeneous and isotropic universe. Based on this, a fluctuation of the energy density will lead to a fluctuation of the scale factor which grows over time. The self gravity amplifies the fluctuations even for length-scales larger than the Hubble radius. The most important fluctuations are the fluctuations which are coupled with the matter density. These fluctuations will dissipate through different processes. Diffusion is one of those processes.

Previously, considerable work have been done on fluctuations regarding the electroweak phase transitions and the QCD epoch. Jedamzik and Fuller [16] worked on nonlinear sub-horizon fluctuations, generated from an epoch of the early universe where there is a deviation from an equilibrium phase transition (i.e., electroweak phase transition). Witten showed that this phase transition may have produced isothermal baryon number fluctuations due to the difference in the number density in the quark-gluon plasma and the hadronic phase.

Primordial fluctuations can decay through different processes: photon inflation, neutrino inflation in the homogeneous and diffusive limits, hydrodynamic expansion, and baryon diffusion. Here in this thesis, we have studied the diffusion of the baryonic inhomogeneities. Applegate, Hogan and Scherrer [17] have shown the decay of the baryon inhomogeneities in a scenario where the neutrons, the protons and the electrons are present. The proton is positively charged particle and the neutron is the neutral particle. So, they will diffuse differently in the plasma. As a result there would be inhomogeneities in the proton and neutron rich regions. Banerjee and Chitre [18] have showed that the diffusion coefficients have explicit dependence on the density of the diffusive particles. They have worked in the non-relativistic limit and also showed that the relativistic kinetic theory can be used to determine the diffusion coefficients for the diffusion of particle before nucleosynthesis, in a classical approximation. Here in this thesis we have discussed the diffusion of these density inhomogeneities for an expanding and non expanding universe. Along with the neutrons, the protons, the electrons and as a fourth particle, we have considered a significant amount of the muons, present in the plasma in the hadronic phase. For the electroweak phase we have analyzed the scenario considering the presence of the quarks, the electrons, the muons and the neutrinos in the plasma.

#### 1.3 The Primordial magnetic field

The magnetic field is a crucial element of the early universe. We can observe the magnetic field from all the astronomical objects, from all parts of the universe. Planets, stars, galaxies, and even intergalactic space between galaxy clusters have significant magnetic fields. It can be measured through various methods like, from radio synchrotron emission data, Faraday rotation measurements and Zeeman splitting etc. The average magnetic field strength in the Milky Way galaxy is  $3-4~\mu G$  in the current time. But the origin of this magnetic field is not clearly understood yet. It is argued that the current magnetic fields can be the result of the magnification of the initial seed magnetic field from the pregalactic era [19–21]. These seed magnetic fields will also have an effect on the Cosmic Microwave Background Radiation, Big Bang nucleosynthesis etc.

How did the primordial magnetic fields arise in the early universe and how did they evolve during the ages, is one of the fundamental questions in cosmology. There should be some charge asymmetry in the plasma to generate a seed magnetic field. But, the early universe plasma is nearly charge neutral and conducting. So, we need to generate a charge asymmetry in the plasma through some mechanism first to get the magnetic field. There could be various ways to generate a magnetic field like, cosmological phase transitions ( generated during the electroweak phase transition or quark—hadron phase transitions), topological defects ( moving GUT/Superconducting strings, collapsing domain walls ), inflation ( generated during the inflationary epoch ), plasma instabilities ( generated when structure formation has started ), and primordial vortices [19].

One of the methods for the production of the Primordial magnetic field is from plasma vorticity due to the Harrison's mechanism, which arises in the radiation dominated era [22]. This magnetic field will be generated in those areas of the electron-ion plasma which have a non-vanishing vorticity. This model was done by Harrison. In this method we can get seed magnetic fields through vorticity produced by the velocity difference in the plasma. According to the Harrison's mechanism the rotational velocities of the electrons and the ions will change differently in the pre-recombination era, because Thomson scattering will have more effect in the case of the electrons than for the ions. Electrons will be in the coupled state for a longer time to the radiation and behave like a relativistic particle whereas ions are already nonrelativistic. The difference between electron and ion velocities will generate an electromotive force in the plasma. Therefore an electric current will follow which will generate the magnetic field. For cosmic strings, two straight moving cosmic strings passing each other can generate vorticity due to the drag effect[23]. Through the Harrison mechanism, the magnetic field can be generated in this moving cosmic string system. In this thesis we have also discussed an unique way of generating magnetic field from moving cosmic string wakes.

The magnetic field generation and amplification will proceed mostly in three steps. At the beginning using the Bierman battery mechanism, we can generate the primordial magnetic field [24]. At this time, the generated magnetic field will be less than the equipartition magnetic field. In the next step this, weak magnetic field will be magnified to be a stronger magnetic field through turbulence. The Reynolds number of the early universe plasma was very high. So from the fluid properties we can say that there will be a turbulence in the early universe plasma. At the last step, this magnetic field will increase again and will reach up to a saturation value due to the turbulent energy. This is known as the equipartition value at that particular epoch.

In this thesis we have shown magnetic field generation in cosmic string wake by the Bierman battery mechanism. We are getting a seed magnetic field in cosmic string wake system. As the early universe plasma has a high Reynolds number that magnetic field also can be amplified to the equipartition level using the turbulence property of the plasma [25].

#### 1.4 Plan of the thesis

After this brief introduction, I will give a brief outline of the remaining thesis.

In Chapter 2, we will start with a short introduction to phase transitions. Then we will give a small review of the symmetry breaking phase transition which have happened in the early universe. These phase transitions can generate topological defects. Next, we will discuss about different types of topological defects that are formed in the early universe. Most of the work of the thesis is related to the Quark Hadron phase transition. So at the end we will discuss the Quark Hadron phase transition and its dynamics in the early universe in more detail.

In **Chapter 3**, we will talk about the inhomogeneities generated in the early universe. Density inhomogeneities play an important role in the early universe as they are one of the key factors leading to all the large scale structures present in our universe. Besides inhomogeneities may also be responsible for the seed magnetic field generated in the early universe. Here we will focus on baryon inhomogeneities. In this chapter we will present a brief overview of the generation and evolution of these baryon inhomogeneities.

Chapter 4 contains the study of the cosmological diffusion of particles from muon rich overdense region in an non-expanding universe. We will discuss how overdensities can be generated after the Quark Hadron phase transition. Next we will explain the high muon abundances. We then inspect the decay of these muon rich inhomogeneities and how these inhomogeneities can affect the big bang nucleosynthesis. There will be a

lot of neutrinos in the plasma at that temperature scale. We will also examine how these neutrinos will influence the helium and lithium abundance at the time of the nucleosynthesis.

Chapter 5 presents cosmological diffusion in an expanding universe. Previously, we have analyzed the inhomogeneities for a stationary universe. Here, we have simulated relativistic diffusion to analyze the scenario in the expanding universe. We have studied the decay starting from the electroweak phase transition up to the hadronic phase. There will be inhomogeneities of different amplitude generated in the electroweak scale and the QCD scale. This analysis will lead us to understand which inhomogeneities will survive up to the nucleosynthesis epoch for an expanding universe and make a difference in the particle abundances after nucleosynthesis.

In **Chapter 6**, we have suggested a new method of generating seed magnetic fields in the early universe. The seed magnetic fields are generated in cosmic string wakes caused by the neutrino density inhomogeneities in the wake of the Abelian Higgs strings. The Abelian Higgs strings are linear topological defects, generated due to the symmetry breaking phase transitions. Generally wakes will form behind a moving cosmic string. Here we discuss about neutrino currents in that wake. We have shown that the neutral particle (neutrino) motion in the wake can give rise to overdensities in the electron which leads to a magnetic field in the early universe. At the end of this chapter, we have briefly estimated the order of magnitude of that magnetic field.

Chapter 7 comprises of plasma property in bulk strange matter. The baryon density in neutron stars is quantified by the chemical potential  $(\mu)$ . Here we have considered a bag constant, which is dependent on temperature and chemical potential. This modified bag model can lead to an isentropic phase transition in the core of the neutron star. Then we have calculated the Maxwell construction for the isentropic phase transition along the phase boundary. For our calculations, we have also considered the conservation of various charges in the plasma. We have found that the mass of the stars depends on both the bag constant and the mass of the strange quark. Next we have matched the mass radius data from our model to some of the experimentally observed data and it is quite consistent with our model.

In the end, we will summarize the thesis in **Chapter 8**.

# Chapter 2

# Phase Transitions in the Early Universe

#### 2.1 Phase Transition

Phase transitions are a well studied phenomena in physical systems. This phenomena can be observed in our daily lives. In the previous chapter, we have discussed about the thermodynamic history of the early universe. There we have mentioned about the different phase transitions, that have occurred after the Big bang in the early universe. In this chapter we will discuss briefly about this phenomenon and its consequences.

Phases are the different states of matter described by the thermodynamic properties of the system and phase transition is the thermodynamical process of transition from one state to the other state of matter. The intrinsic parameters that can describe a phase of a system in equilibrium are temperature, pressure, volume, chemical potential etc. We can draw a phase diagram using these parameters. In that diagram, equilibrium phases are separated by the phase boundaries. There will be a discontinuity in the thermodynamic free energy along these boundary lines. A phase transition moves a system from across the phase boundary from one phase to another. In the fig. 2.1 we have shown the phase diagram of water. At the triple point, the three phases of water can coexist in a system. Fig. 2.2 represents the QCD phase diagram as a function of baryon chemical potential and temperature. The quark-gluon plasma phase, the hadron phase and the superconducting phase have been presented in the phase diagram.

The most common example of a phase transition from our day to day life is the boiling of water and the freezing of ice. The boiling of water is a transition from the liquid phase to the gaseous phase and the freezing of ice is a transition from the liquid phase

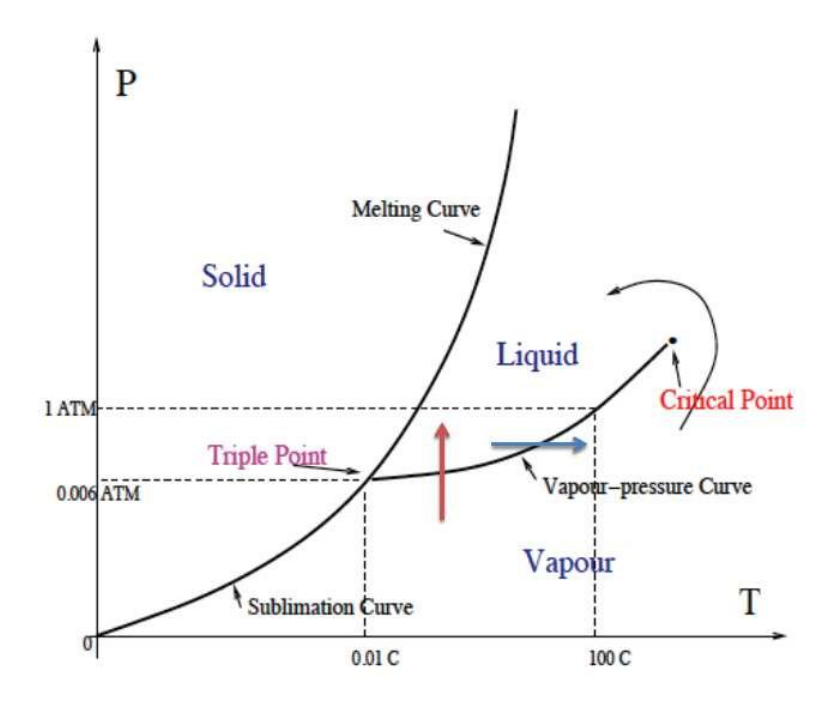


FIGURE 2.1: Phase diagram of water (Ref.[26])

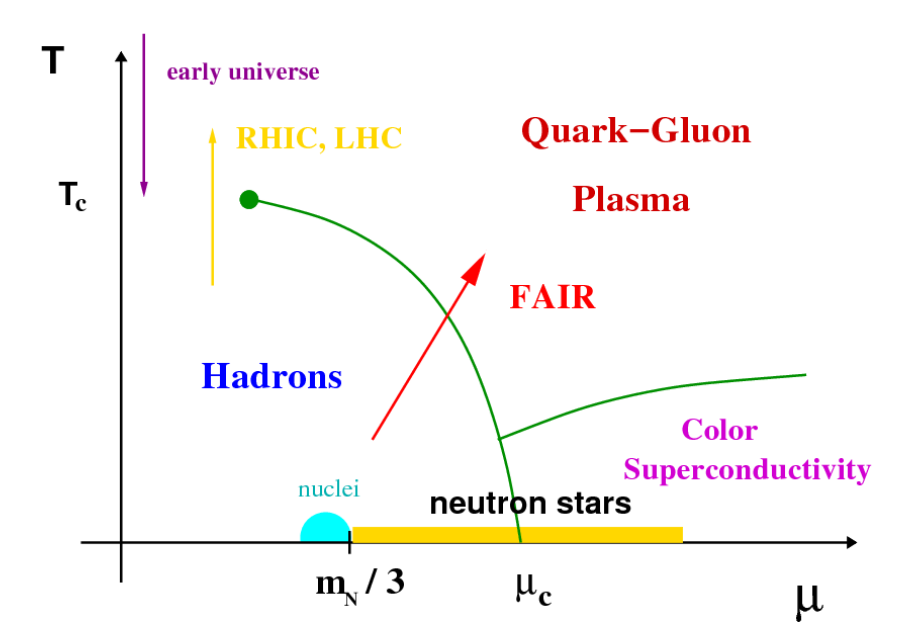


FIGURE 2.2: Phase diagram of QCD plasma (Ref.[27])

to the solid phase. We can also observe melting, condensation, deposition etc between these three states of matter. Besides this, some well known examples that can be observed in experiments are the magnetic phase transition, the superconducting phase transition and the superfluid phase transition. Metals like, iron and nickel show ferromagnetic property. We can convert these metals into a permanent magnet by orienting all the magnetic dipole in the same direction. However above the Curie temperature this alignment breaks to form a paramagnetic phase. This is a phase transition from ferromagnetic to paramagnetic phase. Liquid helium shows superfluidity property. Below the critical temperature it behaves like a superfluid. Metals like, mercury and lead have the superconducting property. Their resistance becomes zero below some temperature and they go into the superconducting phase from the normal phase. A phase transition from Type-I superconductor to Type-II superconductor also occurs. Similar to these examples we have different phase transitions at different temperature scales of the Big Bang Model.

#### 2.1.1 Order of Phase transition and order parameter

A fundamental requirement of a system in equilibrium is energy minimization. Phase transition happens in the process of attaining that ground state of the system. These transitions are categorized into two types the First order and the Second order phase transition. According to Paul Ehrenfest they can be classified depending on the behaviour of the Gibbs free energy. The first derivative of the Gibbs free energy is discontinuous with respect to some intrinsic parameter for the first-order phase transitions. For a second order phase transitions the first derivative of the Gibbs free energy is continuous but the second derivative is discontinuous. Another definition of phase transition says for the first order phase transition there will be the involvement of latent heat in the transition process, while for the second order transition there is no contribution from the latent heat. According to this definition, the water boiling is a first order phase transition. The latent heat is involved in the process. The Ferromagnetic to paramagnetic transition, superconductivity, superfluidity etc. are second order phase transitions. For the magnetic system, magnetic susceptibility changes discontinuously which is the second derivative of the free energy. Besides these two there is another type of phase transition, which is a cross over phase transition. This is a cross over between first and second order phase transition. The quark hadron phase transition is believed to be a crossover phase transition at zero chemical potential.

One other way of describing phase transitions is by the order parameter which describe the symmetry properties of these phases. It takes different value in different phases. Generally in one phase the value of the order parameter is zero and in the other phase it takes a non-zero value. A system need not have an unique order parameter. It is quite possible to define different order parameters for a given system. The order of the phase transition may also become different if a different order parameter is chosen. As an example, for the boiling of water density is the order parameter. In the ferromagnetic phase, the orientation of the magnetic dipole is given by the "Magnetization", and this is used as an order parameter for the magnetic system. The value of the order parameter is zero in the paramagnetic phase, but in the ferromagnetic phase it has a non-zero value. So in the paramagnetic phase, the magnetic dipoles are randomly oriented but in the ferromagnetic phase they have a specific orientation. So for the ferromagnetic phase the rotational symmetry is broken. During a phase transition, the order parameter can change discontinuously or continuously depending on the variation of the thermodynamic parameters. For the first order phase transition the variation of the order parameter with respect to the temperature is discontinuous and for the second order phase transition there is a continuous change in the order parameter. The chiral condensate is one of the order parameters for the QCD phase transition.

The first-order phase transition occurs through the nucleation of bubble like regions. The order parameters changes its value across the bubble wall from zero to non-zero value or vice versa. There is a new phase inside the bubble and an old phase outside the bubble. Bubbles larger than the critical size will grow and merge with each other. This way the entire early universe plasma will be transformed into the new phase. There are several models of the quark hadron phase transitions. Most of them were first order in nature. However, recent simulations and observational constraints indicate that it is probably a cross-over phase transition.

The second-order phase transition is carried out by the continuous change of the order parameter from zero to non-zero value or vice versa in the entire system. At the initial stage, the whole system can be divided into multiple domains of different order parameters. After this stage, the size of the domains increase. As time goes, when complete equilibrium is reached, the order parameters of the entire sample become uniform and the gradient energy is minimized. The second-order phase transition occurs in the transition from a paramagnet to a ferromagnet, the normal superconducting transition of type II superconductor, the transition from normal liquid to helium superfluid, and so on. The strongly interacting chiral symmetric transitions are also expected to be second-order.

#### 2.1.2 Spontaneous symmetry breaking

Phase transitions may also be associated with the spontaneous breaking of the symmetry of a system. Before talking about the symmetry breaking, we will describe what we mean by symmetry first. Symmetry plays an important role in Physics. By definition, a symmetry is a transformation that conserves the physical properties of a system. The most common types of symmetries that is observed in nature is translational symmetry, rotational symmetry, and the reflection symmetry. From the field theoretical point of view, the action of a system will remain invariant through a symmetry transformation. For global symmetry, the physical properties of a system is constant throughout the whole space-time. So the symmetry parameter is not dependent of space-time. But for local symmetries the symmetry parameters depend on the space-time.

Some times at the time of a phase transition a physical system possess symmetry in one phase of the system but the other phase of the system does not follow the same symmetry. As the system undergoes a phase transition, the symmetry of the system changes spontaneously, this phenomenon is called the spontaneous symmetry breaking. However, all the phase transitions are not symmetry breaking phase transitions. The order parameter will change due to the transition but symmetry may not be broken.

In this section, we will focus on those phase transitions which are related to spontaneous symmetry breaking. For the paramagnetic to ferromagnetic transition the Hamiltonian of the system is rotationally invariant, but the ground state does not exhibit rotational invariance. Magnetic dipoles are scattered in every direction in paramagnetic phase, but organized in the same direction in the ferromagnetic phase. So rotational symmetry is broken for the ferromagnetic phase. This is spontaneous symmetry breaking in the magnetic domain.

In the standard model of cosmology and particle physics also we come across spontaneous symmetry breaking phase transitions. In the early universe cosmology the grand unification theory (GUT) model is based on spontaneous symmetry breaking. The grand unification theory can be explained by SU(5) or SO(1O) group. Due to the phase transition this symmetry is broken in to  $SU(3) \times SU(2) \times U(1)$ . This model tries to unify electroweak interaction and strong interaction. In this model, the symmetry breaks to generate the Majorana mass of the neutrino. Electro weak theory which unifies weak and electromagnetic interaction is also based on spontaneous symmetry breaking. Due to the symmetry breaking phase transition  $SU(3) \times SU(2) \times U(1)$  symmetry is broken into  $SU(3) \times U(1)$ . The underlying symmetry associated with this renormalizable theory is gauge invariance. Due to the breaking of the underlying symmetry in electroweak theory, the gauge bosons which mediate the electroweak interaction i.e.  $W^{\pm}$ ,  $Z^0$  acquire

mass. This is due to the Higgs Mechanism and Higgs boson particle is responsible for giving mass to all the elementary particles.

From the field theoretic point of view, spontaneous symmetry breaking is described by a complex scalar field. The effective potential of the fields contain all the information about the phase and the order of the phase transition. During the phase transition the symmetry of the Lagrangian is broken spontaneously. In the context of the particle physics models this scalar field is the Higgs field. Now we will analyze an example of scalar field theory to understand the essential features of spontaneous symmetry breaking. This model was first studied by Goldstone [28]. The Lagrangian density for the scalar field is given by,

$$\mathcal{L} = (\partial_{\mu}\phi^*)(\partial^{\mu}\phi) - V(\phi) \tag{2.1}$$

where,  $\phi$  is the complex scalar field and  $V(\phi)$  is the potential. The potential can be written as,

$$V(\phi) = \frac{1}{4}\lambda(\phi\phi^* - \eta^2)^2$$
 (2.2)

Here  $\lambda$  and  $\eta$  are positive constant. This Lagrangian is invariant under the following transformation,

$$\phi(x) \to e^{i\alpha}\phi(x)$$
 (2.3)

This is global U(1) invariance. This global symmetry transformation is independent of space. This potential has only one minima in the symmetric phase. But it has infinite number of minima in the broken phase. So this potential has degenerate minima and all the minima lies on the circle  $|\phi| = \eta$ . The vacuum manifold  $\mathcal{M}$  structure of the potential is a circle  $\mathcal{S}^1$ . Since the system has to choose a particular minima from among the infinite minima, the symmetry of the system is broken.

Now the vaccum expectation value of the field cannot take a non zero value, but has to choose a finite value. So the symmetry is spontaneously broken and it give rises to the Goldstone bosons [29]. The mass term of the Lagrangian is  $-\frac{1}{2}\lambda\eta^2\phi^*\phi$ . This mass term arises due to a massive particle having mass  $M_G = \sqrt{\lambda}\eta$ .

All the vacuum states, having different  $\theta$  values are equivalent in the broken symmetry phase. To understand the low energy states we can write the complex scalar field in terms of real scalar field as,

$$\phi(x) = \left(\eta + \frac{1}{\sqrt{2}}\varphi(x)\right)e^{i\vartheta(x)} \tag{2.4}$$

Here,  $\varphi$  and  $\vartheta$  is the real scalar fields. Substituting the field expression, the Lagrangian density can be written as,

$$\mathcal{L} = \frac{1}{2} (\partial_{\mu} \varphi)^{2} + \eta^{2} (\partial_{\mu} \vartheta)^{2} - \frac{1}{2} \lambda \eta^{2} \varphi^{2} + \mathcal{L}_{int}(\varphi, \vartheta)$$
 (2.5)

Here,  $\varphi$  represent the real field due to massive scalar field,  $\vartheta$  represent the real field due to the Goldstone boson and  $\mathcal{L}_{int}$  is the interaction term, including the higher order terms from the field. So after the breaking of spontaneous global symmetry, a massless Goldstone boson arises.

In the previous example we have discussed about U(1) global symmetry. Now we will talk about U(1) local symmetry. This local symmetry transformations is called gauge symmetries. If the gauge symmetry is spontaneously broken it leads to the Higgs mechanism. We can study this local symmetry transformation using the Abelian Higgs model [30, 31]. The Abelian Higgs Lagrangian density is given by,

$$\mathcal{L} = \mathcal{D}_{\mu} \phi^* \mathcal{D}^{\mu} \phi - \frac{1}{4} F_{\mu\nu} F^{\mu\nu} - \frac{1}{4} \lambda (\phi \phi^* - \eta^2)^2$$
 (2.6)

Here,  $\phi$  is the complex scalar field,  $\mathcal{D}_{\mu} = \partial_{\mu} - ieA_{\mu}$  is the covariant derivative and  $F_{\mu\nu} = \partial_{\mu}A_{\nu} - \partial_{\nu}A_{\mu}$  is the antisymmetric vector field strength tensor, with gauge vector potential  $A_{\mu}$  and gauge coupling constant e. This Abelian Higgs Lagrangian is invariant under the following transformation,

$$\phi(x) \to e^{i\alpha}\phi(x) \ , \ A_{\mu}(x) \to A_{\mu}(x) + \frac{1}{e}\partial_{\mu}\alpha(x)$$
 (2.7)

This is local U(1) gauge invariance. This local symmetry transformation is dependent on space. The potential has minima which lies on the circle  $|\phi| = \eta$ . The vacuum state is not invariant under this gauge symmetry. Vacuum expectation value of the Higgs field is non zero. In our preferred gauge choice we can write the Higgs field  $\phi(x)$  as real,

$$\phi = \eta + \frac{\varphi}{\sqrt{2}} \tag{2.8}$$

Substituting the above field expression, the Lagrangian density can be written as,

$$\mathcal{L} = \frac{1}{2} (\partial_{\mu} \varphi)^{2} - \frac{1}{2} \lambda \eta^{2} \varphi^{2} + e^{2} \eta^{2} A_{\mu} A^{\mu} - \frac{1}{4} F_{\mu\nu} F^{\mu\nu} + \mathcal{L}_{int}$$
 (2.9)

where,  $\mathcal{L}_{int}$  is the interaction term. Due to the breaking of this local gauge symmetry two masses will arise, the Higgs mass  $M_H = \sqrt{\lambda}\eta$  due to the radial field and the gauge boson mass  $M_W = \sqrt{2}e\eta$  due to the vector field. This field theoretic model would have string like solution. This model leads to the formation of one dimensional topological defects called cosmic strings.

#### 2.2 Topological Defects

Topological defects are the consequences of spontaneous symmetry breaking phase transitions. If there is a symmetry breaking phase transition, topological defects may be produced. At the time of phase transition as the system evolves, in some parts of the system, the system will remain in the old symmetric state, while the remaining system will be in the symmetry breaking phase. These locked regions are in general called topological defects. Depending on the different types of symmetry breaking we can get different defects of different dimension. The existence of topological defects essentially depends on the nature of the order parameter changing through the phase transition, depending on which several types of topological defects can exist. The Monopoles are the point defects. These are point-like regions of one phase immersed in the other phase. Cosmic strings are the string defects of dimension one. These are the thin tubular regions of the previous phase embedded in the other. This occurs due to the breaking of U(1) symmetry. Domain walls are the two dimensional topological defect. These are sheet like defects. Formation of these defects is not necessarily confined to the field of high energy physics, we can observe defects in the condensed matter system also. Common examples of such defects in condensed matter systems are the vortices in liquid He3, flux tubes in type II superconductor, or line defects in liquid crystals.

In 1961, Skyrme showed for the first time that the solution of topological defects comes from nonlinear field theory [32]. Thereafter, the study of this defects has continued for the Higgs and Yang-Mills theories. In 1973, Nielsen-Olesson [33] obtained vortex solutions in the Abelian Higgs model. The cosmological implications of topological defects were first described by Everett [34] and Zeldovich, Kobzarev and Okun [35]. They showed that the domain walls formed during the GUT phase transition would have had enormous mass densities which can generate inhomogeneity in the early universe. In 1976, Kibble demonstrated the first comprehensive theory of the formation of topological defects during phase transitions [36]. Much work has been done regarding the impact of topological defects on cosmology. Zeldovich and Khlopov [37] and Preskill [38] studied the monopole generation during the GUT phase transition. Besides, cosmic strings can play an important role in early universe cosmology. Zeldovich [39] and Vilenkin [40]

have shown that they may be responsible for the formation of large-scale structures. In addition, cosmic strings can generate the baryonic asymmetry of the early universe [41–44]. Recently, it has been investigated how topological defects can affect nucleosynthesis by inducing fluctuations in the evolving cosmic string wake [45]. There is a possibility of cosmic strings contributing to the cosmic microwave background radiation (CMBR) anisotropy.

#### 2.3 The QCD Phase transition

In the Big Bang Model, one important stage is the QCD phase transition, the transition from quark matter to hadrons. Considerable work has already been done on the quark gluon plasma and the dynamics of the quark-hadron phase transition. In this phase transition the coloured quarks are confined to form colour singlet hadrons. Hence the Quark-Hadron transition is also called the deconfinement-confinement transition. The order of the phase transition is still not known satisfactorily. Computational studies of the QCD Phase transition indicates that it might be a weakly first order phase transition or a crossover phase transition. Initially it was treated as a first order phase transition. One of the earliest model used to model this phase transition is the MIT Bag Model which we will describe now.

#### 2.3.1 The MIT Bag Model

A first order phase transition proceeds through the nucleation of bubbles. Bubble formation and their growth have been studied in details in the literatures [46–48]. One of the simplest model to understand bubble nucleation is the bag model. The Bag model gives a equation of state that describes the quark-hadron phase transition. The Lagrangian for the MIT bag model can be written as the following form [49]:

$$L_{Bag} = \left[\frac{i}{2}(\bar{\phi}\gamma^{\alpha}\partial_{\alpha}\phi - (\partial_{\alpha}\bar{\phi})\gamma^{\alpha}\phi) - B\right]\theta_{v} - \frac{1}{2}\bar{\phi}\phi\triangle_{s}$$
 (2.10)

where,  $\phi$  is the free Dirac field, B is the bag constant,  $\theta_{\beta}$  is a step function and  $\triangle_s$  is derivative of  $\theta_{\beta}$  function, it can be described as order parameter. The value of this parameter is 1 inside the bag and 0 outside the bag. The bag Constant can be derived from the above equation.

Bubbles nucleate through thermal fluctuations. The rate of bubble nucleation is given by the following equation [50, 51]:

$$I(T) = CT_c^{\ 4} e^{\frac{-W}{T}} \tag{2.11}$$

Here  $T_c$  is the critical temperature, C is a constant associated with the bubble growth and W is the change in the thermodynamic potential of the two phases and or change in the surface free energy of the boundary between the two phases. The change in the surface free energy is given by:

$$W = \frac{4\pi}{3}r^3(P_q - P_h) + 4\pi\sigma(r)^2$$
 (2.12)

Here  $\sigma$  is the surface tension or the free energy per unit surface area of the phase boundary,  $P_q$  is the pressure in the quark gluon plasma phase, and  $P_h$  is the pressure in the hadronic phase. As the universe gradually cools down, bubbles of hadrons form. Then these bubbles gradually grow and coalesce with each other. If the radius of these bubbles is greater than the critical radius  $r_c$  then only they will grow. Bubble having radius less than the critical value will collapse and disappear. At the critical radius, the surface free energy attain an extremum value. The critical radius of the bubbles is given by the following equation:

$$P_h - P_q = \frac{2\sigma}{r_c} \tag{2.13}$$

At  $T_c$  the pressure in two phases is equal. So, the critical radius will diverge. Nucleation of bubbles starts below the critical temperature. At high temperature (T>1 GeV), we obtain the color charges in the plasma, carried by the quarks and the gluons. With the expansion of the universe the temperature goes down to the critical temperature where, the quark-gluon plasma undergoes a phase transition to the hadronic phase. The new hadronic phase does not appear immediately at the critical temperature. Property of thermal nucleation states that the nucleation rate increases when the temperature goes below the critical temperature. Super cooling happens until the probability of nucleation of hadronic bubbles is high. Once the first generation of bubble nucleation happen, they expands very quickly by releasing latent heat. Due to this latent heat universe reheats and reach the critical temperature again. So, further nucleation of bubble stops. At that time the quark-gluon plasma phase and the hadronic phase coexist in the early universe plasma. Then again the universe expands and these hadronic bubbles grow in size. Gradually through this nearly isothermal evolution process the whole universe is converted in to the hadronic phase.

#### 2.3.2 Consequence of the Quark-Hadron Phase Transition

This first-order Quark-Hadron phase transition in the early universe leads to a rich cosmological scenario. This phase transition will give rise to baryonic lumps or quark nuggets in the plasma [13]. With the decrease in temperature of the universe hadronic bubbles grow in size and after some time they start to coalesce. There are many small regions between the hadronic bubbles where initially the quark gluon plasma become trapped. Baryon density in this trapped region is greater than the phase inside the bubble. Baryon number is carried by the more massive hadrons in hadronic phase and in the QGP phase it is carried by the light quarks. Due to chemical equilibrium condition baryon density in the high temperature QGP phase is greater than low temperature hadronic phase. Quarks like to stay in the quark phase due to lower mass in the quark phase. The expanding bubble will tend to expel baryon number which will be concentrated in the inter bubble spacing region. So this trapped region will have higher baryon density. These QGP phase region will detach from one another and start to shrink. So these excess baryon in that region will start to exert pressure.

With the decrease in temperature of the universe this over dense region will shrink and be forced to hadronize completely and leave behind a baryon overdense region. In the hadronic phase there is no existence of the Quark-Gluon Plasma. So after the phase transition there will be many baryonic lump, generated coming from those small trapped region between the bubbles. Since the baryon number density is higher in the trapped regions there will be higher abundance of neutron and proton in those regions. So instead of a uniform neutron-proton ratio, the universe will have a large scale non-uniformity in the neutron-proton ratio in the plasma. This neutron and proton ratio in the plasma will effect nucleosynthesis calculations. Nucleosynthesis is basically the synthesis of the nuclei of the light elements such as hydrogen and helium and their isotopes. The synthesis of the nucleus is related to the coming together of the neutron and the proton to form a stable object. Hence, depending on the neutron-proton ration different light element will form in different places of the plasma. So generation of these baryon inhomogeneities have large number of consequences in the early universe.

#### Chapter 3

## Density inhomogeneities in early universe

#### 3.1 Density Inhomogeneities

Density inhomogeneities have played a significant part in the early universe. They are one of the reasons for all the large scale structure in the early universe. They can also help to generate the seed magnetic field in the early universe. Apart from these, density inhomogeneities play an important role in nucleosynthesis calculations. In this chapter we will talk about the generation and evolution of these inhomogeneities in brief. Density inhomogeneities can be generated in any time of the universe, starting from the time of inflation, then in the electroweak scale and again in the QCD epoch. Depending on the Hubble scale, these fluctuations are mainly of two types, super horizon and sub horizon fluctuation. Super horizon fluctuations can be generated in the inflationary epoch. But here in this thesis we will discuss about the sub horizon fluctuations only. These fluctuations can be generated in the electroweak scale and the quark hadron scale. These fluctuation can be generated from topological defects like cosmic string, domain walls etc. In the next section we will discuss about inhomogeneities generated by cosmic string in the early universe and there effects on phase transition dynamics.

We will first describe how the cosmic string defects are generated. We will discuss about the static solution for the cosmic string, and the generation of density fluctuations by cosmic string wakes.

#### 3.2 Density inhomogeneities due to cosmic string wake

Density inhomogeneities generated by cosmic string has been discussed in detail in many articles. Here, I will give a brief overview of that.

#### 3.2.1 Cosmic string

The cosmic string is a very thin line like one dimensional topological defect. It has been studied in detail in the literature in the context of early universe cosmology. String defect can be generated due to U(1) symmetry breaking. If the vacuum manifold of a field is circle, a cosmic string may arise over there. This circular vacuum manifold can shrink into a point and for three dimensional space it can generate string like defects. Nielson and Oleson have got a vortex line solution for the Abelian Higgs model[33]. This is the first string like solution ever got. This solution is a cosmic string and it is called the Abelian Higgs string. Cosmic strings can arise from both global and local symmetry breaking.

To describe this defect we can consider the following simplistic model

$$\mathcal{L} = (\partial_{\mu}\phi^*)(\partial^{\mu}\phi) - \frac{1}{4}\lambda(\phi\phi^* - \eta^2)^2 \tag{3.1}$$

where,  $\phi$  is the complex scalar field,  $\lambda$  and  $\eta$  are positive constants. This potential is shown in fig 3.1. It is called a Mexican hat potential. The Mexican hat potential has a circular vacuum manifold. It can give rise to a string like solution. This Lagrangian is invariant under the global transformation. So we will get a global string from this model.

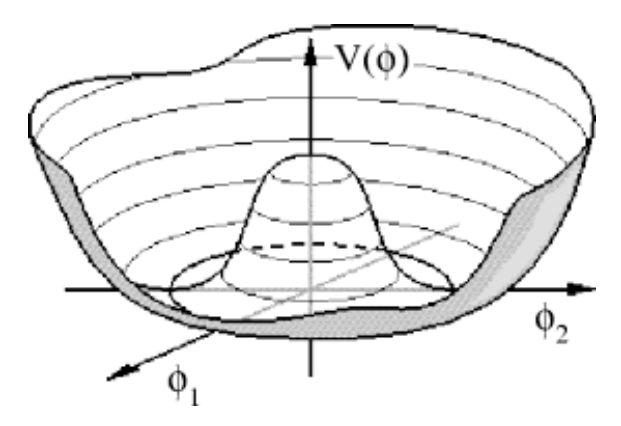


FIGURE 3.1: Defect generated from Mexican hat potential. (Ref.[52])

To understand the local string we have to consider a gauge field. So we can analyze the Abelian Higgs model. The Lagrangian for the Abelian Higgs model has been discussed in the previous chapter.

$$\mathcal{L} = \frac{1}{2} (\partial_{\mu} \varphi)^{2} - \frac{1}{2} \lambda \eta^{2} \varphi^{2} + e^{2} \eta^{2} A_{\mu} A^{\mu} - \frac{1}{4} F_{\mu\nu} F^{\mu\nu} + \mathcal{L}_{int}$$
 (3.2)

It is invariant under U(1) local symmetry transformation. Due to the breaking of this local gauge symmetry two masses will arise,  $M_H = \sqrt{\lambda} \eta$  due to the scalar field and  $M_W = \sqrt{2}e\eta$  due to the vector field. Nielson and Oleson [33] got a vortex line solution from the Abelian Higgs Model. This solution is a local string. We can determine the mass per unit length of the string, which is given by

$$\mu_s \approx 2\pi \eta^2 ln(\frac{M_H}{M_W}) \approx \pi \eta^2 ln(\frac{\lambda}{2e^2})$$
 (3.3)

Here,  $\eta$  is the symmetry breaking scale. Approximate mass per unit length of GUT scale cosmic strings is about  $10^{16}$  tons/cm.

Now if we consider the gravitational property of a cosmic string. We find that the space time of a cosmic string is conical in nature. This conical structure has shown in the fig 3.2. This string property is one of the reasons inhomogeneities are generated by the cosmic strings. The cosmic string metric can be obtained based on two basic assumptions. Cosmic string is an one dimensional line like defect. So the thickness of the string is small and can be assumed as zero. Secondly the gravitational field of the string is weak. Depending on these two assumption we can write the metric for cosmic string along the z-axis as follows [53, 54],

$$ds^{2} = dt^{2} - dz^{2} - d\rho^{2} - (1 - 4G\mu)^{2} \rho^{2} d\phi^{2}$$
(3.4)

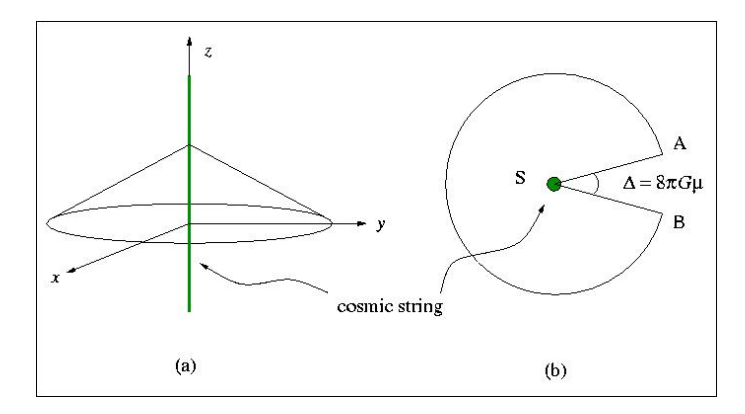


FIGURE 3.2: Deficit angle in cosmic string space time. (Credit-Smoot Group)

If we compare this equation with the normal cylindrical metric, we can see this  $\phi$  coordinate is different. We redefine the  $\phi$  co-ordinate in the above equation by replacing

the following,

$$\phi' = (1 - 4G\mu)\phi\tag{3.5}$$

The above equation will look like,

$$ds^{2} = dt^{2} - dz^{2} - d\rho^{2} - \rho^{2} d\phi'^{2}$$
(3.6)

In normal cylindrical coordinate  $\phi$  varies from 0 to  $2\pi$ , but here  $\phi'$  co-ordinate is varying from 0 to  $(1 - 4G\mu)2\pi$ . So there is a deficiency in the azimuthal angle. This deficit portion is called the deficit angle,  $\Delta = 8\pi G\mu$ . So space time geometry of a cosmic string will be a cone. So if two particle moving in parallel lines pass through the cosmic string space time, they will meet after some time. This has been shown in the fig 3.3.

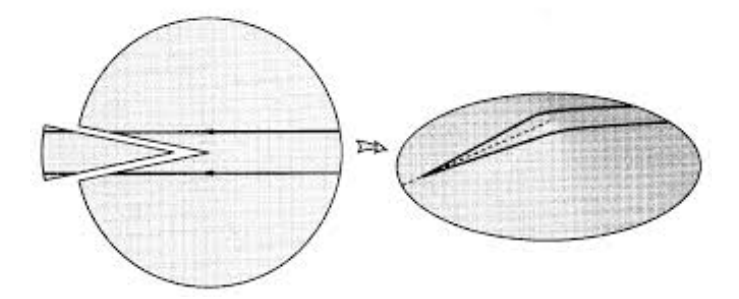


FIGURE 3.3: Motion of two particle moving in parallel line in cosmic string space time. (Ref.[52])

So if a cosmic string is moving in the plasma, due to this conical space time, a wake like structure can form behind the moving cosmic string. In the next section we will discuss about the cosmic string wakes.

#### 3.2.2 Wake formation

Cosmic strings are not stationary in the plasma, they always move with an high velocity. The velocity of a cosmic string is near about the speed of light [55]. Moving cosmic strings generates wake behind them. The geometry of space time is locally flat but globally conical around a cosmic string. If a string moves through a plasma due to the conical geometry of its space time, it will give a velocity perturbation to the nearby matter. As the matter moves toward the region behind the cosmic string from both sides the matter density will increase at that region and it will form some sort of two-dimensional structure. This is called a cosmic string wake.

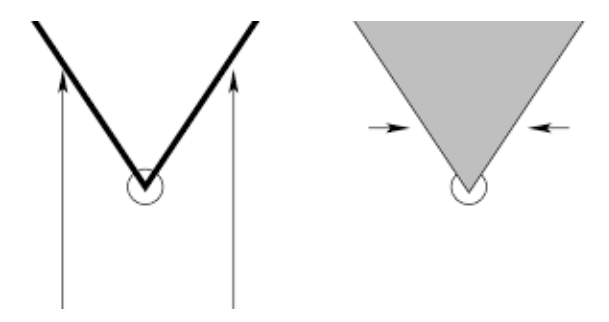


FIGURE 3.4: Cosmic string wake

The formation of cosmic string wake has been studied both analytically as well as numerically. Planar wake formation have been studied with both hot and cold dark matter. Since cosmic string wakes were one of the important candidates for structure formation, therefore, clustering of the baryons in the cosmic string wakes has also been studied. As mentioned before, cosmic string wakes arise due to the conical nature of space time around a cosmic string. A cosmic string has a deficit angle given by  $\delta\theta = 8\pi G\mu$ , where  $\mu$  is the mass per unit length of the string. If a string is moving with a velocity  $v_s$  in a particular direction in a plane, the particles moving along that plane will get a velocity perturbation  $\Delta v$  due to the deficit angle of the string. As the string moves forward, an observer behind the string would see matter streaming past it. Apart from the velocity of the particles, the particles also feel a velocity kick towards the center of the plane behind the string. The magnitude of the kick is given by  $\delta v \approx \delta \theta v_s \gamma_s$  where  $v_s$  is the velocity of the string and  $\gamma_s$  is the relativistic factor. As more and more particles are kicked towards the string, an overdensity or wake is generated behind the string. A detailed description of wake formation is given in ref. [56, 57]. So overdensities are generated in the cosmic string wake. These overdensities have several consequences in the early universe. In the next section we will discuss about the baryon inhomogeneities in the early universe.

#### 3.3 Generation and evolution of baryon inhomogeneities

Baryon overdensities may be formed at the time of the quark-hadron transition in the early universe. Initially, they were formed during the first order phase transition. The first-order phase transition occurs with the nucleation of hadronic bubbles. As these bubbles come together and coalesce, the baryon number is concentrated in small areas between the bubble walls. This is because the baryon number prefers to be in the quark phase rather than the hadronic phase. Details of the formation of such baryon inhomogeneities can be obtained from ref.[45, 58, 59] and references therein. Consequently lattice QCD results showed that the quark hadron phase transition may not be a first

order phase transition. However, there are several situations that may occur in the early universe where the QCD phase transition is still a first order phase transition [60]. In such cases baryon inhomogeneities will form in the early universe. Baryon overdensities can also be generated during the electroweak phase transition [1]. There are other ways to generate such overdensities before the quark hadron transition. The baryon overdensity can be generated by collapsing Z(3) domain walls [2] in the electroweak scale.

The generation of baryon overdensities by moving Z(3) domain walls has been discussed by Layek et. al [2]. The profile of the overdensity is measured by n(R) which is the baryon density left behind at a distance R from the center of the collapsing Z(3) domain wall. This n(R) can be about 1000 times the background density for an area of radius 10m. They had explicitly calculated the transmission coefficients of the up, down and strange quarks through the domain wall. It has been found that the number density of strange quarks is larger by an order of magnitude for the same size of the overdensity. So for R < 1, n(R) for up and down quarks is about 20,000 while it is  $6 \times 10^5$  for strange quarks. Even if the parameters of the model are varied to generate lower overdensities, it has been found for the same radius, if n(R) for up and down quarks is about 400, for strange quarks it is 5000. Therefore these overdensities generated by the Z(3) domain walls are dominated by strange quarks. Some of these overdensities may satisfy the conditions to form stable quark nuggets. However, since there are stringent conditions that need to be satisfied to form a stable object, most of these overdensities will subsequently hadronize when the phase transition temperature is reached.

There are other thermodynamical models that model the hadronization of quarks into hadrons [61]. A detailed review of this hadronization process can be found in [62]. There are two phases here, one phase consists of the up, down and strange quarks while the other phase has the hadrons, which are composites of these three quarks. Since the universe is in thermal equilibrium, we can define the grand canonical partition function for the composite particles. The composite particles are the hadrons. The grand canonical partition function depends on the temperature and the chemical potential of the particles. As the phase transition from the QGP phase to the hadronic phase takes about  $10\mu s$ , at the end of the phase transition chemical equilibrium is firmly established. This allows us to associate the number density of the particles formed after the phase transition from the initial number density of the quarks. This has been discussed in detail in ref. [62]. They have shown that how the chemical potential of the quarks evolves after the hadronization, in the absence of inhomogeneities as well as the hadrons and mesons. According to them the number density of the protons, neutrons, kaons and lambdas are of the order of  $10^{35}$  particles/cm<sup>3</sup> around 100 MeV. The kaons and hyperons, formed after the phase transition, will however be unstable and decay to pions and muons. It has been shown in ref [62] that at around 10 MeV their number densities decrease to about  $10^{20}$  particles/ $cm^3$ . Now we will see how the presence of the baryon inhomogeneities generated by the collapsing domain walls can affect these numbers.

The collapsing domain walls generate inhomogeneities where the number density of strange quarks is 10 times greater than the magnitude of the number density of the up and down quarks. This means that  $n_s \approx 10n_d$ . Now as mentioned in ref.[62], the chemical potential of hadrons is equal to the sum of the chemical potentials of their constituent quarks in equilibrium. However, the universe will still have to maintain the various constraints such as charge neutrality, constant entropy to baryon ratio etc. So after the hadronization, one will see a change in the number densities of the hadrons formed. The number density of the particles is given by the following equation,

$$n_i = \frac{g_i}{2\pi^2} \int_{m_i}^{\infty} dE E \sqrt{E^2 - m_i^2} \times \left( \frac{1}{e^{(E_i - \mu_i)/T} \pm 1} - \frac{1}{e^{(E_i + \mu_i)/T} \pm 1} \right)$$
(3.7)

However, it has been argued [63] that at temperatures close to the QCD phase transition the net number densities can be approximated to

$$n_i = \frac{1}{6}g_i T^2 \mu_i + O(\mu_i^3) \tag{3.8}$$

for fermions. Here, i represents particles present in the plasma at that time.

The hadrons, formed after the phase transition, are the protons, the neutrons, the mesons and the hyperons. Since the number density of strange quarks in the plasma are higher than the other quarks, a larger number of hyperons and kaons will be obtained in the region of the inhomogeneities.

Some of the particles like the  $\Sigma$  particle, which have a very short lifetime  $((7.4\pm0.7)\times10^{-20}~{\rm secs})$  will decay instantaneously after the formation. Since the hadronization occurs around 200MeV, the typical timescales are much longer. At the QCD phase transition, the Hubble time is of the order of  $10^{-5}~{\rm secs}$  [64]. One important thing is that due to the background gas of photons and leptons, the timescale of the hadronic decay processes may not be the same as in vacuum [62]. As the mass of the lambda particle is closest to the protons and neutrons, it has a longer lifetime  $(2.60\times10^{-10}~{\rm s})$ . The lambda particles, after decay, will produce neutrons or protons and pions. The cascade particles will also decay into neutrons or protons and pions in two steps. They have a lifetime of  $(2.90\times10^{-10}{\rm s})$ .

Next we look at the mesons present after the hadronization, these are the pions and the kaons. They have lifetimes of the order of  $10^{-8}$  secs. The other mesons have significantly smaller lifetimes  $10^{-17} - 10^{-23}$  secs. The kaons decay into pions and muons as well as

muon neutrinos. Fromerth et. al. [62] has shown that at least till 10 MeV a large number of pions and muons remain in the plasma. So even in the absence of inhomogeneities, a significant number density of muons (about  $10^{38}$  particles/ $cm^3$ ) already existed in the plasma. In the presence of the inhomogeneities, due to the decay of the excess hyperons and kaons, number density of the pion and the muon in the plasma will increase in the overdense regions. Hence after the completion of the quark hadron phase transition, these overdense regions will have a higher muon concentration than the background plasma.

So baryon inhomogeneities can be generated through different process in different temperature scales. As there are inhomogeneities in the plasma in some places there will a baryon overdensity and in some places the baryon number will be less. So there will be diffusion in the plasma. As neutrons diffuse out of the inhomogeneity faster than the protons, so in these regions the neutron proton ratio will be different from the background. The ratio of neutrons to protons is very important for the outcome of the primordial nucleosynthesis. Neutron proton ratio in some place will change depending on how these particles are diffusing. The amount of Helium produced in the plasma depends on the amount of neutrons present as most of the neutrons contributes to the formation of the helium. Due to the weak interaction, the neutron and the proton will be in equilibrium. Hence if the neutron to proton ratio in the plasma is affected, it affects the abundance of the light elements. But for all these effects to happen the inhomogeneities have to survive up to the temperature of 1 MeV because nucleosynthesis will start at that temperature. Baryon inhomogeneities that survive up to the nucleosynthesis epoch will definitely affect the nucleosynthesis calculation. Hence, models generating these inhomogeneities can be constrained using the results from the nucleosynthesis. Generally inhomogeneities generated in the electroweak scale do not survive up to nucleosynthesis. So they do not affect the light element abundance. But inhomogeneities generated in the QCD scale if they have an amplitude larger than 10<sup>8</sup> will survive and affect the nucleosynthesis calculation. [65]

As mentioned before these baryon inhomogeneities will decay through diffusion. So, in the next two chapter we will have discussed in details about decay of these baryon inhomogeneities in case of a stationary universe and in case of an expanding universe. Our detailed calculations will provide constraints of the size and amplitude of inhomogeneities which survive up to the nucleosynthesis epoch.

#### Chapter 4

# Decay of hadronic inhomogeneities in an non-expanding universe

#### 4.1 Baryon inhomogeneities

As mentioned in chapter 3, baryon inhomogeneities can be generated during the quark hadron phase transition in the early universe. The phase transition itself changes the plasma from the quark gluon phase to the hadronic phase and takes place at 200 MeV. So basically the inhomogeneities are generated at 200 MeV and start decaying after that. The next crucial step in the evolution of the universe is the nucleosynthesis of the light elements, which takes place at 1 MeV. So our interest is to study the evolution of the baryonic inhomogeneities in this time period i.e between 200 MeV to 1 MeV. As we have discussed in chapter 2, it is quite possible that the quark hadron transition is a first order phase transition. It has been shown in the literature that during a first order quark hadron transition, quarks trapped in regions between the hadronic bubble walls gives rise to baryonic inhomogeneities after the phase transition [45, 58, 59]. It was also shown in some of these studies that these inhomogeneities will affect the nucleosynthesis calculations [59]. This lead to various scenarios of inhomogeneous Big Bang Nucleosynthesis. So the formation and evolution of baryonic inhomogeneities are very important for the nucleosynthesis calculations.

The phase diagram of QCD based on the lattice calculations however seemed to indicate that the quark hadron phase transition in the early universe is not a first order phase transition. Since a second order phase transition does not have a coexistence phase where both the phases co-exist, it is not possible to generate baryon inhomogeneities in

a second order phase transition. So it seemed that baryon inhomogeneities could not have formed during the QCD phase transition. Then Layek et. al [2] came up with a method of generating baryon inhomogeneities irrespective of the order of the phase transition. In their method, the baryon inhomogeneities were generated by collapsing Z(3) domain walls. This meant that it was not necessary to have a first order phase transition to generate baryon inhomogeneities. So even though recently there has been some studies which imply that a first order phase transition may still occur during the quark hadron epoch [60, 66, 67], it is no longer a necessary criteria for the study of baryon inhomogeneities. It is also possible to generate dense inhomogeneities like metastable quark nuggets, [68–71] and metastable H dibaryons if the strange quark is also taken into account. However, in this chapter, we will only focus on the baryon over densities in the hadronic plasma.

The two most stable hadrons are the neutron and the proton. So the baryon number is carried by these particles in the hadronic plasma. Since there are regions of the plasma which have a higher baryon number density, the baryon number starts to diffuse through the plasma so that an equilibrium situation may be obtained. The diffusion occurs from the over dense regions to the under dense regions of the plasma. This diffusion of the neutron and the proton has been studied previously in the literature [17, 18, 72]. Other than the neutron and the proton, the other particles which are abundant at those temperature are the electrons, the muons and their respective neutrinos. In the previous studies, the muon was never taken into account since it's number was always less than the neutrons and protons. Other hadrons even if they are formed would be unstable and decay over a short period of time. As we have mentioned before a new mechanism to generate baryon overdensities was proposed by Layek et. al. this was followed by other studies of collapsing Z(3) domain walls by Atreya et. al. [73, 74]. These studies showed that the quarks did not pass uniformly through the Z(3) domain walls. This further meant that there would be some regions in the plasma where the number density of strange quarks would be greater than the number density of the up and down quarks. The collapsing domain walls would then lead to the generation of a large number of hadrons which have a strange quark. These are mostly the lambda hyperons, the kaons etc. But these particles are unstable and would decay within a very short time. The final decay products of these unstable particles are the muons and the pions as well as the neutrinos. The pions again decay to give muons. Kaons also decay into muons. Dense quark nuggets formed during the QCD phase transition evaporate by decaying into kaons. These kaons further decay to give more muons. Thus for all these scenarios, the muon number density in the plasma is quite high and cannot be neglected. We therefore decided to look at the decay of baryonic inhomogeneities in the presence of the muons.

Since the neutrons and the protons are diffusing through the plasma, we have to use the diffusion equation to study the evolution of the baryon number density. This would mean obtaining the diffusion coefficient for the given plasma particles. The diffusion coefficient has to be obtained in the presence of the neutrons, the protons, the muons and the electrons. That the muon contribution cannot be neglected was shown in a recent work [75] where the authors found that the inclusion of the muons increased the bulk viscosity of the plasma. The viscosity is increased by a 100 million times. This means that the contribution of the muon particles in the hadronic plasma cannot be neglected. A similar conclusion can also be reached for the pions, studies have shown that the pion contribution to the plasma affects the total entropy of the universe [76]. Pions, however are unstable and decay into muons. Therefore, we only include the contribution of the muons when calculating the diffusion coefficients of the plasma particles.

In this chapter, we proceed to calculate the nucleon diffusion coefficients (which are necessary for the diffusion equation) in the presence of the muons. We refer to both the neutron and the proton as the nucleon, since the two particles are in equilibrium with respect to weak interactions at temperatures up to 1 MeV. The particles keep changing continuously into each other and are generally indistinguishable. Later, below 1 MeV, the weak interactions fall out of equilibrium and the neutron and proton are no longer indistinguishable. Since the protons are charged they interact with both the neutrons and the electrons. The interaction with the electrons is the Coulomb interaction. The neutron being an uncharged particle does not interact with the electrons in the plasma. This is also because the neutrons are far more heavier than the electrons. Now that we are interested in the muons in the plasma, we have to obtain the scattering cross section of the muon with the proton, the neutron and the electron. That will enable us to do a proper study of the decay of the baryonic inhomogeneities in the hadronic plasma.

Another consequence of the decay of unstable particles is the production of a large number of muon neutrinos. This changes the chemical potential of the muon neutrino. Neutrino degeneracy and its effect on nucleosynthesis has been already studied before [77]. Constraints on antimatter domains and other baryon inhomogeneities are also obtained from nucleosynthesis calculations [78, 79]. We review some of these calculations for the baryon inhomogeneous case dominated by strange quarks. As mentioned earlier, such inhomogeneities would form from the collapse of Z(3) domains around the time of the quark hadron transition. Although it is difficult to derive strict constraints from the results of nucleosynthesis due to the fact that it is a combination of all three neutrino degeneracies, some limitations may still be placed on degenerate muon neutrinos. We use one of the available nucleosynthesis codes based on Wagoner-Kawano code [80] and modified by S. Dodelson [81] to search for constraints coming from nucleosynthesis. The nucleosynthesis code makes it possible to modify the parameters of neutrino degeneracy

and obtain an abundance of primordial elements. There have been previous studies on the effect of neutrino degeneracies on nucleosynthesis [77]. There are a very wide range of baryon to photon ratios. We restrict ourselves to the current value of the baryon to photon ratio and obtain the primordial abundances for different values of the chemical potential for muon neutrinos ( $\xi_{\mu}$ ) and electronic neutrinos ( $\xi_{e}$ ).

In the next section we will briefly discuss the baryon overdensities and deduce the diffusion coefficient of the nucleon through the plasma including the neutrons, the protons, the electrons and the muons.

#### 4.2 Diffusion Coefficients of nucleons

We have already discussed the generation of baryon inhomogeneities in the previous chapter. Here we will discuss about the diffusion from those inhomogeneities. The nucleon diffusion coefficient has been studied extensively in many references [17, 18]. These references have discussed the diffusion coefficients at the time when the weak interaction is out of equilibrium, i.e for temperatures below 1 MeV. However, overdensities are formed around the temperature scale 200 - 100 MeV. Therefore, nucleon diffusion from the overdense regions begins at about the same time. In this temperature scale weak interactions are in equilibrium. So at these temperatures we cannot distinguish between protons and neutrons. However, to attain the equilibrium in the baryon number distribution hadronic particles would still try to move out of the overdense regions. So we need to analyze the diffusion to understand how these overdense regions will decay. Neutrons and protons collide with electrons and decay into each other. Other hadrons, such as hyperons and kaons, will decay to give lots of pions and muons. Finally, the plasma is composed of protons, neutrons, electrons, muons and their respective neutrinos. We need to determine the nucleon diffusion coefficient at this temperature. Therefore, we have to calculate the scattering cross-section for the nucleon-electrons and nucleon-muons interaction.

In a gaseous system if a heavier particle diffuses through a plasma of lighter particles, the diffusion coefficient of a heavier particle is given by the Einstein's equation D = b T. Here, b is the mobility of the heavier particle and T is its temperature. For a Maxwellian distribution of particles, the expression of the mobility is given by,

$$b^{-1} = \frac{16\pi}{T} \int \frac{p^2 dp}{3h} v p^2 \sigma_t e^{-E/T}$$
 (4.1)

Here  $\sigma_t$  is the scattering cross-section, and v is the velocity of the particles.

As we have considered many particles in the plasma, here we are dealing with multiparticle diffusion. Multi-particle diffusion depends on the concentration of the particles that we have considered in our plasma. The effective diffusion coefficient for multiparticle diffusion is given by [82],

$$\frac{(1-x_i)}{D_i} = \sum_{i \neq j} \frac{x_j}{D_{ij}}$$
 (4.2)

Here i and j denote different particles of the plasma.  $D_i$  denotes the diffusion coefficient of the  $i^{th}$  particle and  $D_{ij}$  denotes the diffusion coefficient of the  $i^{th}$  particle in the presence of the  $j^{th}$  particle. As we are not considering the self interaction, to avoid self interaction we have taken  $i \neq j$ . If N is the total particle density, and  $n_i$  is the number density of the  $i^{th}$  particle, then  $x_i = \frac{n_i}{N}$ 

Now we will calculate the scattering cross-sections of the interactions to get the diffusion coefficients for each interactions. The nucleon - electron cross section is dominated by form factors. The neutron - electron and the proton - electron scattering cross-sections are not the same because neutron is a neutral particle but proton is the positively charged particle. So we have to calculate the neutron - electron and the proton - electron scattering cross-sections separately.

Now, let us consider the neutron-electron scattering. The amplitude of the electron vertex is  $-ie\gamma^{\nu}(q^2)$  and the neutron vertex is  $ie\Gamma_{\mu}(q^2)$ , where

$$\Gamma_{\mu}(q^2) = \gamma_{\mu} F_1(q^2) + \frac{i\kappa}{2M} F_2(q^2) \sigma_{\mu\nu} q^{\nu}$$
 (4.3)

Here M is the neutron mass,  $q^{\nu}$  is the transferred four-momentum,  $F_1(q^2)$  and  $F_2(q^2)$  are Dirac and Pauli form factor.  $\gamma_{\mu}$  is the Dirac gamma matrices.

$$\sigma_{\mu\nu} = \frac{1}{2}i[\gamma_{\mu}, \gamma_{\nu}] \tag{4.4}$$

At the energies we consider the form factors can be evaluated at  $q^2 \approx 0$ . For neutron  $F_1 = 0$  and  $F_2 = 1$ . Our neutron vertex will be

$$\Gamma_{\mu}(q^2) = \frac{i\kappa}{2M} \sigma_{\mu\nu} q^{\nu} \tag{4.5}$$

The invariant scattering matrix will be

$$m = [\bar{u}(k')(\gamma^{\nu})u(k)](-\frac{e^2}{q^2})[\bar{u}(p')(\Gamma_{\mu})u(p)]$$
(4.6)

The scattering amplitude will be given by

$$|m|^{2} = \frac{1}{4} \frac{e^{4}}{q^{4}} Tr[(k' + m)\gamma^{\mu}(k + m)\gamma^{\nu}] Tr[(p' + m)\Gamma_{\mu}(P + m)\Gamma_{\nu}]$$
(4.7)

As mentioned before we are looking at the mobility of a heavy particle passing through a gas of light particles. Here, the neutron is the heavier particle and we assume that it is moving through a electron-positron gas. The scattering cross section of the neutron is then given by,

$$\frac{d\sigma}{d\Omega} = \frac{\alpha^2 \kappa^2 q^2}{16M^2 E^2 sin^4(\theta/2)} \frac{E'}{E} \times \left[ 1 + sin^2(\theta/2) \right] = \frac{\alpha^2 \kappa^2}{4M^2} [1 + cosec^2(\theta/2)]$$
(4.8)

Here E is the electron energy before the scattering and E' is the electron energy after scattering and  $\theta$  is the scattering angle. The transport cross section  $\sigma_t$ , is defined by

$$\sigma_t = \int \frac{d\sigma}{d\Omega} (1 - \cos\theta) d\Omega \tag{4.9}$$

Substituting the scattering cross-section we get,

$$\sigma_t = 3\pi \left[ \frac{\alpha \kappa}{M} \right]^2 \tag{4.10}$$

Substituting the expression for the transport cross-section in the definition of the diffusion coefficient, we finally obtain,

$$D_{ne} = \frac{M^2}{32m^3} \frac{1}{\alpha \kappa^2} \frac{e^{1/T}}{Tf(T)}.$$
 (4.11)

M, here is the neutron mass, m is the electron mass,  $\kappa = -1.91$  is the anomalous magnetic moment and the temperature is dimensionless as it is scaled by a factor of  $m_e c^2$ . We also have  $f(T) = 1 + 3T + 3T^2$ .

Similar to the nucleon- electron cross-section, we can also obtain the nucleon-muon scattering cross-section. The amplitude of the muon vertex is similar to the electron vertex. It is given by  $-ie\gamma^{\nu}(q^2)$ . Though the muon is heavier than the electron, it is still lighter than the neutron. Hence we can still consider its mass to be much smaller than the neutron mass. The heavier neutron will not move very fast compared to the lighter particles, therefore we can consider  $q^2 \approx 0$ . The form factors will then be  $F_1 = 0$ 

and  $F_2 = 1$ . The neutron vertex is given by  $\Gamma_{\mu}(q^2) = \frac{i\kappa}{2M} \sigma_{\mu\nu} q^{\nu}$ . The differential cross-section will then be,

$$\frac{d\sigma}{d\Omega} = \frac{\alpha^2 \kappa^2 q^2}{8M^2 E^2 sin^4(\theta/2)} \frac{1}{1 + 2E sin^2(\theta/2)/M} \times \left[ \frac{cos^2(\theta/2)}{1 - q^2/4M^2} \left( \frac{q^2}{4M^2} - 1 \right) - 2sin^2(\theta/2) \right]$$
(4.12)

We assume that the muon energy and mass are less than the neutron mass. This simplifies the cross-section and we can get an approximate cross-section given by,

$$\frac{d\sigma}{d\Omega} \approx K \frac{\alpha^2 \kappa^2}{4M^2} [1 + \csc^2(\theta/2)] \tag{4.13}$$

Here all the constant values are put together and substituted by a single constant  $K = \frac{1}{2}$ . We have also assumed that the heavy neutron particle is moving through a muonantimuon gas. The mobility of the neutron is given by the force on the neutron due to the medium. This force is given by the interaction cross section. Substituting in the definition of the diffusion constant, the diffusion coefficient of the neutron through the muon-antimuon gas is given by,

$$D_{n\mu} = \frac{M^2}{32m_{\mu}^3} \frac{1}{\alpha \kappa^2} \frac{e^{1/T'}}{T'f(T')} \tag{4.14}$$

Here  $T' = \frac{T}{m_{\mu}c^2}$ . Now that we have both  $D_{ne}$  and  $D_{n\mu}$ , we can get the total diffusion coefficient for the neutron moving through the plasma of electrons, muons and their anti-particles. From equation 4.2, we see that it depends on the concentration of the particles in the plasma.

We now proceed to find the diffusion coefficient of the proton moving through the electron positron gas. For proton-electron scattering, we have to take into consideration the Coulomb force. So the scattering cross section is given by,

$$\frac{d\sigma}{d\Omega} = \frac{\alpha^2 m_e^2}{4k^4 sin^4(\theta/2)} \left[ 1 + \frac{k^2}{m_e^2} cos^2(\theta/2) \right]$$
 (4.15)

The transport cross section is then given by,

$$\sigma_t = 4\pi\alpha^2 \left[ \frac{E_e h}{2\pi k^2} \right]^2 \ln(\frac{2}{\theta_0}) \tag{4.16}$$

where  $\theta_0$  is the minimum scattering angle. On substitution, we get the diffusion coefficient as,

$$D_{pe} = \frac{3\pi}{8\alpha^2 ln(\frac{2}{\theta_h})} \left[ \frac{h}{2\pi m_e} \right] \frac{Te^{1/T}}{f(T)}.$$
(4.17)

Similar to the proton electron cross section, we can calculate the proton muon cross section too. The differential cross section is given by,

$$\frac{d\sigma}{d\Omega} = \frac{\alpha^2}{4E^2 sin^4(\theta/2)} \frac{1}{1 + 2E sin^2(\theta/2)/M} \times \left[ \left( 1 - \frac{\kappa^2 q^2}{4M^2} \right) cos^2(\theta/2) - \frac{q^2}{2M^2} (1 + \kappa)^2 sin^2(\theta/2) \right] \quad (4.18)$$

We are interested in the temperature dependence of the diffusion coefficient. There is no simple analytical expression for the diffusion coefficient. However, we can still get the coefficient value numerically by substituting the constants and calculate the final diffusion coefficient by following the same steps as before. After getting the transport cross-section we use it to calculate the diffusion coefficient. The values of the numerically obtained diffusion coefficients are given in the next section. We have not considered here the collision of neutrons and protons, because at high temperatures (above 100 MeV) neutrons and protons are kept in thermal equilibrium with each other by weak interactions. This equilibrium will be maintained as long as the duration of weak interactions is short compared to the time of cosmic expansion. Therefore, we do not think of neutrons and protons as two independent particles colliding.

Immediately after the hadronization of the quarks, the number density of the electrons and the muons can be obtained at thermal equilibrium. We see from ref.[63] that the number densities of leptons after hadronization is given for different values of the lepton asymmetry. We have got that the number density of electrons and muon are of the same order. For electrons and muons both number density is around  $\frac{n_i}{s} \approx (4 \times 10^5) MeV^{-1}$  in the temperature scale 200 MeV - 100 MeV. The number density starts to vary around 150 MeV. If there were no inhomogeneities present then the muon number density is equal to the electron number density. Due to the presence of the inhomogeneities, the number densities can change. Here we make an estimate in the change of the number density and then proceed to study how the diffusion coefficient changes depending on the change in the concentration of the electrons and the muons.

### 4.3 Diffusion Coefficients after the Quark-Hadron phase transition

We are looking at the diffusion coefficients at temperatures greater than 100 MeV. The quark hadron phase transition occurs around 200 MeV. The inhomogeneities are formed after the phase transition. As mentioned before, inhomogeneities with a large number of strange quarks will hadronize to give a large number of hyperons immediately after

the phase transition. These hyperons have a short lifetime and decay into pions and muons. The pions too subsequently decay into muons. So the number density of muons would be high around these temperatures.

In ref.[62], the authors have calculated the number of particles per  $cm^3$  after hadronization in the absence of inhomogeneities. There we find that the number density of the electrons at 100 MeV is of the order of  $10^{35}$  particles per  $cm^3$  and the muon number density is only slightly less than that. In their calculation, they have considered  $\mu_s = \mu_d$ , however in the presence of the inhomogeneities due to Z(3) domain walls we have  $n_s \approx 10n_d$ . This translates to a higher number of hyperons and kaons. These will decay to nucleons, electrons and the muons.

Since the plasma has the nucleons, electrons and the muons, we are using the multiparticle diffusion coefficient mentioned previously. As  $x_i$  is the fractional number density, we have the constraint that  $\sum_{i} x_{i} = 1$ . If all the particles are distributed evenly in the plasma then  $x_i = 0.25$ . However that is not so, hence we now need to find out what should be the values of  $x_n, x_p, x_e, x_\mu$  in the inhomogeneities. Generally at these temperatures, the leptons dominate the energy density and the neutrons and protons constantly change into one another so  $x_n = x_p$  and  $x_n + x_p < x_e + x_\mu$ . The excess of strange quarks in the inhomogeneities implies that the number density of hyperons and kaons have increased. Now as has been mentioned before, the hyperons decay into nucleons and pions. A typical decay mode of a hyperon would be  $\Lambda^0 - > p^+ + \pi^-$  or  $\Lambda^0 - > n^0 + \pi^0$ . The pions decay into muons ( $\pi^- - > \mu^- + \nu_\mu$ ). So the strange quarks would increase the number density of nucleons as well as pions and muons. The decay of the kaon may lead to two possibilities. The kaons can decay into muon/antimuon and muon neutrino or electron/positron and electron neutrino. Now as per the branching ratio of these reactions, the probability of kaons decaying into muon/antimuon and muon neutrino is far greater than the probability of kaons decaying into electron/positron and electron neutrino. According to the particle data group the branching ratio of the former is 64 % while it is only 5% for the latter. Thus it is clear that the inhomogeneities will give rise to an excess muon number density. For the case of the kaons decaying to muon/antimuon and muon neutrino we use the values  $x_n = x_p = 0.2$ ,  $x_\mu = 0.4$  and  $x_e = 0.2$ . This case is referred to in the graphs as  $x_e < x_\mu$ . We have not considered the case of  $x_e > x_\mu$  since the current data suggests that it is highly improbable. The case  $x_e \approx x_\mu$  is the absence of any inhomogeneity.

We start by calculating the diffusion coefficients of the neutrons and the protons in a plasma that has a high density of muons. The number densities of the electrons and the muons are kept the same. This is done so that we can focus on the presence of the muons in the plasma. The fig. 4.1 shows the plot of the total  $D_n$  vs temperature while

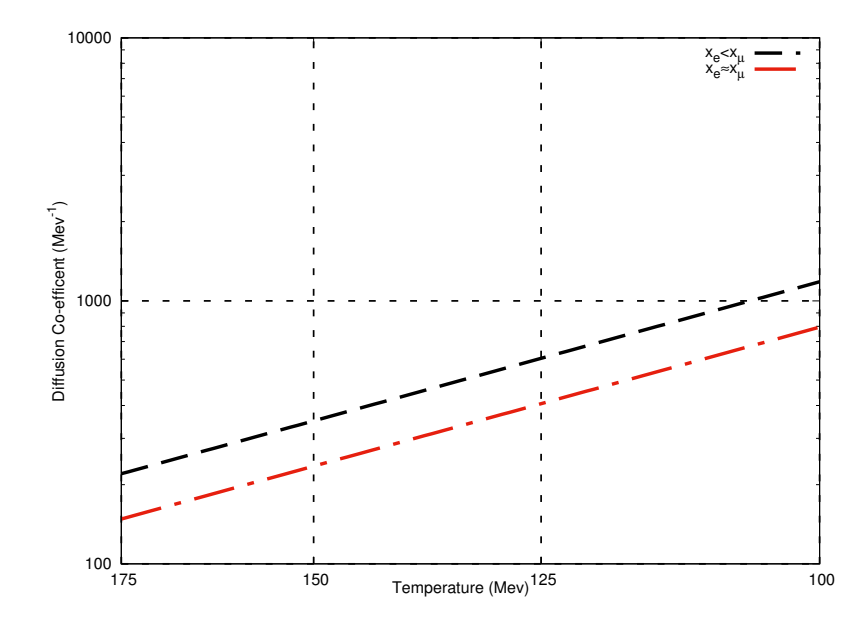


FIGURE 4.1: Diffusion coefficient of neutrons in the electron, neutron and muon plasma. The (black) dashed line denotes  $x_e < x_{\mu}$  and the (red) dot- dashed line denotes  $x_e \approx x_{\mu}$ .

fig 4.2 has the plot of the  $D_p$  vs temperature. The two lines denoting the two cases are as follows, the (black) dashed line denotes case (1) ( $x_e < x_\mu$ ) and the (red) dot-dashed line denotes case (2). Now, if the particle densities depend solely on temperature (i,e in the absence of any inhomogeneities) then between 175 MeV and 100 MeV the electron particle density will be close but higher than the muon particle density [75]. As the temperature decreases, the diffusion coefficients increase. The presence of the inhomogeneities however increases the number density of the muons. As the number density of muons increase, we notice that the diffusion coefficient is increasing more. Thus the presence of muons changes the diffusion coefficient of the neutron considerably. This will definitely affect the decay of hadronic inhomogeneities at temperatures above 100 MeV.

While we have calculated the number densities of the particles based on the standard decay paths and branching ratios, there is always the possibility that non-standard decays can occur and the nucleon density may be greater in the baryon inhomogeneity then in the background plasma. This can occur if a large number of hyperons decay via  $\Lambda^0 - > n^0 + \pi^0$ . The  $\pi^0$  will decay into photons and we will have a neutron excess in the plasma. This means that the neutron density need not be fixed with respect to the muon density. We have checked what happens if the neutron density are more but we see no significant differences.

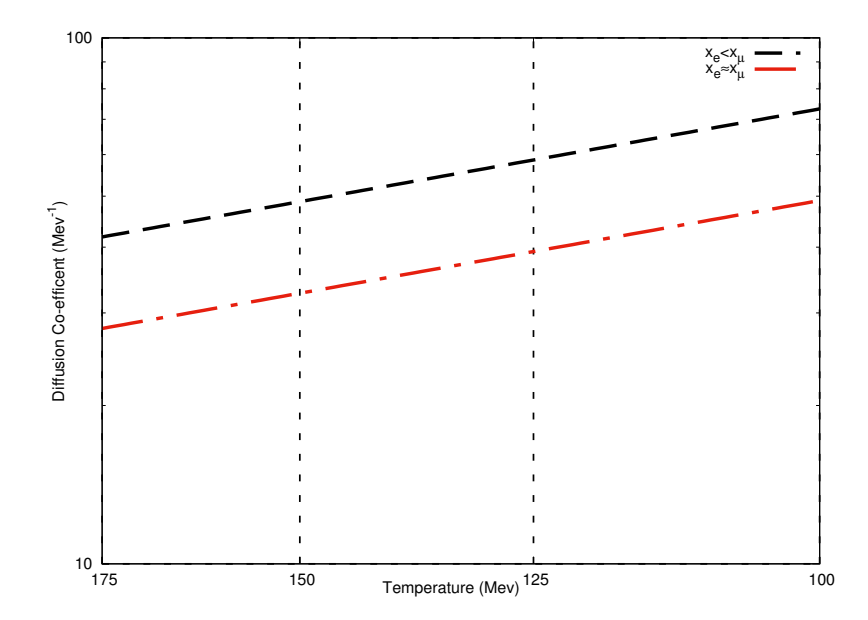


FIGURE 4.2: Diffusion coefficient of protons in the electron, neutron and muon plasma. The (black) dashed line denotes  $x_e < x_{\mu}$  and the (red) dot- dashed line denotes  $x_e \approx x_{\mu}$ .

From all the figures we can conclude that the diffusion coefficient starts to increase as the muon density is increased. Thus these graphs show that the presence of the muons changes the diffusion coefficient of the neutron/proton through the plasma. The diffusion coefficient being increased, the nucleons move faster through the plasma. So a baryon over dense region will diffuse at a faster rate if the muon number density is higher. However, this only happens when temperatures are quite high. As the temperature cools to 1 MeV, the number density of muons go down. During this period, the contribution to the diffusion coefficient from the muons becomes negligible. Fig. 4.3 gives the diffusion coefficient at temperatures less than 1 MeV. As seen from fig. 4.3, the presence of the muons does not really change the diffusion coefficient around 1 MeV. We have thus established that the diffusion coefficient of the neutrons and protons change significantly due to the presence of the muons in the plasma in the overdense regions immediately after the quark hadron transition. We would now like to see what effect these new diffusion coefficients would have on the diffusion of hadronic inhomogeneities formed around the time of the quark hadron phase transition.

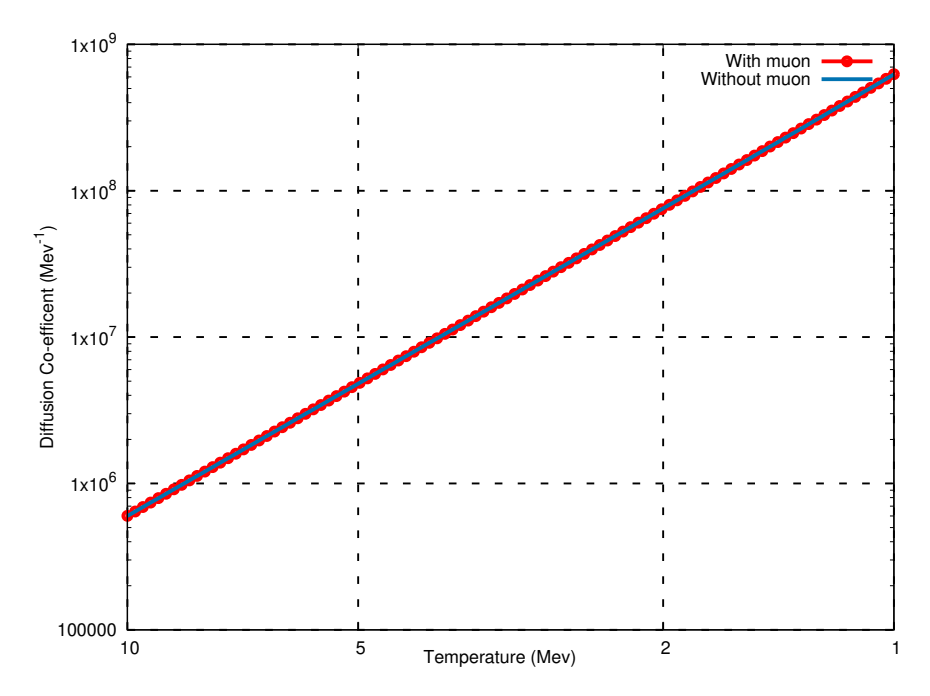


FIGURE 4.3: Diffusion coefficient of neutrons in the electron, neutron, proton, and neutrino plasma at temperatures below 10 MeV. The (red) dotted line denotes the presence of muons in the plasma. The (blue) solid line denotes the plasma without the presence of muons.

#### 4.4 Decay of inhomogeneities

We now look at the decay of baryon inhomogeneities in the plasma around those temperatures. Baryon inhomogeneities generated at the quark hadron phase transition should be at least of the scale of 0.4 m (at 200 MeV) to affect nucleosynthesis [83] calculations. So the overdensities that may affect the nucleosynthesis results will be greater than 0.5 m. The horizon scale in the QCD epoch is of the order of a few kilometers. So an inhomogeneity with a lengthscale of 0.5 m does not span the whole of the universe. This means that for the over density the universe is practically stationary. Thus we will neglect the expansion of the universe when considering the diffusion equation for these overdensities.

We treat the inhomogeneity as a Gaussian function whose peak value at the initial time  $t_0$ , is given by  $10^{15} MeV^3$ . The average number density of the background plasma is of the order of  $10^7 MeV^3$  and baryon overdensities can be as large as  $10^8$  times the background density [2]. In general, the diffusion equation is given by,

$$\frac{D(t)}{a^2} \frac{\partial^2 n(x,t)}{\partial x^2} = \frac{\partial n(x,t)}{\partial t}$$
 (4.19)

where D(t) is the diffusion coefficient which is dependent on the temperature and therefore the time in the early universe. Here  $a^2$  is the scale factor of the expanding universe.

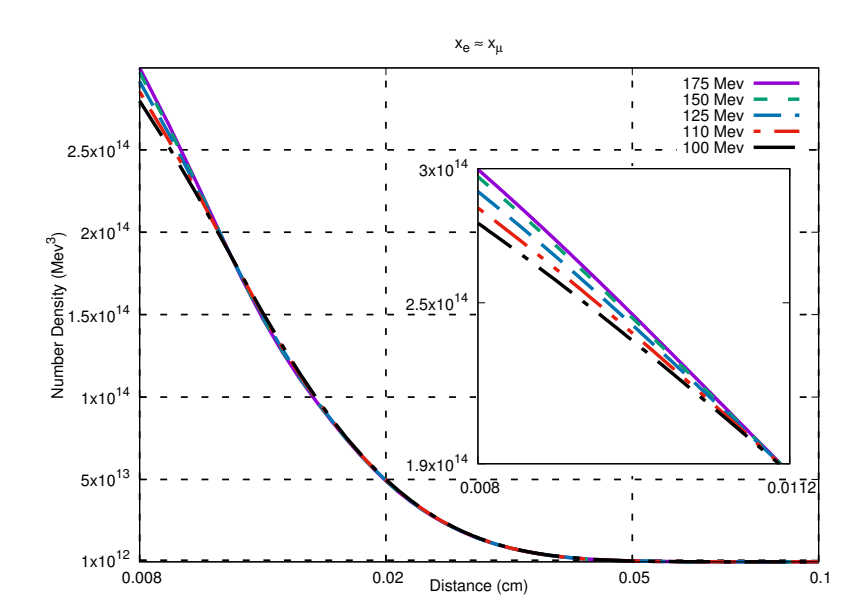


FIGURE 4.4: The decay of the inhomogeneity in a plasma with equal number of electrons and muons.

Since the diffusion coefficient is time dependent, we solve the time dependent diffusion equation numerically to see the evolution of the inhomogeneities with time. We use a finite difference method to obtain the numerical solution of the diffusion equation for the different diffusion coefficients obtained previously. Since our diffusion coefficients are expressed in terms of temperature, we use the standard time temperature expression to obtain the diffusion equation in terms of temperature. Therefore, now our number density depends on space and temperature n(x,T). We consider the inhomogeneity at T = 175 MeV, we then evolve the inhomogeneity with a given diffusion coefficient.

We assume for the time being that the ratio of the fractional number densities of the different particles are more or less constant through out the time of evolution of the diffusion equation. That way the diffusion coefficient is only dependent on temperature. Initially the number density decreases slowly. As time increases (temperature decreases), the peak of the inhomogeneity goes down and it spreads out in space. We initially show how an overdensity decays in a plasma which has equal numbers of electrons and muons in fig. 4.4, in fig. 4.5 we have plotted the decay of the overdensity in a muon rich plasma.

From the two plots, it is clear that the muon rich inhomogeneities decay faster. The difference in the decay increases as the temperature cools down. The initial profile is taken to be the same at a temperature of 175 MeV. The final profile of the inhomogeneity

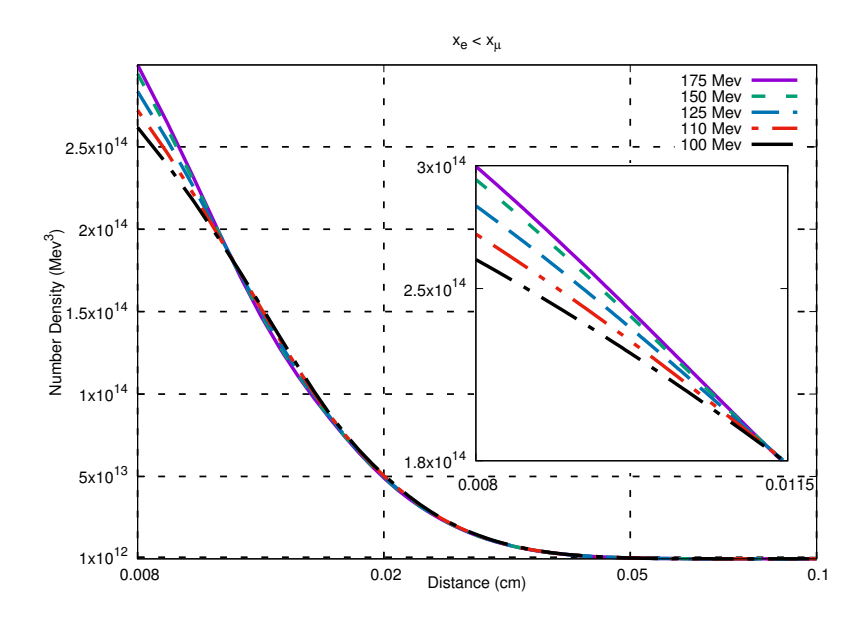


FIGURE 4.5: The decay of the baryon inhomogeneity in a muon rich plasma.

for the muon rich plasma is close to  $2.5 \times 10^{14} MeV^3$ . In the case when the electron and muon densities are the same the overdensity is close to about  $2.75 \times 10^{14} MeV^3$ . The initial size of the inhomogeneity was the same in both cases, so it indicates that the hadronic inhomogeneity decays faster, in the presence of a large muon density. This leads us to conclude that over densities which have a larger number of strange quarks will decay away faster after hadronization. Thus they will have little or no impact on the Big Bang Nucleosynthesis calculations.

#### 4.5 Neutrino degeneracy parameters

Collapsing Z(3) domain walls will form inhomogeneities in the early universe and these inhomogeneities will have a large number of strange quarks. After hadronization these quarks will produce lots of unstable hyperons. These hyperons will decay through weak interaction and will generate mesons and neutrinos. Since most of them decay through the production of pions, pions continue to decay into muons and muon neutrinos, so there will be a large number of muon neutrinos in the plasma.

The three standard model neutrinos oscillate among themselves and have the same chemical potential at a particular temperature. So in the nucleosynthesis calculations the three neutrinos are usually given the same chemical degeneracy parameter. However, it has also been shown previously, that if the lepton number densities are different for the electron neutrino and the muon and tau neutrino, then the abundances of primordial elements are affected [77]. Therefore if Z(3) domain walls collapse and form inhomogeneities during the quark hadron phase transition, we can expect a larger number density of muon neutrinos compared to electron neutrinos. In nucleosynthesis calculations, the net lepton number is defined for each of the neutrinos. This is a dimensionless number defined by,

$$L_i = \frac{n_{\nu_i} - n_{\bar{\nu_i}}}{n_{\gamma}} \tag{4.20}$$

This is related to the neutrino degeneracy parameters,  $\xi_i = \frac{\mu_{\nu_i}}{T_{\nu}}$  by the equation [84],

$$L_{\nu_i} \approx \frac{\pi^2}{12\zeta(3)} \left(\frac{T_{\nu}}{T_{\gamma}}\right)^3 (\xi_i + \frac{\xi_i^3}{2\pi^2}).$$
 (4.21)

During this time, the photon are slightly heated with respect to the neutrinos.  $T_{\nu}$  is the temperature of the neutrinos and  $T_{\gamma}$  is the temperature of the background photons. The integral can be simplified and solved in terms of the Riemann Zeta function of order three ( $\zeta(3)$ ). This is what determines the energy density of the neutrinos during nucleosynthesis.

We have used a standard code for the nucleosynthesis calculations. The core of the computational routines is based on Wagoner's code [80] but the code itself has been modified by Scott Dodelson [81]. The code allows us to change the neutrino degeneracies at the beginning of the calculation. The neutrino degeneracies depend on the chemical potential of the neutrinos as well as the baryon to photon ratios. The current bound on the baryon to photon ratio is quite stringent. Hence we just adhere to only one value of the baryon to photon ratio and vary only the chemical potential of the neutrinos. The chemical potentials depend on the number density and an order of magnitude estimate can be obtained from eqn. 3.8 considering only the first term on the right hand side. The temperature is taken as a constant and the degrees of freedom are the same for all the neutrinos.

Neutrino degeneracies have been studied previously and some bounds on the degeneracy values have already been obtained [77]. The neutrino degeneracy affects the helium and the lithium abundances more than the other abundances so we just look at the primordial helium and lithium abundances. In fig. 4.6, we show the abundances for  $\xi_e = \xi_\mu$  in bold while we have  $\xi_e < \xi_\mu$  as the dashed line. We have considered  $\eta = 3.4 \times 10^{-10}$ . There are two pairs of values we have considered. One of them is  $\xi_e = 0.2$  and  $\xi_\mu = 2.0$ , while the other is  $\xi_e = 0.4$  and  $\xi_\mu = 4.0$ . Our motivation for using these values are the constraints derived previously in ref.[85]. Accordingly, the neutrino degeneracy parameters have to be in the ranges  $-0.06 \le \xi_e \le 1.1$  and  $|\xi_\mu| \le 6.9$  to satisfy the CMB constraints. Our

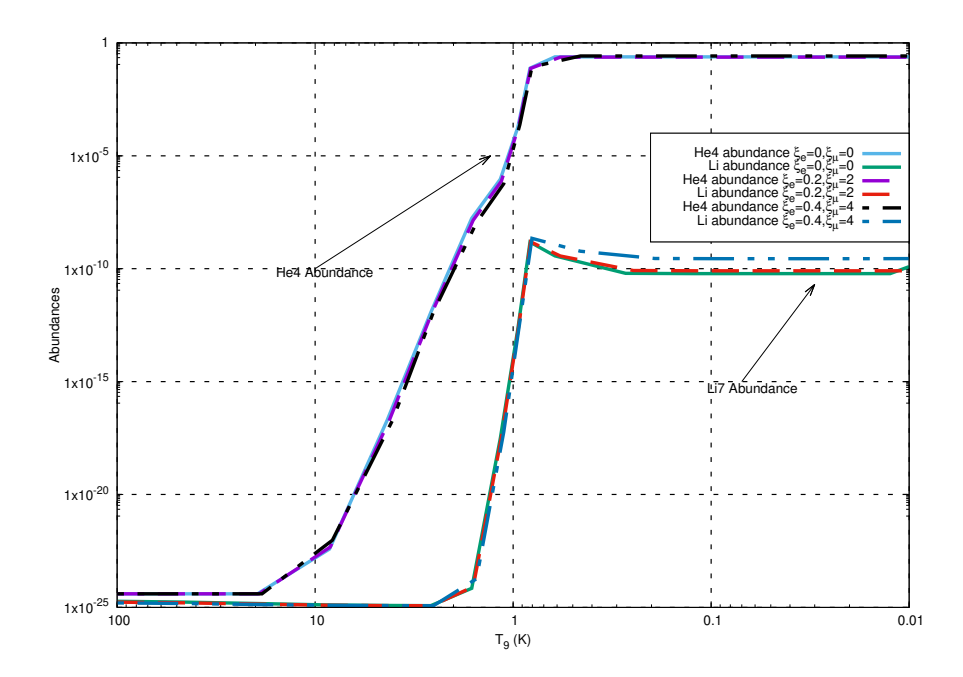


Figure 4.6: Comparison of abundances in the presence and absence of inhomogeneities for muon degeneracy greater than the electron degeneracy.

 $\xi_e, \xi_\mu$  are in these ranges and the number density of the muon neutrino is about ten times that of the electron neutrino. As mentioned before, we cannot specify the decay branches of the hyperons and kaons exactly hence we tried to see what could be the maximum possible effect. Since the number density of s quarks is at least 10 times that of the u and d quarks hence we have calculated  $\xi_\mu$  and  $\xi_e$  by using eq.3.7. This gives us the maximum possible bound. We have also tried other combinations within these parameters but none of them showed any improvement in the final results.

Our results show that there are some small changes in the abundances of helium. The changes are not too significant to put constraints on the inhomogeneities. However, the lithium abundance is enhanced if we go to higher values of the degeneracies. Here, we have kept the muon neutrino degeneracy to be higher than the electron neutrino degeneracy at all times. Since the inhomogeneities in our model tend to decay into pions and muons, the muon neutrino degeneracy will definitely be higher than the electron neutrino degeneracy. This means that the lithium abundance will be higher than the current calculated value. As is well known, the observed lithium abundance is less than the calculated value, hence we can conclude that large inhomogeneities with a pre dominance of strange quarks will be constrained by the lithium abundance.

Apart from the inhomogeneities from the collapsing Z(3) domains, there can be charged inhomogeneities too. Charged inhomogeneities can be formed if the plasma has a small charge imbalance during the quark hadron transition [86]. So we also look at the case

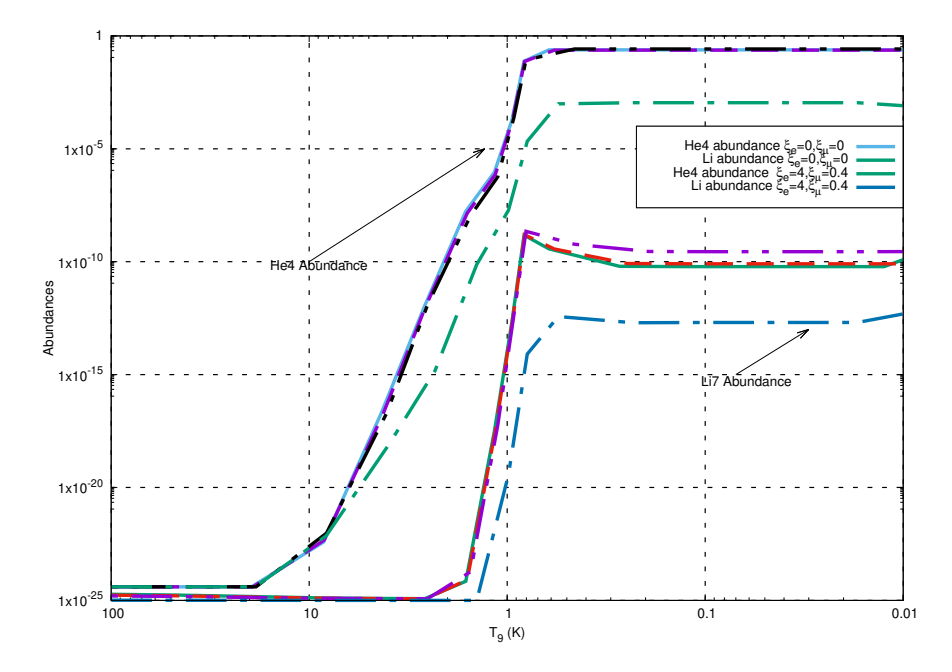


FIGURE 4.7: Plot of the abundances in the presence and absence of inhomogeneities for electron neutrino degeneracy greater than the muon neutrino degeneracy included.

where the electron neutrino degeneracy is greater than the muon neutrino degeneracy. This can happen if there are charged inhomogeneities in the plasma. The plot is given in fig. 4.7. Here however we see that both the helium abundance and the lithium abundance is reduced. Not only that, the large electron neutrino density also affects the neutron to proton transformation rates. Thus the beginning of the lithium production is also delayed.

Here, we notice that when the two parameters  $\xi_{\mu}$  and  $\xi_{e}$  are varied there is variation in the abundances of lithium and helium. When  $\xi_{\mu} > \xi_{e}$ , the two abundances are enhanced while if  $\xi_{\mu} < \xi_{e}$  the abundances are decreased. Since the decay of the inhomogeneities results in the variation of the degeneracy parameters, a detailed simulation would give us further insight in understanding the quark hadron phase transition.

#### 4.6 Summary

In summary, we have shown that baryonic inhomogeneities which have a larger number of muons decay faster compared to inhomogeneities that exist in a muon underdense region. In most cases, in the temperature ranges that we are considering, in the absence of inhomogeneities, the plasma has a higher electron density compared to the muon density. In the presence of inhomogeneities, the number density of muons are increased depending on how the inhomogeneity is generated. It is quite possible that the muon

density would be higher than the electron density in some of the inhomogeneities which are formed by the collapse of Z(3) domain walls. Such a scenario had never been studied before in the literature. Our first result concerns the diffusion coefficient of the neutron and the proton in a muon rich plasma. We find that there are significant variations to the numerical value of the diffusion coefficient that we obtain for the muon rich plasma. This significant change will result in the faster decay of inhomogeneities above 100 MeV. It is well known that an inhomogeneity decaying in a plasma with equal numbers of electrons and muons, has to be of the order of 0.4 m to survive till the nucleosynthesis epoch. But in a muon rich plasma, the size of the inhomogeneity has to be at least 5% bigger to survive to the nucleosynthesis epoch. So any mechanism that segregates the strange quarks more than the up and down quark must generate very large inhomogeneities to have any effect on the nucleosynthesis calculations. Inhomogeneities which have a predominance of strange quarks thus decay faster than inhomogeneities which have the different quarks in a more or less equal proportions.

## Chapter 5

# Decay of baryon inhomogeneities in an expanding universe

### 5.1 Introduction

The electroweak phase transition as well as the quark hadron transition generates baryon inhomogeneities [1, 58, 59, 87–89]. Usually in the electroweak scale most of the inhomogeneities are generated by topological defects [90–99]. Baryonic inhomogeneities in the early universe, are usually constrained by the nucleosynthesis calculations. Though they do have other consequences, we are interested in inhomogeneities that survive till the nucleosynthesis epoch. Inhomogeneities which are generated in the electroweak epoch affect the quark-hadron phase transformation [100] but will probably not survive till the nucleosynthesis epoch. The only study of the decay of these inhomogeneities was done by Jedamzik et.al.[16] and they concluded that the inhomogeneities decay very little due to the neutrino inflation in the quark gluon plasma. The study of Jedamzik et.al did not include the presence of all the other particles in the plasma. There have been quite a few studies of the decay of these overdensities in the hadronic plasma. However, as discussed in the previous chapter not all particles were taken into account for these studies. In this thesis, we want to do a complete study of the decay of these inhomogeneities in an expanding universe using the diffusion equation.

Previously as mentioned in the last chapter, the diffusion equation has already been studied for the case of baryon diffusion in a proton-neutron plasma [101–103]. In this chapter, we will discuss the diffusion of baryon number carried by the quarks. This has not been studied in the literature before. Since we develop a FORTRAN code for solving the diffusion equation in an expanding universe, we also use it to redo the study of diffusion in an expanding hadronic plasma. This is an extension of the diffusion in

the hadronic plasma studied in the previous chapter [103]. The expansion term in the diffusion equation is found to make a significant difference in the final results.

The inhomogeneities generated in the electroweak epoch and the inhomogeneities generated in the QCD epoch are different in scale and size. We have previously discussed the generation of these inhomogeneities in the previous chapters. The universe size is smaller in the electroweak epoch and so the size of the inhomogeneities are also smaller. For the QCD epoch, the universe size is larger and therefore the sizes of the inhomogeneities are also larger. Apart from this, the amplitude of the overdensities are greater in the QCD epoch than in the electroweak epoch [45]. The particle content of the plasma is also very different in the two epochs. The plasma in the electroweak epoch consists of the quarks, the muons, the electrons and the neutrinos, while the plasma in the QCD epoch consists of the neutrons, protons, muons and the three flavors of neutrinos. Due to all these differences, we consider the cases of the electroweak epoch and the hadronic epoch separately.

Since it is non trivial to solve the diffusion equation in an expanding universe, we make some basic assumptions to simplify our problems. First and foremost, we look only at sub horizon scale fluctuations. The second important assumption is about the size of the fluctuations. The size should be larger than the mean free path of all the particles in the plasma. Our third assumption is that all the baryon number violating processes are neglected. Such processes can only occur around 200 GeV so this assumption will not affect the diffusion in the hadronic phase. We also assume that the baryon density fluctuation is a Gaussian. The Gaussian distribution function is the most general distribution function. Generally, the diffusion equation is solved in the Minkowski metric, but here we have solved it in the Friedmann-Lemaître-Robertson-Walker (FLRW) metric. To obtain the sizes and amplitudes of the Gaussian distribution, we refer to the literature on the generation of the inhomogeneities in the electroweak epoch and the QCD epoch. For the Gaussian distribution in the electroweak epoch we use the size and amplitude from reference [1]. The scale is taken as  $10^{-3}$  cm and the amplitude is taken as  $10^4$  over the background baryon density. In the QCD epoch, the scale is about one meter and the amplitude is between  $10^{12} - 10^{13}$ . Before going into the details of the simulation, we would like to discuss the diffusion equation in an expanding universe.

### 5.2 The diffusion equation in the FLRW metric

The FLRW metric for the flat universe is defined by,

$$ds^2 = c^2 dt^2 - a^2(t) d\vec{r}^2 (5.1)$$

Here a(t) is the scale factor of the expanding universe and  $\vec{r}$  is the spatial coordinate. This is the comoving distance in an expanding universe. We consider a region of the universe with an inhomogeneity given by  $n(\vec{r},t)$ . As time evolves, the particles in the over dense region tend to move towards the lesser dense region to restore equilibrium and a particle flux is generated. In this case, we consider the diffusion to be isotropic. The local observer then sees the particle flux as,

$$j_k = -D(t)\frac{\partial}{\partial x^k} n(\vec{r}, t)$$
(5.2)

The diffusion coefficient D(t) depends on the scattering cross section and the velocity of the particles. Since there are different kinds of particles in this plasma, we are dealing with multi-particle diffusion here. The conservation of current gives us,

$$\frac{\partial}{\partial x^{\mu}}(\sqrt{g}j^{\mu}) = 0 \tag{5.3}$$

Here  $\sqrt{g} = a^3(t)$  and using the definition of the Hubble parameter as  $H(t) = \frac{\dot{a}(t)}{a(t)}$ , the diffusion equation can be written as,

$$\frac{\partial}{\partial t}n(\vec{r},t) + 3H(t)n(\vec{r},t) - \frac{D(t)}{a^2}\nabla^2 n(\vec{r},t) = 0$$
 (5.4)

So we have obtained the diffusion equation for the FLRW metric. There is no exact solution to this equation. Also, the diffusion coefficient in the equation is time dependent. An exact form of the diffusion coefficient is also not available. Hence we need to solve this equation numerically. The diffusion coefficient depends on the scattering cross section of the particles present in the plasma. The scattering cross sections of relativistic particles depend on temperature. Since the temperature of an equilibrium universe is related to the time we can change the variable in the diffusion equation to temperature. This would give us the numerical solution at a given temperature instead of a given time. In the early universe, time is related to the temperature by,

$$t = \frac{(0.95 \times 10^{10})^2}{T^2} \tag{5.5}$$

Here t is in secs and T is in Kelvin. Now our independent variable is temperature instead of time and we will solve the diffusion equation in terms of temperature ranging from 200 GeV - 200 MeV. Before we proceed to solve the diffusion equation, we must however obtain the diffusion coefficients of the different particles in the plasma.

### 5.3 Diffusion in the electroweak scale

For the inhomogeneities in the electroweak epoch, the relevant temperature scale is 200 GeV. The particles in the plasma at this temperature scale are the quarks, the electrons, the muons and the neutrinos. Since the baryon number is carried by the quarks, we need to study the diffusion of quarks through the electrons, the muons and the neutrinos. The baryon over densities therefore translate to over densities in the quark number in this epoch. We have to treat the individual interactions separately, since the masses of the particles vary considerably. The diffusion of a massive particle through a gas of lighter particles has to be analysed differently compared to the diffusion of a lighter particle moving through a plasma of heavier particles. The detailed scenarios are discussed in the textbook by Lifshitz [104]. Here we do not go into the derivation of the diffusion coefficient from the transport equations of the individual particles. We obtain the equations directly from the textbook that we have referred to. The derivation of the coefficient D is straightforward and hence we do not reproduce them here again.

The quarks are lighter than the muon and hence we will have the diffusion coefficient of the quarks moving through the muon as,

$$D = \frac{1}{3N} \left\langle \frac{v}{\sigma_t} \right\rangle = \left(\frac{T}{\pi m}\right)^{1/2} \frac{2^{3/2}}{3\sigma_t} \tag{5.6}$$

Unlike the previous case, the quarks are heavier than the electrons so we find out the mobility of the particle in a background fluid which is lighter than the particles moving through it. This is done by choosing an appropriate distribution function. The distribution of the particles is assumed to be Maxwellian. This means that the mobility of the particle is given by,

$$b^{-1} = \frac{16\pi}{T} \int \frac{p^2 dp}{3h} v p^2 \sigma_t e^{-E/T} = \frac{16\sigma_t m^2 t^2}{3\pi^2}.$$
 (5.7)

Here  $\sigma_t$  is the scattering cross-section, m is the mass of the particle. We consider the velocity of the particle to be  $\vec{v}$ . So the mobility b can be related to the external force  $(\vec{f})$  by,  $\vec{v} = b\vec{f}$  and the diffusion coefficient is given by,

$$D = bT (5.8)$$

Therefore, to obtain the value of the diffusion coefficients, we first need to calculate the scattering cross sections. As there is no general expression for obtaining the scattering cross section of the multiple particles present in the plasma, we calculate the scattering cross section between any two individual particles separately in the next few subsections.

We then substitute these in the expression for the diffusion coefficient D and solve the diffusion equations numerically. We emphasize once more that our independent variable here is the temperature and not the time.

#### 5.3.1 Quark-electron scattering

We start with the motion of quarks through the electron gas. For this we need to find the scattering cross section for the  $e^-e^+ \longrightarrow q\bar{q}$  interaction. The differential cross section is given by,

$$\frac{d\sigma}{d\Omega} = \frac{Q_f^2 \alpha^2}{2s} \left( \frac{u^2 + t^2}{s^2} \right) \tag{5.9}$$

Here  $\alpha \sim 10^{-2}$  is the fine structure constant and  $Q_f$  is the momentum transfer in this interaction. The variables u, t and s are the Mandelstam variables. This gives,

$$\sigma_t = \frac{Q_f^2 \alpha^2}{2s} \int \left(\frac{u^2 + t^2}{s^2}\right) (1 - \cos\theta) d\Omega$$
 (5.10)

The total scattering cross section can be obtained after integrating over the solid angle. The numerical value can be obtained once the energy scale of the colliding particles is known. Since we are working around the electroweak scale, the colliding energy of the particles are also in the GeV range. The mobility factor is thus given by,

$$b^{-1} = \frac{2\sigma_t m^2}{3\pi^2} \left[8T^2 (1 - e^{-E/T}) - 2E(2E + 4T)e^{-E/T}\right]$$
 (5.11)

As mentioned before, we obtain the mobility at different temperatures. This mobility is then substituted in the expression for the diffusion coefficient. All this is incorporated in the numerical simulation code that we have used for this study.

### 5.3.2 Quark-neutrino scattering

One of the numerous particles in this epoch are the neutrinos. Both neutrinos and quarks come with different flavors. However, neutrinos are not electrically charged particles, so the only interaction they have with the quarks is the weak interactions. Different flavours of neutrinos interact differently with the different kinds of quarks. This would result in a multitude of cross sections. On studying these cross sections, we noticed that they have very similar order of magnitudes. So we consider the quark neutrino scattering cross section as,

$$\sigma_t = \frac{G_F^2 \hat{s}}{\pi} \tag{5.12}$$

Here  $G_F$  is the Fermi constant given by,  $G_F = 1.166 \times 10^{-5} GeV^{-2}$ . Numerically, the cross section turns out to be  $\sigma_t = 17.2 \times 10^{-42} cm^2 \times \frac{E_{\nu}}{GeV}$  [105]. Though we are working at very high temperatures in the GeV scale, the value of the diffusion coefficient is difficult to handle numerically with this value of  $\sigma_t$ . For the numerical calculation we therefore rescale the variables suitably to obtain a stable numerical solution.

### 5.3.3 Quark-muon scattering

In both the previous cases we had a heavier particle moving through a lighter gas of particles, however the scenario changes considerably when we consider the quarks moving through a gas of muons. For the  $\mu^-\mu^+ \longrightarrow q\bar{q}$ , though the expression for the interaction cross sections are similar to the electrons, but here the quark is the lighter particle which is moving through a heavier gas of particles (the muons). This means that, the diffusion coefficient is given by eqn. 5.6,

$$D = \left(\frac{1}{2\pi}\right)^{\frac{3}{2}} \left(\frac{s^{\frac{1}{2}}}{Q_f \alpha}\right)^2 \left(\frac{1}{mT}\right)^{\frac{1}{2}} \left[2T(1 - e^{-E/T}) - 2Ee^{-E/T}\right]$$
 (5.13)

We have the total cross section given by,

$$\sigma_t = \frac{4\pi Q_f^2 \alpha^2}{3s} \tag{5.14}$$

As can be seen from the expressions we have derived, the numerical values of the diffusion coefficient are very large. The numerical code we use to simulate the decay of the baryon over densities in the early universe cannot handle such large numbers. We tackle this issue by rescaling the energy values. This gives us reasonable values of the diffusion coefficient. This rescaling does not affect our results as we plot the amplitude of the inhomogeneity at different temperature scales. We define the amplitude of the inhomogeneity as the ratio of the enhanced density to the background density  $(\frac{n'_B}{n_B})$ . Here  $n'_B = \Delta n_B + n_B$  and  $n_B$  is the average baryon density at that temperature and  $\Delta n_B$  is the increase in the baryon density in the inhomogeneity. The amplitude is therefore dimensionless and not affected by the rescaling.

# 5.4 Decay of inhomogeneities in the quark gluon plasma phase

For the numerical study, we have used a finite difference method for the second order space derivative and an explicit forward Euler approximation for the first derivative in

time. The Courant-Friedrichs-Loewy coefficient changes with temperature but care is taken so that it never exceeds 0.5 for maintaining the stability of the program. We consider the solution of Eq.5.4 to be spherically symmetric and dependent upon the radius r. This is the length scale of the inhomogeneity. The origin is taken to be at the centre and the particles diffuse out causing the radius of the inhomogeneity to increase. The maximum value of the radial lattice is the horizon size. As we are working in the FLRW metric, the universe size will also increase with decrease in temperature. This feature is incorporated in our program by increasing the maximum size of the radius as time increases and temperature decreases. We have kept the minimum step size fixed at dr = 0.01. Time is represented by temperature and the maximum lattice size is therefore calculated at each temperature before the r loop. The relationship is given by,  $r_{max} = \frac{314.01155}{T}$ . For both the electroweak and the QCD case, we start with a Gaussian fluctuation given by  $f(r) = Ae^{(-\frac{r^2}{2b^2})}$ . The amplitude A and the variance b are different in the two epochs. The amplitudes are different as the generation of baryon inhomogeneities in the two epochs are different and the variance are different as length scales in the two epochs are different.

We now look at baryon inhomogeneities generated during the electroweak phase transition. In ref.[1, 88], it is shown that a strong first order phase transition generates a radially symmetric baryon inhomogeneity whose amplitude depends upon the ratio of the minimum and maximum bubble wall velocity. They have shown that baryon inhomogeneities having amplitudes of the order of  $10^2$  are generated. Though we are not emphasizing that these are the inhomogeneities we are interested in, they do provide a measure of the possible magnitude of baryon inhomogeneities generated at the electroweak scale. So we consider the amplitude of the inhomogeneities generated in the electroweak epoch to be of the order of 10<sup>3</sup>. We are also considering inhomogeneities whose decay will be affected by the expanding universe. The horizon at these temperatures is of the order of 1cm [64]. The size of the inhomogeneities we have considered are always less than the horizon size. However we do not want them to be so small that their lengthscale is negligible in comparison to the radius of the universe. So basically we have looked at inhomogeneities which have a radius of less than a millimeter. We have presented results for inhomogeneities having a radius of 0.03 cm. Larger inhomogeneities (with radius closer to 1 cm) will also decay in a similar way but it is rather difficult to present the graphs in the same plot due to the vast change in the radius. Hence for presenting our results we have chosen the radius of the initial inhomogeneity to be about 0.03 cm. The diffusion coefficients can be obtained numerically, but the problem is that they vary considerably in their numerical values. This indicates that the particle content in the inhomogeneity would ultimately define how they decay. Though there are multi particles present in the plasma, we do not go for multi particle diffusion as it

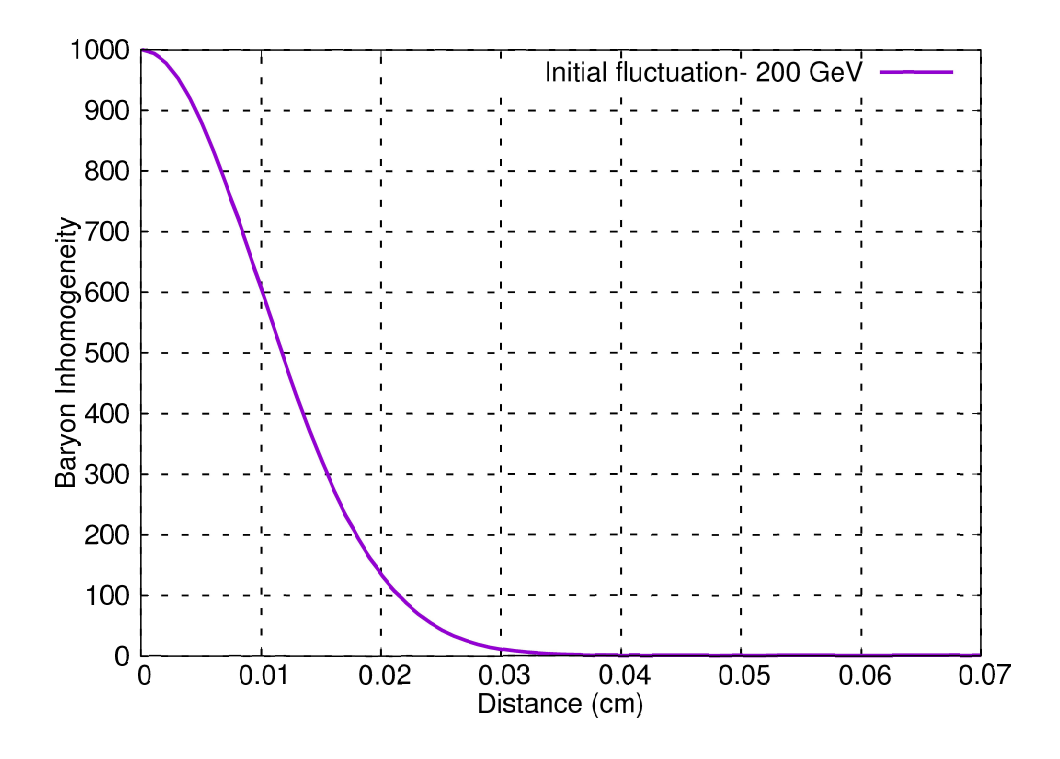


FIGURE 5.1: The initial fluctuation at 200 GeV in the linear scale.

becomes numerically quite challenging. We look at each of these interactions separately and see how much each of them contributes to the decay of the baryon inhomogeneity. We believe this will give us some idea of how the baryon inhomogeneity decays in this temperature range.

There are several challenges in the electroweak epoch. The biggest challenge is the large change in the horizon size between 200 GeV and 200 MeV. At 200 GeV, the horizon is of the order of 1 cm while at 200 MeV the horizon is of the order of 10 kms. We divide this into two parts. We evolve the inhomogeneity from 200 GeV to about 1 GeV and then again from 1 GeV to 200 MeV. Interestingly, we find that the inhomogeneity decays considerably during this period depending on the particle interactions being considered. We find that on the log scale, the amplitude decays quite rapidly irrespective of the interactions considered. This means that low amplitude inhomogeneities will be completely wiped out before the quark hadron phase transition. Let us first look at the decay of the inhomogeneities between 200 GeV and 1 GeV. We give the figure of the initial fluctuation in fig. 5.1. The graph is plotted in the linear scale, however in the rest of the paper, the results are plotted in the log-log scale instead of the linear scale. In the logarithmic scale, the function appears to end abruptly as the zero is not defined on this scale. Since the lattice size of the simulation also changes with temperature, the

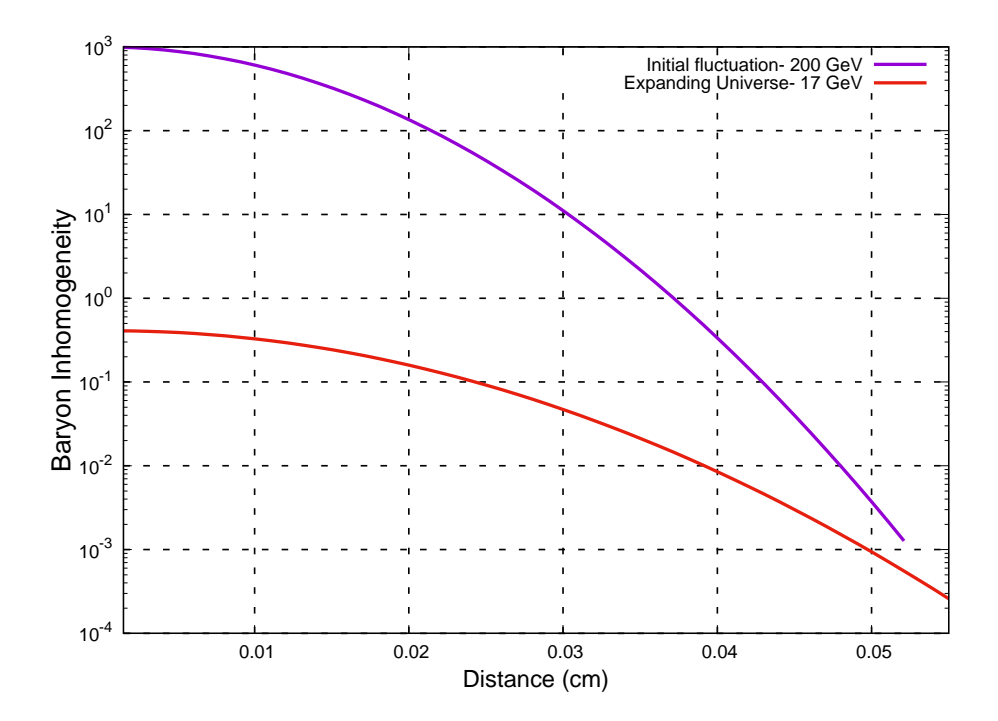


Figure 5.2: The decay of the fluctuation is shown in logscale between 200 GeV - 17 GeV as the quarks moves through a sea of electrons. The fluctuation is smaller at higher temperatures and spreads out further as temperature decreases.

data for the higher temperatures are for a smaller radius (horizon) size, while the data for lower temperatures reflects the larger radius of the horizon. In the graphs, we have focussed on the decrease in the amplitude of the inhomogeneity rather than the increase in it's size. Even with the increase in size, the fluctuations always remain within the horizon.

In the electroweak epoch, the diffusion coefficients differ considerably as they are dependent on the temperature and this is quite a large temperature range. So we look at the decay of the inhomogeneities for different interactions separately. For all the different figures, we have the baryon inhomogeneity  $\binom{n_B'}{n_B}$ , on the y axis and the radial length scale (denoted by distance) on the x- axis. In figure 5.2, we see the decay due to the quarks moving through the electrons. The initial fluctuation is taken at 200 GeV and the final is taken at 17 GeV. As we see the peak of the inhomogeneities goes down by more than three orders of magnitude. The inhomogeneity also spreads out. If we plot the solution up to the maximum radial distance, then for the initial curve we observe an abrupt cut off. The abrupt cut off is an artefact of plotting the solution in the log-log scale. The same plot in the linear scale resembles fig 5.1 but with a reduced peak and larger variance. However, since there is a considerable decrease in the amplitude, it is not possible to show both the graphs in a linear plot. The decay is similar in the

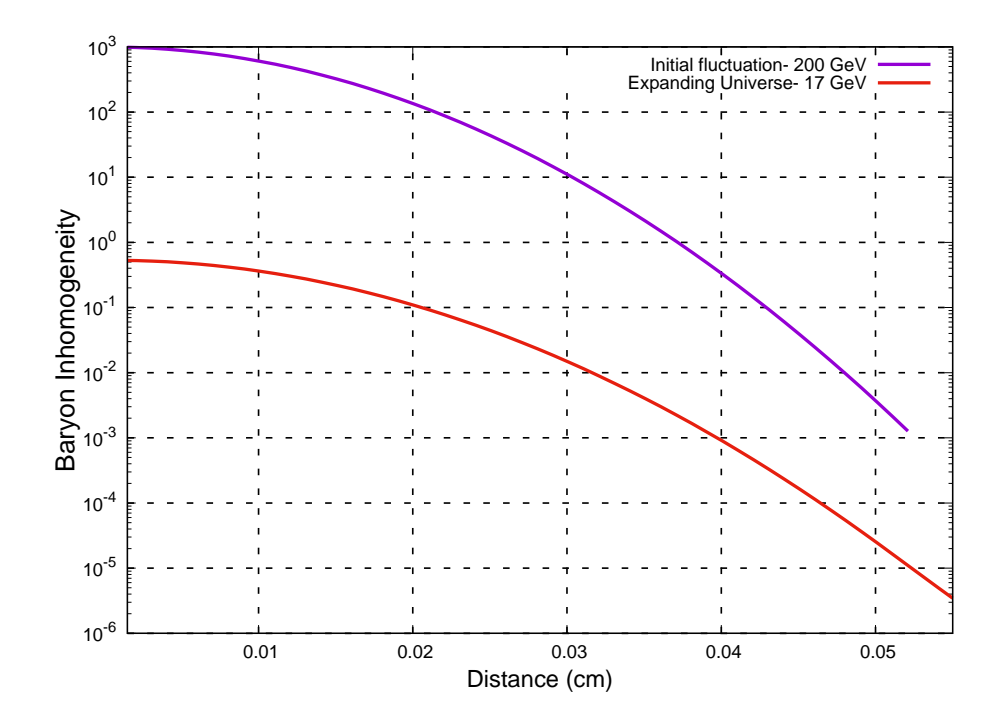


FIGURE 5.3: The decay of the fluctuation is shown in logscale between 200 GeV - 17 GeV as the quarks are predominantly surrounded by neutrinos. The fluctuation is smaller at higher temperatures and spreads out further as temperature decreases.

case when the surrounding particles are muons and neutrinos. We have used a different scaling for the neutrinos but as mentioned before the scaling will not affect the relative decay of the amplitude. Though the final amplitude is lower in the case of the neutrinos, the order of magnitude is similar. Since all the graphs have similar decay in orders of magnitude, we have only shown selected graphs. Fig 5.2, shows the decay due to the motion of the quarks through the electrons while fig 5.3 shows the decay due to the motion of the quarks through the neutrinos. Since the plasma at those high temperatures is predominantly dominated by electrons, our results clearly show that the baryon inhomogeneities decay by about three orders of magnitude in the high temperature GeV range. This is true, even if there are a large number of muons and neutrinos in the plasma.

We now look at the decay of the inhomogeneities between the temperatures 1 GeV to 200 MeV. We find that the order of magnitude decay is again quite large for the three diffusion coefficients. The individual numbers vary but we plot only the order of magnitude estimates as before. In figure 5.4, we find that the inhomogeneity has decreased by three orders of magnitude. In the case of fig. 5.4, the initial fluctuation is at 1 GeV while the final is plotted at 236 MeV. We find that the curve flattens out considerably. The radial distance up to which the inhomogeneity persists is actually

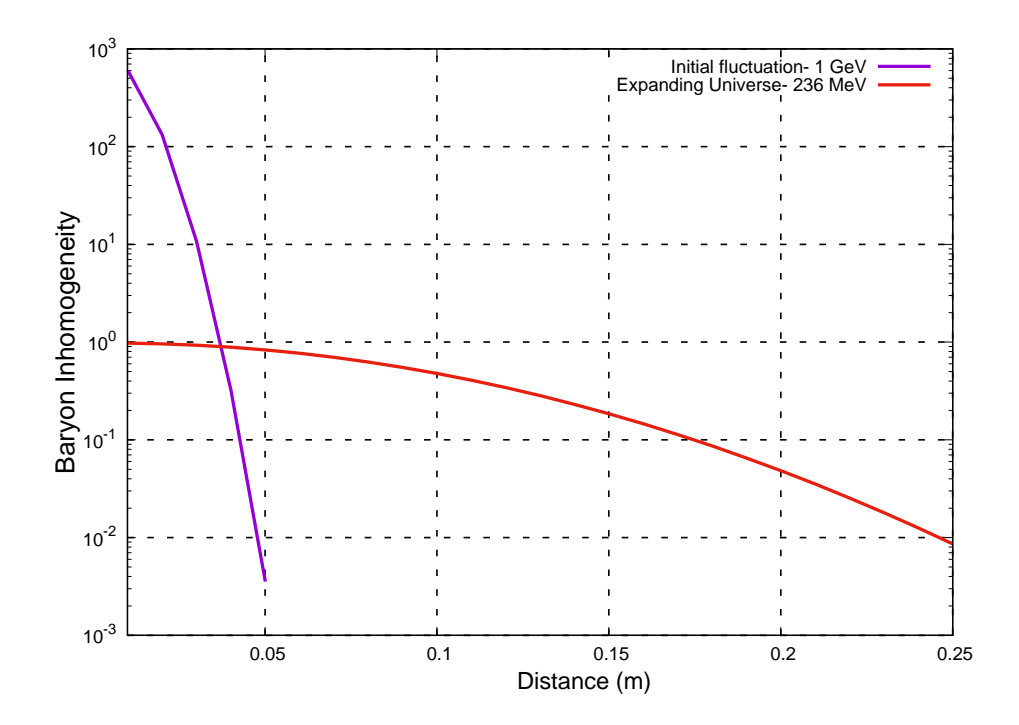


Figure 5.4: The decay of the fluctuation is shown in log scale between 1 GeV - 236 MeV for a plasma where a quark is moving through a sea of electrons.

more than what is shown in the plot. Again we find that the initial inhomogeneity appears to have a sudden cut off around 0.05 cm. This is again due to the log log nature of the plot. The size of the inhomogeneity is also much smaller initially. Since the maximum radius of the lattice is smaller at higher temperatures, the initial fluctuation looks very narrow and sharp when plotted at a later time. This makes the shape of the fluctuation different at different times. Not only are the particles diffusing away from the centre of the inhomogeneity, the maximum size of the one dimensional lattice is also increasing with time.

For the case of the quarks moving through a large number of muons, the amplitude decay is less than the decay in the case when the particles surrounding the quarks are the electrons. However, the decay is still quite significant. For the neutrinos, again we have the inhomogeneity decaying by three orders of magnitude. So independent of the particle distribution in the plasma, the amplitude of the inhomogeneities goes down significantly. In fig 5.5, we have the quarks moving in a region of muons while in fig. 5.6, the quarks move through the neutrinos. As is seen from the plot, the inhomogeneity decays much faster in the presence of neutrinos and quickly reaches an amplitude of  $10^{-2}$ . Compared to the initial amplitude, this is negligible and can be considered to be zero. That is why in fig. 5.6 the plot is cut off at a distance 25 cm. Beyond this point,

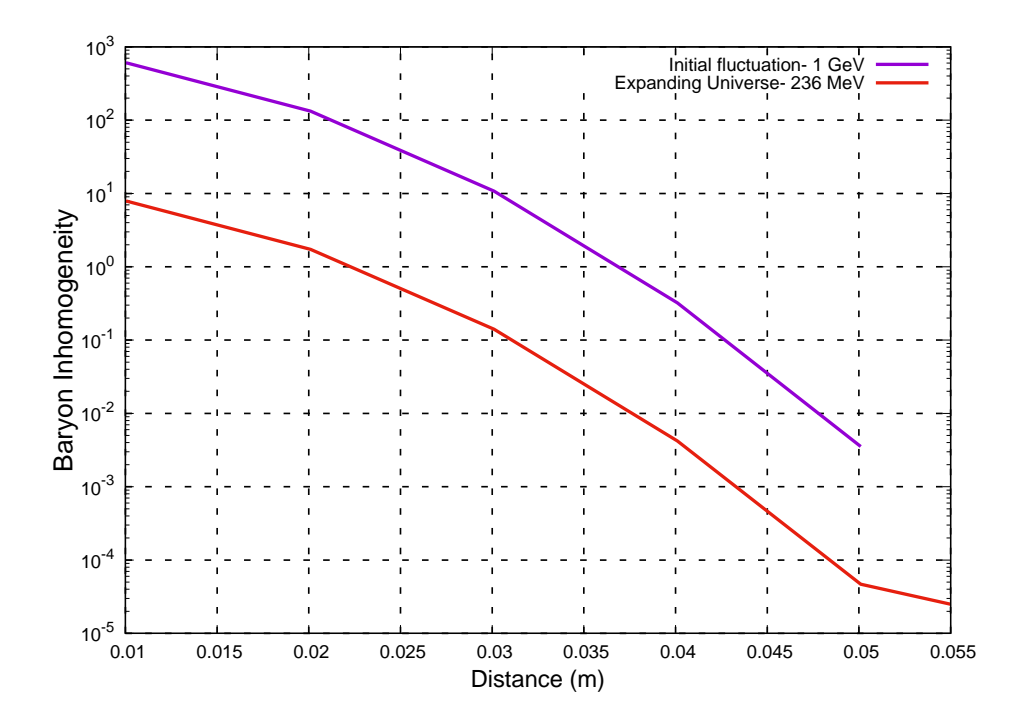


Figure 5.5: The decay of the fluctuation is shown in log scale between 1 GeV - 236 MeV for a plasma where a quark is moving through muons.

the inhomogeneity gradually goes down to zero. We thus find that the inhomogeneity decays by three orders of magnitude between 200 GeV to 1 GeV, and again decays by at least two orders of magnitude between 1 GeV to 200 MeV. This means that any inhomogeneity generated at the electroweak epoch needs to have an amplitude greater than  $10^5$  times the background density to survive till the quark hadron transition. Thus if we had an inhomogeneity at the electroweak scale with an amplitude less than  $10^5$ , it would be completely wiped out before the quark hadron transition.

### 5.5 Decay of inhomogeneities in the hadronic phase

We have discussed our work on the decay of inhomogeneities in the hadronic phase in the previous chapter [103], however in that case we were interested in specific inhomogeneities generated by Z(3) domain walls whose size was much smaller compared to the horizon size. The expansion of the universe was ignored in those cases. We are now interested to see the decay of larger inhomogeneities in the hadronic phase. As mentioned before, inhomogeneities generated during or after the quark hadron phase transition are not only larger in amplitude but they may also be larger in size. Consequently, the decay of these inhomogeneities would be affected by the expanding universe. The plasma

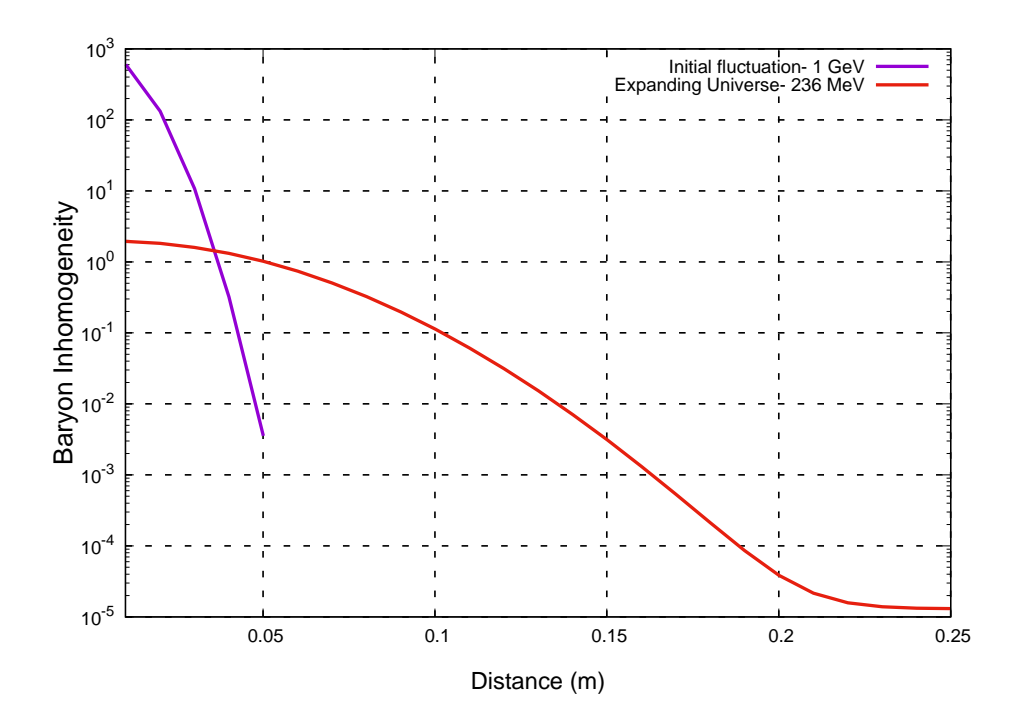


FIGURE 5.6: The decay of the fluctuation is shown in log scale between 1 GeV - 236 MeV for a plasma where a quark is moving through neutrinos. Since the inhomogeneity decays faster here, as the magnitude goes down, the radial distance increases. The full curve at 236 MeV is not given, it is cut off at some point where baryon inhomogeneity is close to 0.01. Compared to the initial fluctuation which had an amplitude of 10<sup>3</sup>, this can be taken to be zero.

during this period consists of the muons, neutrons, protons. electrons and neutrinos. We now solve the diffusion equation in the hadronic plasma for the expanding universe and find that the expansion of the universe causes the inhomogeneities to decay much faster. In the current section, we briefly describe the diffusion coefficient in the hadronic phase and then proceed to present the results of the decay of the inhomogeneities in the hadronic plasma. In this case, the size of the inhomogeneities is taken to be of the of the order of kilometers as the horizon size is around 10 Kms after the quark hadron transition.

As we have mentioned, the calculation of the diffusion coefficient will depend on which particle is moving through the plasma. The baryon number is carried by the neutrons and the protons, hence here we will be considering the motion of a heavier particle through a lighter gas. The heavier particle is the neutron or the proton, while the lighter gas is a gas of electrons and neutrinos. The muons only play a role till 100 MeV. We thus have to use eqn.5.8 and the scattering cross-section of the neutrons with the electron-positron gas to obtain the diffusion coefficient of the neutrons in the electron positron gas. All the scattering cross-sections and diffusion co-efficients of the relevant

interaction in context of hadronic plasma has been discussed in detail in the previous section. So here we will briefly write about the diffusion co-efficient.

The diffusion coefficient for neutron-electron interaction is,

$$D_{ne} = \frac{M^2}{32m^3} \frac{1}{\alpha \kappa^2} \frac{e^{1/T}}{Tf(T)}.$$
 (5.15)

Here M, is neutron mass, m is electron mass and  $\kappa = -1.91$  is the anomalous magnetic moment. The temperature in this case is dimensionless as it is scaled by a factor of  $m_e c^2$ . Finally, the function f(T) is given by,  $f(T) = 1 + 3T + 3T^2$ .

The diffusion coefficient for neutron-muon interaction is,

$$D_{n\mu} = \frac{M^2}{32m_{\mu}^3} \frac{1}{\alpha \kappa^2} \frac{e^{1/T'}}{T'f(T')}$$
 (5.16)

Here  $T' = \frac{T}{m_{\mu}c^2}$ . After obtaining both  $D_{ne}$  and  $D_{n\mu}$ , we calculate the total diffusion coefficient of the neutron moving through the plasma.

Apart from the neutron, we need to find the diffusion coefficient of the proton moving through the electron positron gas. The diffusion coefficient for proton-electron interaction is

$$D_{pe} = \frac{3\pi}{8\alpha^2 ln(\frac{2}{\theta_0})} \left[ \frac{h}{2\pi m_e} \right] \frac{Te^{1/T}}{f(T)}.$$
 (5.17)

where  $\theta_0$  is the minimum scattering angle

We obtain the numerical value of this diffusion coefficient by substituting the constants in the transport cross section. Once we have the diffusion coefficients, we numerically solve the diffusion equation in the FLRW metric. In this case, we use the same program but double the stepsize to accommodate the larger radius of the horizon.

We are considering inhomogeneities whose sizes are in the range of 1 km. Since the horizon size is around 10 kms in the hadronic phase, these are large inhomogeneities. We have considered high amplitudes of the order of  $10^{14}$  as well as smaller amplitudes, we find that the decay rate does not depend significantly on the amplitudes. However, we find that in an expanding universe the overdensity falls far more rapidly than in an non-expanding universe. We have shown both the cases in figure 5.7. for comparison. We have checked for the decay separately in the range 200 MeV - 100 MeV as the muon is still present in the plasma at these temperatures. At lower temperatures the muon density in the plasma becomes negligible.

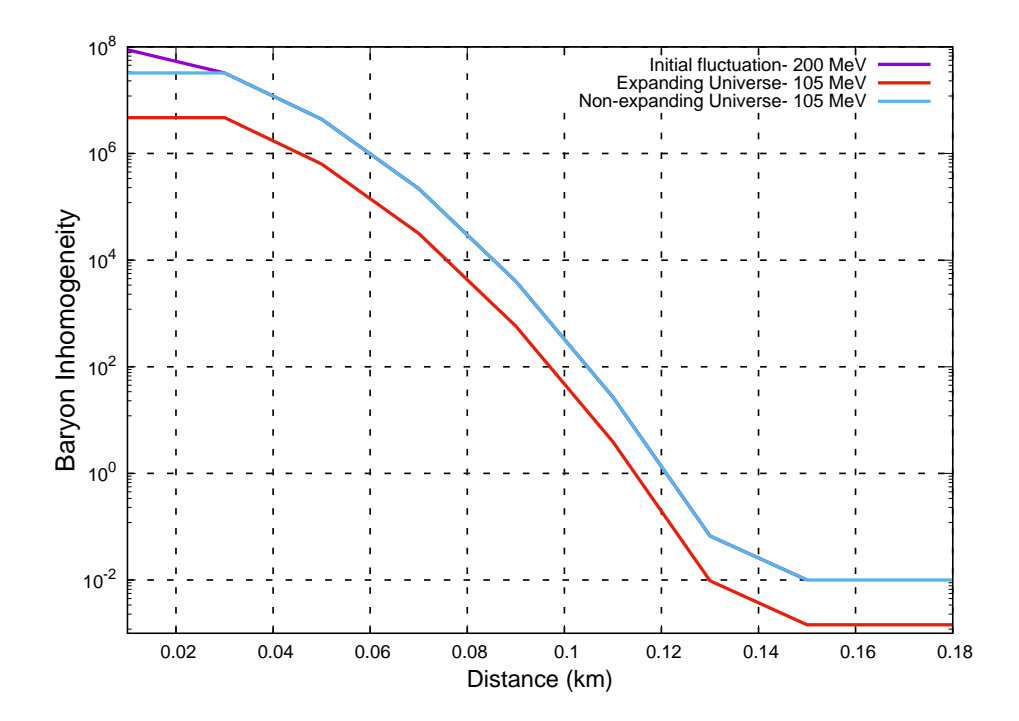


Figure 5.7: The decay of the initial fluctuation is shown in log scale between 200 MeV  $\,$  - 100 MeV.

It seems that large inhomogeneities do decay significantly in an expanding universe but as long as they have very large amplitude, they may still survive up to the nucleosynthesis epoch. So an inhomogeneity whose amplitude is of the order of  $10^8$  will be decreased to an amplitude of the order of  $10^7$ . Hence inhomogeneities with low amplitudes of the order of 10 will be wiped out. Finally, we look at the temperature range from 100 MeV - 1 MeV. The muons will be negligible in this epoch but the diffusion coefficients will not change. Figure 5.8 shows the decay of the inhomogeneities in this epoch. We find that the amplitude of the inhomogeneity decreases by an order of  $10^4$  in this period. This means that any inhomogeneity with an amplitude less that  $10^4$  will be wiped out before the nucleosynthesis epoch. So large baryon inhomogeneities generated during the quark hadron transition must have amplitudes greater than  $10^5$  times the background density to survive till the nucleosynthesis epoch.

### 5.6 Summary

Finally we summarize this chapter briefly, we have studied the decay of the baryon inhomogeneities generated at both the electroweak scale and the QCD scale. If the baryon inhomogeneities generated at the electroweak epoch survive till the quark hadron

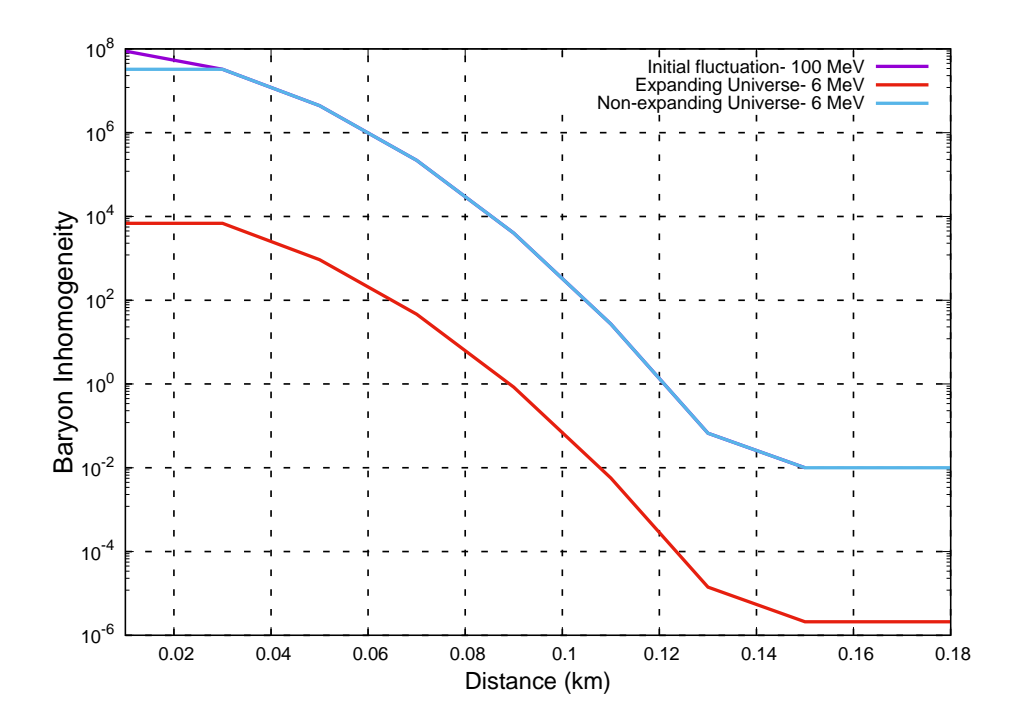


FIGURE 5.8: The decay of the initial fluctuation is shown in logscale between 100 MeV - 1 MeV.

phase transition they will affect the phase transition dynamics. The quark hadron phase transition is very important in the thermal history of the universe. Similarly, baryon inhomogeneities generated during the quark hadron phase transition will have an effect on the Big Bang Nucleosynthesis calculations. There has been no previous studies of the decay of baryon inhomogeneities in the early universe during the electroweak scale. Our study is the first study that shows that the decay of these baryon inhomogeneities is affected by the expanding universe in the electroweak scale. To obtain the decay of the baryon inhomogeneities, we have first obtained the diffusion coefficient of the quarks through the electroweak plasma. We have then substituted it in the diffusion equation for an expanding universe. The diffusion equation of the expanding universe is obtained by writing the diffusion equation in the FLRW metric.

Our detailed study shows that baryon inhomogeneities generated at 200 GeV should have an amplitude greater than 10<sup>5</sup>, otherwise they will not survive till the quark hadron phase transition. This makes it difficult for the baryon inhomogeneities generated in a first order electroweak phase transition to have any effect on the quark hadron epoch. In ref. [1, 88], spherical inhomogeneities with a radial profile are formed at the electroweak phase transition. However, the amplitude of these inhomogeneities are bounded by the ratio of the highest and lowest wall velocities reached during the bubble expansion

phase. In most cases, this is of the order of  $10^2$ . This is an order of magnitude lower than the amplitude of the baryon inhomogeneities we have considered in our simulations. Thus the baryon inhomogeneities generated due to a strong first order electroweak phase transition would be completely wiped out before the QCD phase transition. To survive up to the QCD phase transition, the baryon inhomogeneities have to have a very high amplitude as they decay substantially during the period between 200 GeV - 200 MeV. This is because the diffusion coefficient is temperature dependent. The quark hadron transition occurs around 200 MeV. We have found that the amplitude of the baryon inhomogeneity decreases to about five orders of magnitude during this period. This means any inhomogeneity with an amplitude of  $10^5$  (or less) will be wiped away before the quark hadron phase transition. We therefore conclude that any model which generates inhomogeneities with less than  $10^5$  amplitude in the electroweak epoch cannot affect the quark hadron phase transition. They will therefore not contribute to inhomogeneous BBN either.

In this work, due to the vast differences in the values of the diffusion coefficients of the different particles in the electroweak epoch, we have not considered multi particle diffusion. We have studied the diffusion of the quarks through a gas of similar particles only. However, for all the different particles we find that the inhomogeneities will decay. This indicates that even for a multi particle diffusion our results will hold. However, in any region which has a predominance of neutrinos and electrons, the inhomogeneities will probably decay faster, than in regions which have a predominance of muons.

Finally in the previous chapter, we had looked at the decay of baryon inhomogeneities in the QCD epoch for a stationary universe. This would work only for small scale inhomogeneities for which the expansion of the horizon does not matter. We have extended that work for an expanding universe where we can work with large baryon inhomogeneities. So we look at the decay of large baryon inhomogeneities in the QCD epoch. We find that the baryon inhomogeneities decrease by 5-6 orders of magnitude. This means that if large baryon inhomogeneities are generated by collapsing domain walls and other topological defects during the quark hadron transition they will survive till the nucleosynthesis epoch. We conclude that the big bang nucleosynthesis, can thus be used to constrain models which generate large amplitude inhomogeneities in the QCD epoch only.

## Chapter 6

# Generation of magnetic field in cosmic string wake

We have discussed the generation of topological defects previously in chapter 3, there we had mentioned that the linear defects generated in symmetry breaking phase transitions are called the Abelian Higgs strings [33]. The Cosmic Microwave Background (CMB) imposes certain restrictions on the masses of these defects [106]. The evolution of the string network [107] and the consequences that these can have on several epochs in the early universe are well documented in the literature [108]. As the string networks evolve they lead to density fluctuations in the early universe. This is especially true for the long Abelian Higgs strings which are known to generate wakes as they move through the plasma of the early universe [56, 57, 109]. Various signatures related to cosmic string wakes have also been discussed in the literature. [110, 111]. We have already discussed about the wake formation in detail in chapter 3.

As mentioned before, the space time around a cosmic string is conical. This means that the geodesics of particles moving around a cosmic string is curved. The Abelian Higgs string also has two fields associated with it, so the geodesics of the particles around these strings are often non trivial. A detailed study by Hartmann et. al [112] showed that there are some particles which move in closed orbits around these strings. A subsequent study by Saha et. al. [113] indicated that the closed orbits lead to a clustering of particles around the cosmic string. The nature of the force and the geometry of the surface combine together for certain values of angular momentum and energy and lead to these closed orbits. This only happens for massive particles. Now, as we have mentioned before, the long strings once formed will move through the cosmic plasma and generate wakes behind them. Some of the most abundant particles in the early universe plasma are the neutrinos. We also know that it is possible to have massive neutrinos. Hence

neutrinos moving with certain energies and angular momentum close to a cosmic string will get trapped in closed orbits and cluster around the cosmic strings. As there is an inherent asymmetry in the neutrinos, the rotational motion will generate a neutral current. The motion of the string will cause a density gradient of all particles in the wake region, the neutrino will also be one of them. The combination of the motion of the string and the neutral current generated by the neutrinos will result in a charge separation in the plasma. An electron current is thus generated in the plasma which will then give rise to a primordial magnetic field. Though electrons have mass themselves, the motion of the electrons around a cosmic string do not generate an electron current since in the early universe plasma, there are equal number of positrons in the plasma. The positrons rotating in the opposite direction will neutralize the net electron current around the cosmic string in the early universe plasma. That is why electrons rotating around the cosmic string will not lead to a charge separation in the plasma. For neutrinos however, an asymmetry between neutrinos and anti-neutrinos is well established [114, 115]. The order of magnitude of the lepton asymmetry varies from  $10^{-10}$  to higher values of  $10^{-4}$ depending on the various leptogenesis models. It is this lepton asymmetry in the neutrino sector which will give rise to a neutrino currents around the Abelian Higgs strings.

The electron current is generated from the non-uniform fluxes of neutrinos which interact with the electrons by weak interactions. A weak ponderomotive force has been predicted by several authors [116–118]. This force has also been used for the generation of magnetic fields before [119]. Even though, the analogy with the ponderomotive force was not well established but the results could also be established from the kinetic theory. It was shown that neutrino gradients can also lead to instabilities in the plasma. Detailed studies [120, 121] using quantum field theory inspired models have led to the conclusion that gradient of the electron and neutrino densities can generate an electric current in an electroweak plasma. As is well known from Maxwell's theory of electromagnetism, a changing current can generate a magnetic field. The universe plasma at such high temperatures is a turbulent plasma with a large Reynolds number. So the charge separation caused by the neutrinos in the cosmic string wakes can be used to generate a magnetic field using the Biermann battery mechanism. In this chapter we present the novel way of generating magnetic fields from neutrino currents in cosmic string wakes. We also estimate the magnitude of the generated magnetic field and find that it is within the limits of the observational bounds on magnetic fields set by nucleosynthesis calculations.

### 6.1 Neutrino current density around cosmic strings

As discussed in the previous section, we would now like to calculate the neutrino current density around the cosmic strings. Though neutrinos in general have a very low mass, some models have predicted more massive neutrinos[122]. The neutrinos in general have a long mean free paths. It has been shown that the neutrino mean free path above 100 GeV is small but it increases with the decrease in temperature[16]. The mean free path would affect the diffusion of the clustered particles around the string. If the energy scales are high then the clustering is also enhanced due to the energy values giving rise to large number of closed orbits around the string. It has been shown that the overdensity is quite high and spreads over a lengthscale of 10 fm around the string [113]. To calculate the current we first find the Fermi distribution of the neutrinos in a rotating system. This is given by,

$$f(E, l_z, \beta) = \left[ exp\left(\frac{E - l_z\Omega - \mu\beta}{T}\right) + 1 \right]^{-1}$$
(6.1)

where  $\Omega$  is the angular velocity,  $\mu$ , is the chemical potential of the neutrinos, and  $l_z$  is the projection of the particle's total angular momentum on the direction of  $\Omega$  and E is the energy of the neutrinos. The factor  $\beta$  takes on the values 1 or -1 depending on whether the neutrinos are more than the antineutrinos in the plasma. The Abelian Higgs string is cylindrical in shape so we use the cylindrical coordinates. The most general line element obeying all the symmetry properties pertaining to the Abelian Higgs string is given by,

$$ds^{2} = N^{2}(r)dt^{2} - dr^{2} - L^{2}(r)d\phi^{2} - N^{2}(r)dz^{2}$$
(6.2)

The factors L(r) and N(r) are determined by the boundary conditions. They are related to the values of the fields at a distance r from the axis of the string (the z axis in this case). Our string moves in the x-y plane and there is a magnetic field associated with the Abelian Higgs string along the z-axis whose value depends on the scalar and the vector potentials. The metric corresponds to a cylindrical metric with a deficit angle  $\delta\theta$  as mentioned in Chapter 2. The deficit angle far from the core of the string is proportional to the energy per unit length of the string. Further, the Lagrangian of the Abelian Higgs string is usually rescaled and written in terms of two dimensionless constants  $8\pi G\eta^2$  and  $\frac{\lambda}{e^2}$ . The deficit angle depends upon these two constants. The cosmic string has a finite width with a core of magnetic flux as well as a scalar core. The width of these cores are the inverse of the gauge boson mass and the Higgs mass respectively. The lengthscales of the moving particles around the cosmic string are much smaller compared to the Hubble radius at any time, so the expansion of the universe is

neglected throughout this chapter. For all the calculations in this chapter the universe is considered to be stationary.

The geodesics of the neutrinos around the cosmic string are open or closed circular orbits [112]. So the neutrino particles appear to rotate about the z-axis. To obtain the neutrino current density around the cosmic string, we first need to calculate the appropriate spinor wave function  $\psi(E, p_z, l_z, \beta)$ . We start with the neutrino field equations in the metric of the cosmic string.

$$\gamma^{\mu}(\partial_{\mu} - \Gamma_{\mu})\psi - m\psi = 0 \tag{6.3}$$

Since we are looking at neutrinos with mass, m denotes the mass of the neutrinos. A suitable choice of Gamma matrices for this metric are,  $\gamma^t = \gamma^0$ ,  $\gamma^r = \gamma^1, \gamma^\phi = \frac{\gamma^2}{L(r)}, \gamma^z = \gamma^3$ . Here we have considered N(r) = 1 as the particles are considered quite close to the string and their distance from the core is small. Using these Gamma matrices, we then solve the field equations by choosing the trial solution in the form,

$$\chi = e^{-iEt}e^{ip_z z}e^{-il_z \phi} \begin{bmatrix} \xi \\ \zeta \end{bmatrix} \tag{6.4}$$

Here E is the energy,  $p_z$  in the component of linear momentum in the z direction and  $l_z$  is the projection of angular momentum along the z-axis. On solving the equations, we get

$$\xi = \begin{bmatrix} i(E+m-p)^{1/2} J_{l_z+1/2}(\alpha r) \\ \beta (E+m+p)^{1/2} J_{l_z-1/2}(\alpha r) \end{bmatrix}$$
(6.5)

Here  $J_{l_z+1/2}(\alpha r)$  are the Bessel functions. For a system with zero chemical potential  $\xi = \zeta$  [123]. However, for a non zero chemical potential  $\zeta = \beta \xi$ . As we have mentioned before, since there is a lepton asymmetry in the early universe and it is manifested in the neutrino sector, we take  $\zeta = \beta \xi$ . The wavefunction is then given by,

$$\psi_{(Ep_zl_z\beta)} = \frac{1}{4\pi} e^{-iEt} e^{ip_z z} e^{-il_z \phi} \begin{bmatrix} \xi \\ \beta \xi \end{bmatrix}$$
 (6.6)

The normalization condition for the wavefunction would be,

$$\int \psi_{Ep_z l_z \beta}^{\dagger} \psi_{E' p_z' l_z' \beta'} r dr d\phi dz = \delta_{l_z, l_z'} \delta_{\beta, \beta'} \delta(p_z - p_z') \delta(E - E')$$
(6.7)

Once the wavefunction is obtained, one can obtain the neutrino current. The direction of the current is along the axis of the string i.e along the z-direction, however as the wavefunction depends on the distance from the string, the magnitude of the current also varies with the distance from the axis of the string. The current as a function of r, (the

distance from the string axis) is given by,

$$j(Ep_z l_z \beta) = \beta \psi_{Ep_z l_z \beta}^{\dagger} \gamma^t \gamma^z \psi_{Ep_z l_z \beta}$$
(6.8)

Hence the total current density as a function of r, is given by,

$$J(\alpha r) = \int_0^\infty dE \int_{-E}^E dp \sum_{\beta = \pm 1} \sum_{l_z} f(E, l_z, \beta) j(Ep_z l_z \beta)(\alpha r)$$
 (6.9)

To obtain the neutrino current around the cosmic string we have to solve eqn.6.9. Analytically this provides quite a challenge, as it is a summation over Bessel functions. One can obtain an approximate solution close to r=0 but it is the finite values of r that generate the magnetic field. We need to obtain an estimate of the current numerically since we are going to use it for the calculation of the magnetic field generated later on in the paper. As expected a sum of Bessel functions will generate a sinusoidal curve. We find that the numerical solution is in the form of a sinusoidal curve.

We now explain in detail the numerical values chosen to obtain this graph. The cosmic string is generally characterized by it's symmetry breaking scale. The two cores of the cosmic string have width inverse to the Higgs mass  $(M_H)$  and the W boson mass  $(M_W)$ . The masses are given by  $M_H = \sqrt{\lambda} \eta$  and  $M_W = \sqrt{2} e \eta$ , where  $\eta$  is the symmetry breaking scale. Generally for solving equations numerically all the quantities are made dimensionless. This has been done in previous papers involving particle motion around cosmic strings [112, 113]. The symmetry breaking scale is usually used to rescale the variables; so that the momentum  $p_z$  is scaled to  $p_z/e\eta$ ,  $l_z$  by  $l_z/e^2\eta^2$  and similarly for the energy. To obtain the values in the cosmological scenario, all we have to do is to identify the symmetry breaking scale. For the numerical values of energy and momentum, we have taken the values from ref.[113]. The values are chosen such that they give rise to clustering of particles around the string. In dimensionless variables, they are E = 1.083,  $l_z^2 = 0.025$  and  $p_z = 0.02$ . The symmetry breaking scales for these cosmic strings are very high, usually above the electroweak scales [124]. The electroweak symmetry breaking scales are of the order of 100 GeV. If we substitute the value of  $\eta$  in the equations, we get the current in terms of  $GeV^3$ . The numerically obtained values of  $J(\alpha r)$  are plotted in figure 6.1. The distance from the core is in terms of  $\alpha r$ . Here  $\alpha = \sqrt{(E+m)^2 - p_z^2}$ . Hence  $\alpha$  is in GeV. This makes  $\alpha r$  dimensionless. The neutrino current will also depend on the amount of lepton asymmetry in the plasma. However we find that in the range of  $10^{-10}$  to  $10^{-4}$ , there is no significant change in the magnitude of the neutrino current.

The current is oscillatory in nature and decreases with increase of distance from the string. The maximum value is close to the core of the cosmic string. Though the values appear to be small, in the context of the early universe plasma it is not negligible.

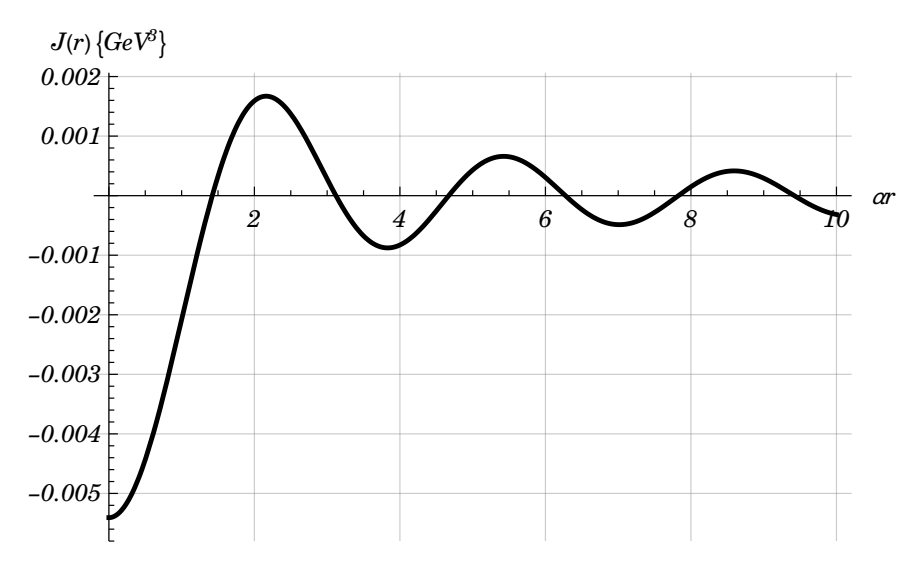


FIGURE 6.1: A plot of the neutrino current as a function of r (distance from the cosmic string). Here  $\alpha r$  is dimensionless. The current is oscillatory in nature and decreases with increase of distance from the string.

Detailed studies of neutrino currents in the plasma have been done and both charged currents and neutral currents have been discussed in the literature [125]. However, there are no numerical estimates of these currents. These currents depend on the interaction cross section of the particles. Unlike these currents we want to emphasize our current is a directed flux of particles moving collectively through the plasma. The numerical estimate given in fig 6.1 shows that at high temperatures it is not negligible. We will use this estimate when we calculate the magnetic field in the next section. This solution is for a stationary string; but a cosmic string in the early universe is never really stationary. It moves through the plasma with a velocity  $v_s$  mentioned before. Behind the string a wake is formed. Now the oscillatory neutrino distribution will thus change with time due to the velocity of the moving string. The overdensity behind the string will enhance the current further. As mentioned previously, generally the wake density is double the background density of the plasma. So the neutrino distribution will be less in front of the string while it will be much more behind the string. Both a spatial as well as a temporal gradient in neutrino density is thus generated in the plasma.

### 6.2 Neutrino currents in moving cosmic string wakes

#### 6.2.1 Ponderomotive force

Initial studies by Bingham et. al.[116, 117] showed that neutrino gradients in the early universe led to a ponderomotive force in the background plasma. The ponderomotive

force was initially a force that occurred in a dielectric in an arbitrary non-uniform electric field. However, it was generalized in [118] to the interaction of any non uniform field with a background medium. The non-uniform field was the neutrino field and the background medium were the electrons. The ponderomotive force was due to the weak interaction between the neutrinos and the electrons in a high temperature plasma. They had shown that a force is exerted on the electrons due to the non-uniform distribution of neutrinos in the plasma. This is the generalized ponderomotive force. The electrons are thus forced to move away from the regions in which the neutrino density is higher. Considering only the electrons in the plasma, the ponderomotive force was given by [119],

$$F_{\nu} = \frac{1}{8\pi} (f_{\nu}^2 - 1) \nabla \sum_{k_{\nu}} \langle |\psi_{k_{\nu}}|^2 \rangle.$$
 (6.10)

Here  $f_{\nu}$  is the refractive index of neutrinos in plasma. However, the ponderomotive force obtained here only contained the terms proportional to the gradients of the neutrino number densities and not the term corresponding to the vector current. Bento [120, 121] obtained the expression that included the terms due to the vector currents using a quantum field theory approach. The other approach was using the relativistic kinetic theory for describing the interaction between the neutrinos and the plasma [126]. They showed that for relativistic neutrino jets, plasma instabilities can develop with growth rates of the order of Fermi constant  $G_F$ . In all these studies, it was well established that a electromagnetic current is generated due to the neutrino currents in the early universe. The interaction term in the Lagrangian leads to the force on the electron and both weak-electric and weak-magnetic fields are generated as well as the familiar electromagnetic fields. The electromagnetic fields are given by, [127]

$$\vec{E_e} = -\nabla \vec{J_e^0} - \frac{\partial \vec{J_e}}{\partial t} \qquad \qquad \vec{B_e} = \nabla \times \vec{J_e}$$
 (6.11)

The weak-electric and weak magnetic fields are given by,

$$\vec{E}_{\nu} = -\nabla \vec{J}_{\nu}^{0} - \frac{\partial \vec{J}_{\nu}}{\partial t} \qquad \qquad \vec{B}_{\nu} = \nabla \times \vec{J}_{\nu}$$
 (6.12)

The flow of neutrinos in a plasma medium is given by the following fluid equations

$$\frac{\partial N_{\nu}}{\partial t} + \nabla . \vec{J_{\nu}} = 0 \tag{6.13}$$

$$\frac{\partial \vec{P_{\nu}}}{\partial t} + (\vec{v_{\nu}}.\nabla)\vec{P_{\nu}} = \vec{F_{\nu}} = \sqrt{2}G_F \left(\vec{E_e} + \frac{\vec{v_{\nu}}}{c} \times \vec{B_e}\right)$$
(6.14)

Similarly we can also obtain the continuity equations for the electron plasma dynamics,

$$\frac{\partial N_e}{\partial t} + \nabla \cdot \vec{J_e} = 0 \tag{6.15}$$

$$\frac{\partial \vec{P_e}}{\partial t} + (\vec{v_e} \cdot \nabla) \vec{P_e} = \vec{F_e} = -e\vec{E_e} + \sqrt{2}G_F \left( \vec{E_\nu} + \frac{\vec{v_e}}{c} \times \vec{B_\nu} \right)$$
 (6.16)

We then use the standard perturbative approach to obtain the relation between the neutrino perturbation and the electron perturbation in the plasma. We consider  $\delta N_e$  to be the electron number density fluctuation and  $\delta N_{\nu}$  to the neutrino number density perturbation. The two density perturbations are then related by,

$$\left(\frac{\partial^2}{\partial t^2} + \omega_p^2\right) \delta N_e = -\frac{\sqrt{2}G_F N_e}{m_e c^2} \left(\frac{\partial^2}{\partial t^2} - c^2 \nabla^2\right) \delta N_\nu \tag{6.17}$$

Here  $N_e$  is the mean electron density of the plasma and  $\omega_p$  is the plasma oscillation frequency. The neutrino current in the plasma will thus generate a plasma potential  $\phi_e$  due to the charge separation given by  $\nabla^2 \phi_e = 4\pi \delta N_e$ . An electron current is thus generated in the shock wave.

Now we look at our specific case, in our case, behind the cosmic string we have a non - uniform stream of neutrino current. The cosmic string is generated very early in the universe. Once created the string moves through the plasma generating a wake behind it. Apart from the neutrinos, the early universe plasma contains a large number density of electrons. Depending on the temperature of the surrounding plasma in the early universe, the other particles may be quark and gluons (for temperatures above the quark - hadron phase transition ) or the neutrons and protons (for temperatures below the quark hadron temperature). We will look at very high temperatures in the GeV range. The background particles will then be given by the quarks and the leptons. At these temperatures, the particles in the plasma, experience both strongly coupled forces as well as weakly coupled forces. In such a plasma, perturbative calculations and the quasi-particle description used in deriving the generalized ponderomotive force in the literature [118, 119] is not valid. A study by Muller et. al. [128] has shown that in a high temperature plasma, the shear viscosity of the leptons is dominated by the interaction between the leptons and the quarks. Thus the thermal leptons form a more viscous fluid than the quarks. At lower temperatures below the quark hadron transition, the plasma consists of the leptons and the neutrons/protons. The lower temperature plasma is well studied. The velocity of the cosmic string being lower, the plasma can be considered to be non-relativistic. Neutrino plasma interaction in non-relativistic plasmas has been studied in the two fluid hydrodynamic description. Since both at high

temperature and at low temperature, the plasma interaction can be considered as a two fluid hydrodynamic description, we will use this to explain how magnetic fields can be generated in the string wakes at any temperature due to the presence of the neutrino density gradients.

As has been established in previous studies the neutrino gradient exerts pressure and results in a local charge separation in the plasma. This leads to a current in the plasma. The current is like a cross-perturbation across the shock. The perturbation is in the form of density gradients in the direction of shock motion. Such perturbations have been studied both numerically and experimentally in the classical regime. There are however no studies for such perturbations for relativistic shocks. Generally if the perturbation is small, the shock remains stable, though the perturbation itself can be accelerated in the direction of the shock. The fact that the leptons in the quark gluon plasma behave as a fluid with a higher viscosity means that accelerated neutrinos may generate shear induced vorticity in the plasma. A better understanding can only be obtained by a numerical simulation which is beyond the scope of this current work.

### 6.2.2 Magnetic field generation

In this section we will talk about the magnetic field generation in the moving cosmic string wake using the Biermann battery mechanism and try to calculate the order of magnitude of the magnetic field. The angle of scattering between the neutrinos and the background plasma determines whether an instability will be generated in the plasma. In this case, there is no head on collision between the neutrino current and the string wake. The angle of scattering is closer to  $\pi/2$ . A detailed study has shown that for small scattering angle, the elastic process dominates and the energy is transferred from the neutrinos to the plasma, however here in this case the angles are closer to  $\pi/2$ . This means that not much energy is transferred from the neutrinos to the plasma. So no instability is expected to be generated in the plasma. However, the Reynolds number in the plasma is very high. So we have shear induced vorticity in the plasma as well as a high Reynolds number, therefore localized magnetic fields are generated in the string's wake by the Biermann battery mechanism. In a two-fluid description of the plasma with massless electrons, the magnetic field evolution, as given by the Biermann battery mechanism is [116],

$$\frac{\partial \vec{B_e}}{\partial t} = \nabla \times (\vec{v_e} \times \vec{B_e}) + \frac{\eta_{res}}{4\pi} \nabla^2 \vec{B_e} - \frac{1}{eN_e} \nabla \times (\vec{j} \times \vec{B_e}) - \frac{1}{N_e e} \nabla N_e \times \nabla T_e \qquad (6.18)$$

Here,  $\vec{v_e}$  is the electron fluid velocity,  $N_e$  is the number density of the electrons,  $T_e$  is the electron temperature and  $\eta_{res}$  is the resistivity of the plasma. The last term on the right

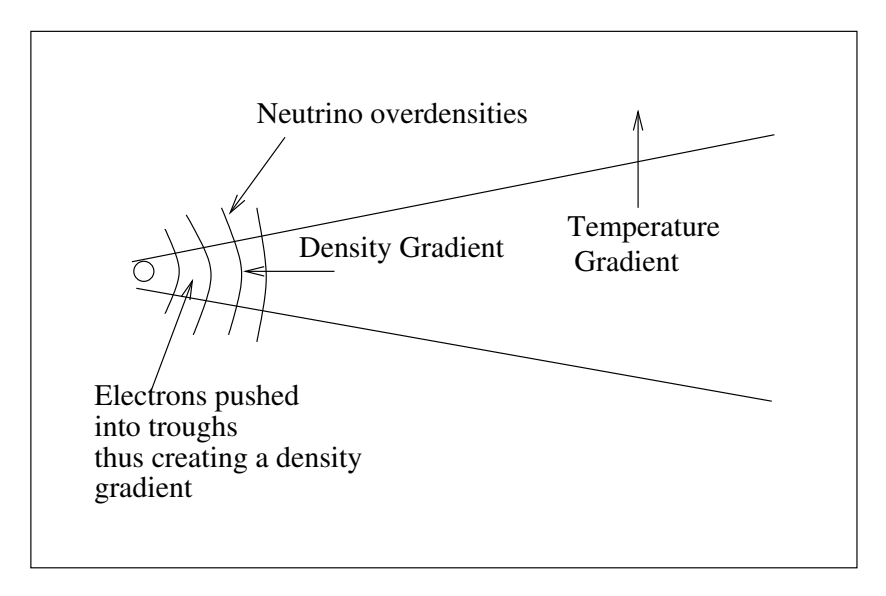


FIGURE 6.2: An illustration to show the generation of magnetic field in the wakes of cosmic strings due to the non uniform neutrino overdensities.

hand side is the Biermann battery term. In the case where there is no magnetic field  $(\vec{B_e} = 0)$ , this term generates the magnetic field due to the misalignment between the density and the temperature gradients of the electrons. We now demonstrate why the density gradient and the temperature gradient would be misaligned due to the neutrino currents in the shocks of the cosmic strings.

Let us assume that the string is moving in the y - direction in the x-y plane. The shock is therefore stretched along the y axis with a small width in the x-axis. The temperature difference between the overdensity and the background plasma is primarily along the x-axis. Now, as mentioned before, the neutrino current exerts a force on the electrons which pushes them into regions where there are less neutrinos, so the electron gradients will be complementary to the neutrino gradient caused by the Abelian Higgs strings. This means that if the string was moving in the y-direction, they would also be in the y-direction. Fig 6.1. plots the neutrino density with respect to  $\alpha r$ , where r is the radial distance away from the string, since  $r = \sqrt{x^2 + y^2}$ , the neutrino gradient and the temperature gradient will not be parallel to each other. Since the neutrino gradient and the electron gradient will be complimentary to each other, therefore, the Biermann battery term will give rise to a small but finite magnetic field.

In fig 6.2, we have given an illustration to further explain the magnetic field generation. Though an exact calculation is beyond the scope of this work we would like to make an order of magnitude estimate for fields generated at around 100 GeV temperature scales in the early universe. We assume that the density perturbation for neutrinos is proportional to the density perturbation of the electrons which is taken to be in the y

direction. The temperature gradient across a cosmic string shock (in the x-direction) is of the order of  $10^{-5}T$  [129]. So from the Biermann mechanism,

$$\frac{\partial B}{\partial t} \sim \frac{\sqrt{2}G_F}{m_e c^2} \frac{\partial N_{\nu}}{\partial y} \frac{\partial T_e}{\partial x}$$
(6.19)

We consider  $G_F = 10^{-5} GeV^{-2}$ ,  $\frac{\partial N_{\nu}}{\partial y} \sim 0.02 GeV^3$  and  $\frac{\partial T_e}{\partial x} \sim 10^{-5} \times 200 GeV$ . The lengthscales at around the electroweak scales are about  $1 GeV^{-1}$  and if we take a similar time scale (about  $1 GeV^{-1}$ ) then the order of magnitude of the generated magnetic field is about  $10^{13}$  Gauss. Though this is not a very large field, we point out that this is a conservative estimate as we have not considered the enhancement of the current due to fluid dynamical processes. The  $\frac{\partial N_{\nu}}{\partial y}$  is for a stationary cosmic string, as we have mentioned previously, the density inhomogeneities will also be enhanced by a moving string due to the high Reynolds number at those high temperatures. At the electroweak scale the equipartition magnetic field is  $\sim 10^{24} G$  [130]. Though the field generated in the shock region is far smaller than this, the Reynolds number is very high at such scale  $\sim 10^{12}$ , so it is quite possible that this small field can grow into a larger field due to turbulence.

There are various methods of generating magnetic fields in the wakes of cosmic strings through vorticity in the wake region in the literature [131, 132]. The correlation lengths of these fields are of the order of 100 kpc after the recombination epoch. Though the primordial fields generated were sufficiently large in magnitude, it was not clear whether stable vorticity can be generated in wakes of these cosmic strings. The correlation length of the cosmic strings generated by the neutrino currents in the cosmic string wake will be of the order of magnitude of the wake itself. However it is expected that there would be more than one string in one horizon volume. It may be quite possible that there would be string loops or string networks. This would significantly change the correlation length of the magnetic field generated; as the hydrodynamics of a string loop is quite different from that of a straight string. Though we have found that the magnitude of the generated field is lower than what is required, there is the possibility that the turbulence generated in the wake will magnify this field. Turbulence in cosmic string wakes has also been studied before [133, 134]. Turbulence will definitely occur in the cosmic string wake and coupled with the Biermann battery mechanism will enhance the generated magnetic field.

### 6.3 Summary

In this work, we have shown that Abelian Higgs strings moving through the plasma generate a neutrino current which has density gradients in the direction of motion of the string. The wake formed behind the string will therefore have a cross perturbation across it. This cross-perturbation creates density discontinuities in the wake. These can be looked as interfaces through which the wakes pass. At very high temperatures, shocks are formed in the wakes of cosmic strings. As the shocks cross the interface, the magnitude of the neutrino current is too small to generate an instability but the particles in the interface are accelerated by the shock wave. Due to the neutrino electron interaction in the plasma, an electron current is generated in the plasma. The difference in the viscosity of the neutrino-electron fluid and the neutrino - quark fluid will generate vorticity in the shocks. The Reynolds number of the plasma being high at these temperature, this could lead to the generation of magnetic fields in the shocks of Abelian Higgs strings by the Biermann mechanism.

At lower temperatures i.e after the quark - hadron phase transition, the plasma consists of the heavier hadrons (neutron/proton) and the lighter leptons. The shock formed behind the string will again have a cross-perturbation. Now, the collision angle between the shock and the neutrinos will be closer to  $\frac{\pi}{2}$ , hence the energy transfer to the plasma will be less. Again no instabilities develop but an electric current is generated which will lead to the generation of a magnetic field. This seems to indicate that the motion of Abelian Higgs strings will always generate accelerated particles and magnetic fields in their wake.

We have obtained an order of magnitude estimate for the generated magnetic field and find that though low it is not negligible. Our estimate is very conservative as it does not include the effect of the high Reynolds numbers in the early universe. There are other mechanisms (such as bubble collisions at the electroweak scale ) which generate lower magnetic fields which are subsequently enhanced due to the high Reynolds number in the plasma. A detailed simulation of the wake structure including the neutrino current will give an idea of the actual magnitudes of the fields generated.

In conclusion, neutrino currents around Abelian Higgs string act as a cross perturbation to the wakes generated by the strings. This cross - perturbation leads to the generation of magnetic fields in the wakes of the string at all temperatures. In the case of the cosmic string, the electron current which is generated by the interaction of the neutrinos with the plasma is of primary importance for us. The electron current leads to charge separation and the generation of a magnetic field. So Abelian Higgs strings will always

generate magnetic fields in the wakes behind them. This can occur at all temperatures in the early universe.

We have done the analysis for an isolated straight cosmic string, apart from straight cosmic strings one can also have loops of cosmic strings. The geodesics around cosmic string loops are far more complicated [135]. This means that the clustering around loops of Abelian Higgs strings might also be quite different from clustering of particles around long cosmic strings. A detailed simulation is required to study the clustering of massive particles around cosmic string loops.

Abelian Higgs cosmic string networks have been studied in detail recently [136]. Just as we found clustering of particles around straight cosmic strings, there will be a possibility of generating a large number of such clusters in evolving string networks. However, such a scenario would be difficult to analyse as the neutrino currents may not lead to significant charge separation. Only detailed simulations of cosmic string networks can determine whether they can generate seed magnetic fields or not and that is beyond the scope of our current work.

### Chapter 7

## Quark cores in modified MIT Bag model

### 7.1 Introduction

In the previous chapters we have discussed the various consequences of cosmic string wakes and density inhomogeneities in the early universe. We have dealt with finite baryon densities non-uniformly distributed in an electroweak or hadronic plasma. In this chapter we will deal with finite baryon densities in compact objects such as quark stars/hybrid stars. These are hypothetical compact objects which have been predicted to account for quite a few unexplained phenomenon in the current universe. These are capable of generating gravitational waves. Since in recent years, large scale collaborations have been able to detect signals of gravitational waves, it is quite possible that soon we will start detecting more exotic objects in the current universe. The first prediction of stable quark stars was by Witten [13] in 1984. Other authors also contributed to the study of these exotic objects [137]. Neutron stars have already been predicted. There were some models predicting that the core of these stars was also made up of quarks [138–140]. In recent times, the Neutron Star Interior Composition Explorer (NICER), which is a X- ray telescope stationed at the International Space Station has measured the radius and mass of several massive neutron stars. These include the pulsars like PSR J1614-2230 and PSRJ0348+0432. The theoretical challenges brought about by these exciting new observations has lead to many new theories of the neutron stars. The latest approach to modelling of neutron stars involves a Bayesian approach. In this method different measurements of macroscopic observables are combined to put constraints on the EoS of neutron stars and hybrid stars [141]. In most of these cases, a phenomenological parametrization of the EoS is used. These studies have put tighter constraints

on the radii of the neutron stars. More details about the neutron stars and the current challenges faced from recent observations can be obtained from a recent review of neutron stars by Baym et. al. [142].

As we have discussed in chapter 2, the quark hadron transition is usually studied using the bag model. Since the neutron star is composed mostly of neutrons, it's equation of state (EoS) can be modelled using this bag model [143–146]. Since now there are several observational signals available, the EoS has to be modelled such that it fits the observables. The simple bag model cannot give rise to these observational signals, hence extensions to the bag model were proposed by several authors [147, 148]. The sizes and masses of recent observed stars are very large. Primary among these are the PSR J1614-2230 and PSRJ0348+0432 stars. But even the masses of these stars have been successfully modelled by extensions of the bag model [149–153]. In reference [148], the bag constant is considered to be dependent of the density. Such extensions have also been used to study strange stars in ref. [154]. Various models of strange and hybrid stars are mostly motivated by observational constraints. As has been mentioned before the mass and radius of these stars can be measured quite accurately with today's telescopes. To fit these observations, it is often theorized that the core of the neutron star is different from the crust of the star. The stability of quark matter has been well established by ref. [155]. In ref. [156], a neutron star is gradually changed to a quark star by the trapping of strange matter in the core of the star. Apart from the bag model, the Nambu Jona Lasino model has also been used to model the core of a neutron star [157]. A color flavor locked phase has also been predicted in the core of the star by several groups [158, 159].

The EoS also determines the boundary between the quark and hadron phases. The boundary is important as it gives the order of the phase transition as well as its nature. A fixed entropy per baryon has been suggested across the phase boundary [160]. There are proto-neutron stars where several boundaries are defined as the star cools down. Generally, these boundaries are modelled by a Maxwell construction for an isentropic phase transition. Detailed simulations have been carried out to study the birth of neutron stars and usually an isentropic phase transition is used for these simulations [161, 162]. The model that we will describe in this chapter was first discussed by Leonidov [163] for two quark flavours. This was mostly in the context of relativistic heavy ion collisions [163–165]. In the case of the relativistic heavy ion collisions, the phase transition takes place at a finite value of the chemical potential. However, in the case of the early universe the chemical potential is negligibly small. So the concept of the isentropic phase transition was not required for the case of the early universe. The cores of hybrid stars and neutron stars have a high baryon chemical potential so we choose to use the model by Leonidov to study the cores of these stars. Our work was to apply Leonidiv's model

to the case of the cores of hybrid/neutron stars. Since strange quarks are expected to be present in the cores of these stars, we have extended Leonidiv's model to include all the three flavors of quarks. Our principle aim in using this model was to show that extensions of the bag model can be used to explain the current observations of massive stars with a large radii.

Since our model is an extension of the bag model, we have several parameters in the model. We have studied all the parameters in detail but we find that the mass and the radius of the stars primarily depend upon two factors. These two parameters are the bag constant and the mass of the strange quark. A caveat here is necessary, though we have multiple parameters, we do not use a temperature dependent mass term nor do we consider any medium effects. This is because medium effects have been shown to have negligible effect on the mass and the radius of these stars [166]. There are several constraints that we maintain in our model. The first and most important constraint is that the quark matter we obtain has to be energetically favourable over the  $^{56}$  Fe crystal. This is because this crystal has the lowest mass per nucleon and is thus one of the most stable nuclei in the periodic table. The second constraint comes from the mass of the strange quark. The mass of the strange quark is constrained by multiple observations to be in the range of 90-110 MeV. We therefore maintain this range except for the case where the strange quark is considered to be massless. Finally, the object should be gravitationally stable. For this, we solve the standard Tolman - Oppenheimer - Volkoff (TOV) equations. The TOV equations are generally used to study the stability of gravitational objects. The inputs of these equations are obtained from the partition function corresponding to the EoS of our model. The equations have to be solved numerically as there are no analytical solutions. The solution of the equations gives us the mass radius ratio of the stars. We have solved these equations for different values of the chemical potential and for different temperatures. These studies have lead us to conclude that the stars are stable for a large range of chemical potentials at lower temperatures.

In our studies we have concentrated on the cores of these stars, there will be an outer crust for all these stars. In this current study we have neglected this outer crust. Though there have been some EoS which have described both the core and the crust [167], in our case we concentrate only on the core and assume that the crust is negligibly thin compared to the core. While the mass and radius can be deduced from the experimental observations, one of the direct observables is the surface redshift of the star. Since this is the gravitational redshift, hence it is related to the compactness of the star. The redshift can be calculated from the parameters of our EoS. We calculate it for several values of the parameter space. We find that there are several candidates that match all

these constraints. We will discuss these candidates after discussing in detail about our model.

### 7.2 The extended bag model

We briefly discuss the model proposed by Leonidov and then explain how we have extended it to include the third flavour of the quark, the strange quark. Leonidov's model was based on the MIT bag model that was discussed in chapter 2. This is a phenomenological model which led to a first order phase transition from the quark gluon plasma (QGP) state to the hadronic phase. The model has a constant known as the bag constant. The model proposed by Leonidov et. al [163] had a bag constant which was not a constant, but a variable dependent on chemical potential  $\mu$  and temperature T. Their model was consistent with the Gibbs equilibrium criteria for a phase transition. The model also conserved baryon number and entropy across the phase boundary. Following Leonidov's approach others also modified the bag constant by making it dependent on the chemical potential and temperature [164, 165]. This modification of the bag constant resulted in a EoS which was stiff compared to the EoS obtained from the MIT bag model. It is known that a stiff EoS results in more massive neutron stars [168]. In recent observational data from telescopes, the mass of neutron stars was found to be of the order of two times that of the solar mass. This indicates that the EoS in the core of the star has to be reasonably stiff to give rise to such massive stable objects. We therefore use Leonidov's approach to obtain the EoS for the star. Since it is well known that strange quarks may be found in the core of the stars, we extend the model to include the strange quark. We study the model first for a massless strange quark and then for a massive strange quark where the strange quark mass is constrained by experimental observations.

The number density and the pressure of these stars can be calculated from the grand canonical partition function obtained from Leonidov. For massless quarks, both two flavors (u and d) as well as three flavors (u, d and s), the energy density and pressure is given by,

$$\epsilon = \frac{N_c N_f}{2} \left( \frac{7}{30} \pi^2 T^4 + \mu^2 T^2 + \frac{\mu^4}{2\pi^2} \right) + \frac{\pi^2}{15} N_c T^4 + B(\mu, T) - \frac{\partial B(\mu, T)}{\partial \mu} T - \frac{\partial B(\mu, T)}{\partial T} \mu$$
(7.1)

Here  $N_c$  and  $N_f$  are the number of color and flavor degrees of freedom.  $\mu$  is the chemical potential and T is the temperature of the core.  $B(\mu, T)$  is the chemical potential and

temperature dependent bag constant.

$$P = \frac{N_c N_f}{6} \left(\frac{7}{30} \pi^2 T^4 + \mu^2 T^2 + \frac{1}{2\pi} \mu^4\right) + \frac{\pi^2}{45} N_g V T^4 - B(\mu, T)$$
(7.2)

As mentioned before, the bag constant is not a constant in this model. It is dependent on the chemical potential and the temperature of the core. In ref. [169], it is shown that for a quark gluon plasma with a temperature dependent particle mass, standard thermodynamical relations need to be supplemented by special requirements for maintaining thermodynamic consistency. Though we do not have a temperature dependent mass here, since the pressure is dependent on the bag pressure, we need to check for thermodynamic consistency in our case too. This is similar to checking for thermodynamic consistency in the case of medium effects in systems with medium dependent effective quark masses [166]. Such medium effects have also been considered in calculating the bulk viscosity in interacting strange quark matter [170]. As has been pointed out in ref. [166], changes due to these special requirements affect the mass radius relationship of compact objects negligibly. They are only pertinent for the phase transition dynamics. The question of thermodynamic self consistency for a first order phase transition in a non-constant pressure has been discussed in detail in ref. [171]. For our case, we have performed the Maxwell construction along the phase boundary and also taken into account the conservation of various charges. The expression of the bag constant has been obtained after considering the energy difference between the two phases. Thus the special requirements for maintaining thermodynamic consistency are taken care of. Moreover, finally we are interested in the mass radius relation of the compact objects and hence the extra constants required to maintain thermodynamic consistency will have a negligible effect on our final results.

In our model, we consider the EoS in the limit of high baryon density. As was shown by Leonidov [163], in this limit, the thermodynamical quantities can be written as the sum of two parts. One part gives the zero temperature contribution and the second part gives the finite temperature contribution. When we consider the s quark to be massive, these contributions change significantly. Hence in the next subsections, we will first consider the quarks to be massless and obtain the mass and radius relations for the three flavor case. Then we will consider the strange quark to be massive and obtain the mass and radius relations for that case separately. We have found that the plasma is meta stable for the two flavor case.

#### 7.2.1 Case 1: Two massless flavors (up and down)

We first look at the two flavor u and d case. We consider the core to be charge neutral. Generally in the early universe the charge neutrality is maintained by the leptons but in this case we do not consider the leptons. To maintain the charge neutrality we therefore assume that the number of d quarks is twice that of the u quarks. As has been shown in ref.[172], the plasma stability parameters are only weakly dependent on lepton contributions in the case of the two flavor plasma so the lepton contribution to the charge neutrality can be ignored. The general way to construct the EoS is to describe the EoS in each of the two phases and then perform the Maxwell construction to join the two phases along their common boundary. We follow Leonidov's approach in modifying the bag constant. This means that at the phase boundary the following equation must hold,

$$\frac{S_q - \frac{\partial B(\mu, T)}{\partial T}}{n_q - \frac{\partial B(\mu, T)}{\partial \mu}} = \frac{S_H}{n_H}$$
(7.3)

Here S is the entropy and n the number density, the suffix "q" denotes the thermodynamical variables in the quark phase, while the suffix "H" denotes the same variables in the hadronic phase. The modified bag's constant in our case is the following,

$$B(\mu, T) \simeq B_0 + \mu^2 T^2 - \frac{\mu^4 T^2}{\theta_H^2}$$
 (7.4)

where  $\theta_H = (\mu^2 - m_H^2)^{1/2}$  and  $m_H$  is hadron mass.

While the core consists of the quarks, the other side of the boundary called the crust is in the hadronic phase. Though we have mentioned right at the beginning that we are interested in the EoS for the cores of the stars and the outer crust is considered to be negligible, we do have to specify the nature of the outer crust. In this case, the outer crust which is in the hadronic phase consists of a non-interacting neutron - pion gas. The hadronic partition function, is based on a hard core neutron neutron repulsion. Due to this, it is necessary to divide any thermodynamic quantity for point like particles by a volume factor [163]. The volume factor is given by,  $(1 + \frac{4}{3}\pi r_n^3 n_H)$ , where  $r_n$  is the radius of the neutrons and  $n_H$  is the number density of the hadrons. For the case of the two flavor massless quarks, a change in the volume factor does not give any significant change in the results. However, in the case of three flavor massless quarks, a change in the volume factor affects the values of the chemical potential of the quarks and the value of the corresponding bag constant for which the star is stable. The important quantity that can bring in a change in the volume factor is the radius of the neutron. We will discuss this later when we discuss the three flavor massless case. As mentioned in the introduction, we need to check the gravitational stability of the massive objects. For

this we need to solve the TOV equations using the pressure obtained from our EoS. So the pressure, in our case turns out to be,

$$P = \frac{1}{3}(\epsilon - 4B_0) - \frac{1}{3} \left( \frac{2\mu^4 T^2}{\theta_H^2} - \frac{18\mu^6 T^2}{\theta_H^4} \right). \tag{7.5}$$

Apart from the gravitational stability, to form a stable plasma state the energy per baryon number of the quark gluon plasma has to be calculated. For the two flavor quark matter at low pressures, the energy per baryon number should be larger than that of the nuclear plasma (which is around 940 MeV) and also a  $^{56}Fe$  crystal which has the minimum binding energy per nucleon [172, 173]. Substituting all these constraints, we find the chemical potential is constrained between 313.5 MeV to 331 MeV. The bag constant is also constrained within a narrow range between 149 MeV to 154 MeV. The temperature does not have much effect on these constraints as long as it is below 1 MeV. The maximum size, can be obtained for the minimum bag constant and highest value of chemical potential. The baryon density turns out to be  $0.32/fm^3$ . However, the plasma in this case is meta stable and one cannot give a definite mass and radius to this plasma, hence we introduce the strange quark and look at the plasma composed of three massless quark flavors.

#### 7.2.2 Case 2: Three massless flavors (up, down and strange)

The plasma with three massless flavors of quarks can be treated as a degenerate Fermi gas with equal numbers of quarks of different flavors. This and the fact that the plasma is beta equilibrated gives the necessary charge neutrality to the plasma. The only change in the expressions for the bag constant and the pressure come from the fact that the number of flavors have increased to three. The number densities of the three different quarks may thus be different and so can their chemical potentials. We therefore use the suffix u, d, s to denote the chemical potential of the three flavors. As of now the assumption of  $\mu_u = \mu_d = \mu_s$  holds as all the flavors are considered to be massless. The bag parameter becomes,

$$B(\mu, T) \simeq B_0 + \frac{3}{2} \left( \frac{1}{9} \mu^2 T^2 - \frac{1}{81} \frac{\mu^4 T^2}{\theta_H^2} \right)$$
 (7.6)

and the corresponding pressure equation is given by,

$$P = \frac{1}{3}(\epsilon - 4B_0) - \frac{1}{2} \left( \frac{2\mu^4 T^2}{\theta_H^2} + \frac{18\mu^6 T^2}{\theta_H^4} \right)$$
 (7.7)

Here  $B_0$  is the bag parameter at T=0. For this case too, we have to check the stability of the plasma. Since the number of flavors has increased, the energy per baryon will also change accordingly. The preferred state of a stable plasma comprising of all the quark flavors should have energy per baryon less than that the nuclear energy of 940 MeV so that the plasma does not hadronize. Similarly, the energy per baryon should be less than the binding energy of the  $^{56}Fe$  crystal. The lower energy per baryon will make the quark gluon plasma the preferred state for the bulk matter [172, 173]. As mentioned before, the stability of the plasma puts a constraint on the values of the chemical potential as well as the bag constant. We see that the stability of the plasma increases with smaller bag constant values.

Again similar to the previous case, since the hadronic phase is also present, there are some parameters in the hadronic phase which also contribute to the stability of the plasma. We find that in the three flavor case, the radius of the neutron which contributes to the volume correction in the neutron - pion gas does change the stability values of the core pressure. This is because we have equated the pressure of the hadronic phase and the quark phase to obtain the bag constant. We have plotted the pressure in the core for different values of bag constant for different values of the neutron radius for which the quark plasma is stable in fig 7.1. As can be seen from the figure, the increasing bag constant decreases the pressure in the core.

The graph further shows that the the core pressure rises abruptly to rather high values once the neutron radius becomes 0.66fm. Beyond this radius, we notice all the curves overlap. We have checked till 1fm. Below 0.6 fm, there is a rise in the pressure with increase in the radius of the neutron, however above 0.66fm, the pressure in the hadronic phase ceases to be dependent on the volume factor. The neutron radius from scattering experiments is in this range for nuclear forces at short distances [174]. There have also been some work on the correlation of the neutron radius of  $^{208}Pb$  and the radius of a neutron star [175]. Generally, it has been observed that a larger value of neutron radius generates a stiffer EoS with a larger pressure. We have observed the same thing in our model except that in our model there is a critical radius beyond which the neutron radius does not affect the stiffness of the EoS anymore.

We thus find that the change in the volume corrections to the non-interacting neutronpion gas affect the limiting values of the pressure and the density at the core. In all the cases, we have considered we have kept the hadronic phase to be the same as we are interested in the quark phase. We find that as long as the hadronic part consists of a neutron - pion gas, the only parameter that affects the stability of the plasma is the radius of the neutron through the volume corrections. Though this effect also occurs when the strange quark mass is taken into account, the dominance of the strange quark

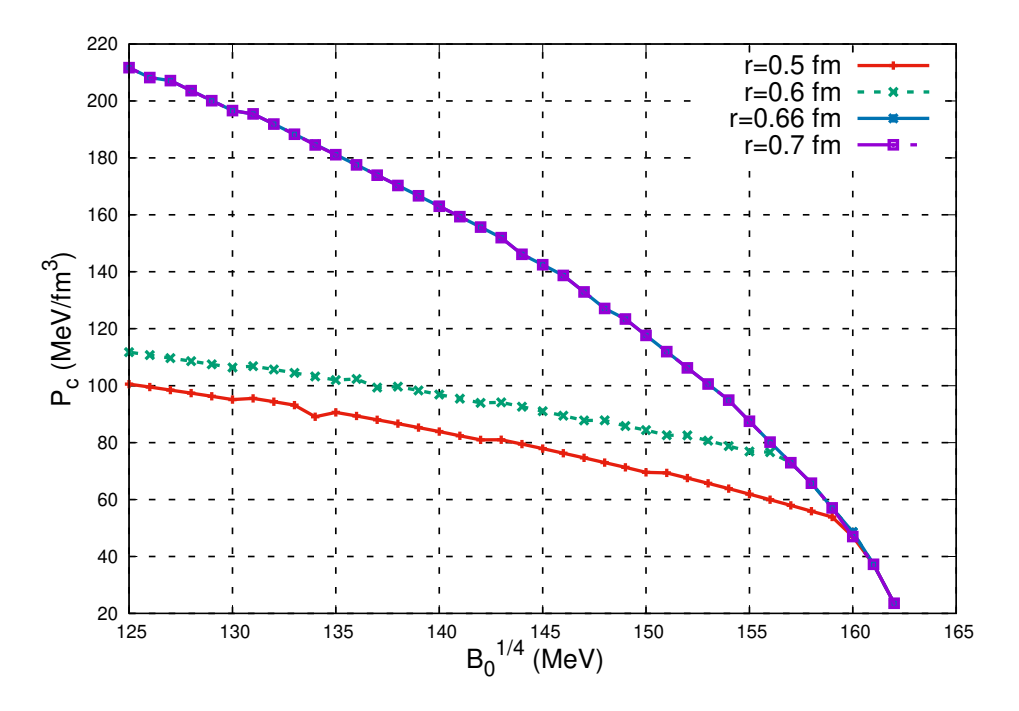


Figure 7.1: The graph shows the core pressure for stable masses at different bag constants for different values of the neutron radius. Beyond 0.66 fm all the curves overlap.

mass leads to very small variations in the core pressure due to the change in the volume corrections.

#### 7.2.3 Case 3: Massless up, down and massive strange quarks

If we consider the s quark to be massive then we cannot have  $\mu_u = \mu_d = \mu_s$ . So it is important to consider the first order correction terms to the temperature and the entropy. As in the previous case, strange matter is modelled as a Fermi gas of up, down, and strange quarks. This time the charge neutrality of the system is maintained by the electrons. Weak interactions ( $\beta$  equilibrium) will then lead to  $\mu_s = \mu_d = \mu$  and  $\mu_u + \mu_e = \mu$  [176]. The number densities are related by,  $\frac{2}{3}n_u - \frac{1}{3}n_u - \frac{1}{3}n_s - n_e = 0$ . This means that effectively we are dealing with only two chemical potentials  $\mu_u$  and  $\mu_s$ .

To deal with high baryon densities and low temperatures, finite temperature corrections are added to the zero temperature terms. This means that,

$$P_s \simeq P_s^0 + P_s^1 T^2 + P_s^2 T^4 \tag{7.8}$$

$$n_s \simeq n_s^0 + n_s^1 T^2 + n_s^2 T^4 \tag{7.9}$$

$$S_s \simeq S_s^1 T + S_s^2 T^3 (7.10)$$

The zero temperature terms are given by,

$$P_s^0 = \frac{1}{6\pi^2} (\mu_s \theta_s (\theta_s^2 - \frac{3m_s^2}{2}) + \frac{3m_s^4}{2} ln(\frac{\mu_s + \theta_s}{m_s}))$$
 (7.11)

$$n_s^0 = \frac{2\theta_s^3}{9\pi^2} \tag{7.12}$$

Here  $m_s$  is the mass of the s quark and  $\theta_s = \sqrt{(\mu_s^2 - m_s^2)}$ . The suffix "s" denotes the parts with the finite temperature corrections. At high baryon densities and low temperatures  $\frac{\partial B}{\partial T}$  dominates over  $\frac{\partial B}{\partial \mu}$ , based on that at the phase boundary one can obtain the bag constant as,

$$B(\mu, T) \simeq B_0 + (\mu_u^2 + \mu_d^2 - \frac{2}{3}\mu_s\theta_s)\frac{T^2}{2} - \frac{\mu_s T^2}{2\theta_H^2}(\mu_u^3 + \mu_d^3 + \frac{2}{3}\theta_s^3)$$
 (7.13)

Once the bag constant is obtained the pressure can be expressed as,

$$P = \frac{1}{3} \left(\epsilon - 4B_0 + \frac{4\mu_e^4}{3\pi^2} + \frac{m_s^4}{\pi^2} ln(\frac{\mu_s + \theta_s}{m_s}) - (\mu_u^3 + \mu_d^3 - \frac{1}{3}\theta_s^3)(\frac{\mu_s T^2}{\theta_H^2}) + \frac{\mu_s \theta_s}{2\pi^2} (\theta_s^2 - \frac{3m_s^2}{2}) - \frac{\mu_s^3 \theta_s T^2}{\theta_H^2} - \frac{\mu_s}{2\pi^2} (\mu_s^2 \theta_s + \frac{m_s^2}{2\theta_s (m_s^2 - \mu_s^2)}) + \frac{\mu_s T^2}{2} (\frac{18\mu_s^2}{\theta_H^4} (\mu_u^3 + \mu_s^3 + \frac{2\theta_s^2}{\theta_H^4})))$$

$$(7.14)$$

As we can see apart from the chemical potentials of the u and s quark, the main parameter is the s quark mass. The s quark mass is already constrained by other experiments. So though we do get large stable mass stars with a smaller value of the s quark mass, we do not vary the s quark mass below 90 MeV. Generally this is the lower limit of the s quark mass from various other sources [177]. The temperature is also below 1 MeV. The constraint on the temperature comes as the entropy per baryon number has to be continuous even in the bulk. Increasing the temperature violates this continuity and hence we are constrained to temperatures below 1 MeV. The electron fraction in the core increases in this temperature range reaching a maximum at 1 MeV, consequently the strangeness fraction goes down. So we find that lower the temperature, higher is the strangeness fraction in the core. However, the strangeness fraction saturates to a value of 0.33 and becomes independent of temperature at lower values.

In the previous section, we had seen that some parameters in the hadronic phase also affect the stability of the quark cores. We had found that changes in the volume corrections to the neutron - pion gas cause variation to the core pressure. In this case, the chemical potential of the quarks u and s along with the mass of the strange quark dominate the core pressure. In fact as the chemical potential of the u quark is increased, the electron fraction and the strangeness fraction required for a stable core goes

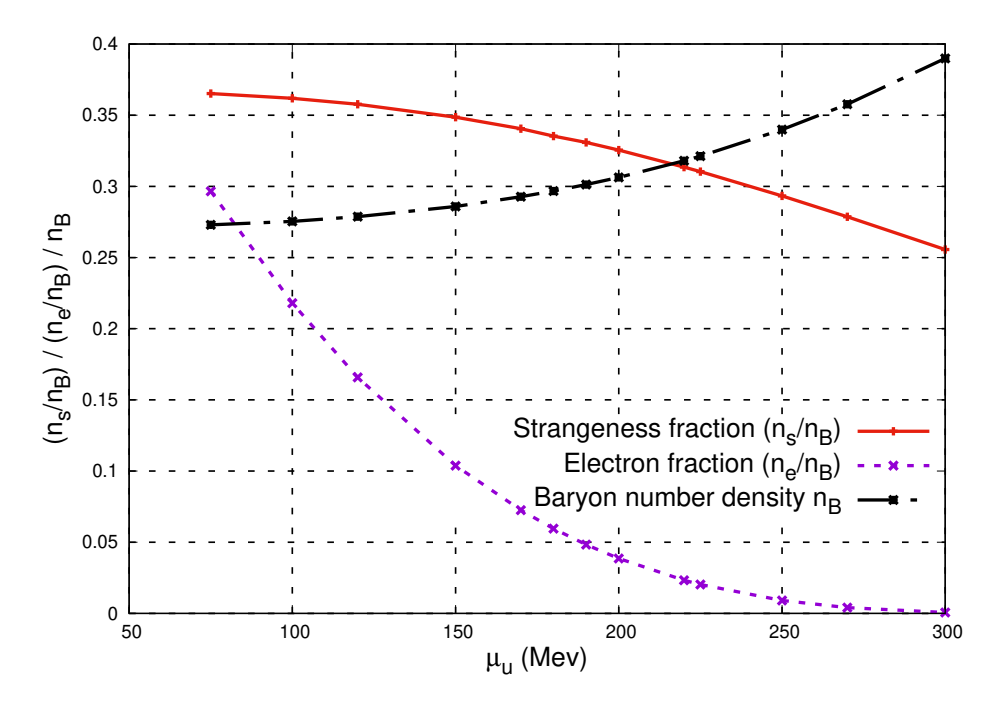


FIGURE 7.2: The rate of change of the electron fraction  $(\frac{n_e}{n_B})$ , the strangeness fraction  $(\frac{n_s}{n_B})$  and the baryon number density  $(n_B)$  with respect to the chemical potential of the u quark.

down while the baryon number density increases to maintain the stability. The rate of increase(decrease) of the electron fraction, the strangeness fraction and the baryon number density has been plotted against the chemical potential of the u quark in fig 7.2. Generally a larger value of the chemical potential of the u quark ( $\mu_u$ ) results in more stable quark cores provided the strange quark mass is on the lower side. This is seen by calculating the energy density of the quark core, which has to be more stable than the  $^{56}Fe$  nucleus. For all the values in fig 7.2, we get stable quark matter. The stability is checked by calculating the energy per baryon in the plasma.

Thus we have found that it is possible to have energetically stable quark matter using three flavors of the quark gluon plasma. As these are massive objects, we know that gravitation plays an important role in establishing the stability of these stars. The macroscopic quantities of mass and radius are thus calculated using the Tolman - Oppenheimer - Volkoff equations [178, 179]. In the next sections, we briefly describe these equations and their solutions.

### 7.3 The Tolman - Oppenheimer - Volkoff equations

We consider the TOV equations for a spherical and isotropic metric. We assume that the core of the quark star has a uniform density in all the directions. The TOV equations

are then given by,

$$\frac{dP}{dr} = \frac{G}{r} \frac{(\epsilon(r) + P(r))(M(r)c^2 + 4\pi r^3 P(r))}{(rc^2 - 2GM(r))}$$
(7.15)

and

$$\frac{dM}{dr} = \frac{4\pi r^2 \epsilon(r)}{c^2} \tag{7.16}$$

where the mass density  $\rho(r) = \frac{\epsilon(r)}{c^2}$  and c (cm/sec) is the speed of light and  $\epsilon(r)$  is the energy density of the plasma in MeV. The TOV equations are solved numerically with appropriate boundary conditions to obtain the mass distribution of the stars. The solution also gives us the gravitationally allowed values of the mass and radius of the stars. We solve the TOV equations numerically for the high baryon density regime. We find that stable stars are possible for various values of the bag constant. Detailed results and graphs are shown in the next section. We have only given plots for the parameters which give a mass/radius diagram consistent with experimental results. Though, we have done a through study of a large parameter space but we have only presented those results which are consistent with experimental observations.

Apart from the mass radius ratio, we would also like to look at a direct observable that is affected by the compactness of the star. One such observable is the surface gravitational redshift values of the stars. It is a parameter that corresponds to the redshift experienced by a radially propagating photon travelling from the star's surface to infinity. It can be directly calculated from the mass - radius ratio of a star.

$$z_s = \left(1 - \frac{2GM}{Rc^2}\right)^{-1/2} - 1\tag{7.17}$$

For all the cases, where we have a stable configuration from plasma stability as well as gravitational stability, we have calculated the gravitational red shift values of the stars. In the next section, we will show that the surface gravitational redshift values obtained for the strange stars in our case are consistent with experimentally observed gravitational red shift values for different strange star candidates.

#### 7.4 Results

# 7.4.1 Mass-radius ratios with three massless flavors (up, down and strange)

Since the two flavor plasma only gives us a metastable plasma we do not solve the TOV equations for the two flavor plasma. In the case of the three massless flavors of quarks

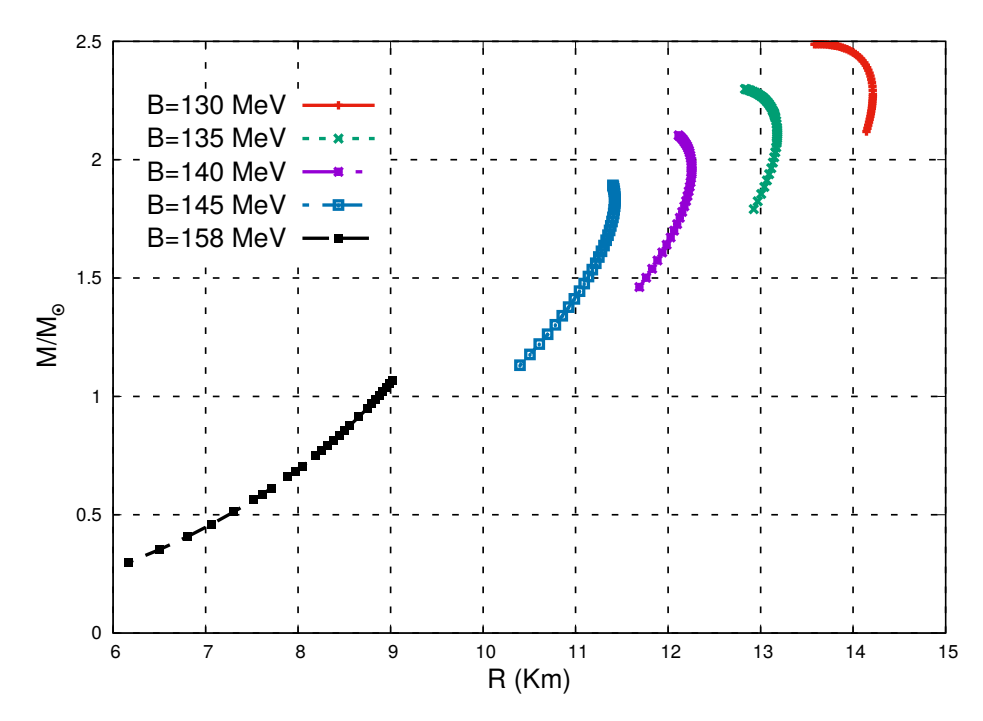


Figure 7.3: Graph of the mass M (in solar masses) Vs R obtained from the stiff EoS at different bag constants for massless quarks.

we vary the various parameters and do a systematic search to put constraints on the various parameters of the model.

For massless quarks, we do get large mass values close to  $2.2M_0$  with a radius of 14 km. This occurs for lower bag constants. The strange quark is considered massless here and therefore we get the mass values greater than two solar masses. The recent measurements of PSR J0740+6620 from NICER [180] is in this region and would hold for bag constants below 145 MeV. We have plotted only one value above this to show the limits of the bag values that are possible. We then obtain the surface gravitational red shift values for these large mass stars and the resultant plot is shown in fig 7.4.

As seen from fig 7.4., we obtain redshift values of 0.4 for massive stars of  $2M_0$  or higher. It has been predicted that PSR J0348+0432 has a radius of about 12 kms and mass of  $2.1M_0$  [149–151] with a red shift value of 0.4. So our model with massless quarks is able to reproduce the mass - ratio required to have stable quark stars as seen from the surface red shift data. The combined plots constrained by the PSR J0740+6620 data and the PSR J0348+0432 data constrain the bag constant for large mass stars to be around 130 - 140 MeV.

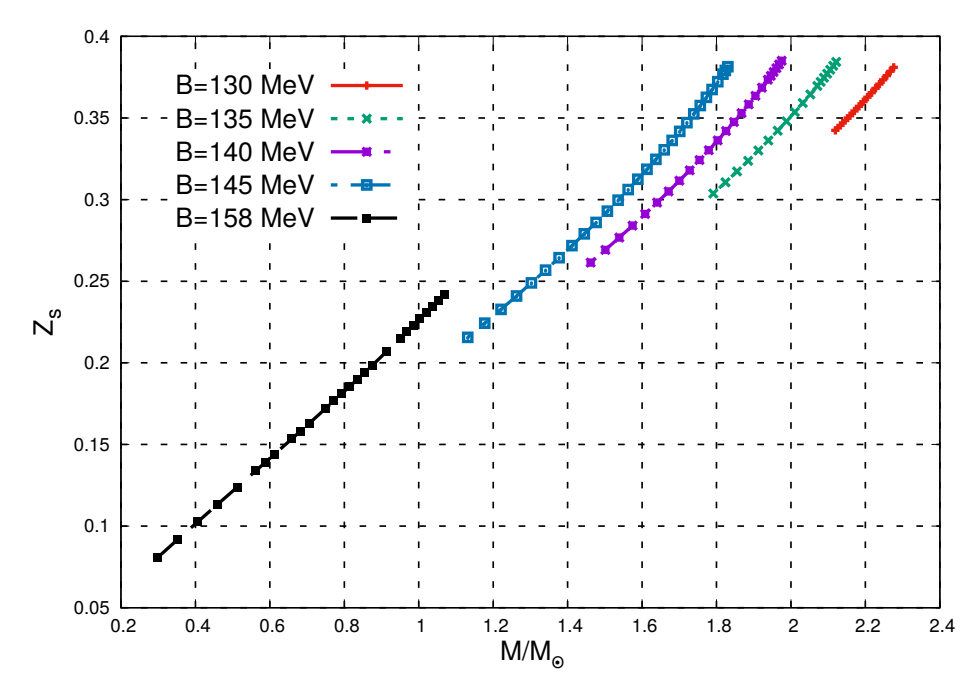


Figure 7.4: Graph of the gravitational red shift values for stars with cores having massless quarks.

#### 7.4.2 Mass-radius ratios for the massive strange quark

We now present the results of the TOV equations with the pressure obtained from the EoS corresponding to the massive strange quarks. The mass of the quark puts a constraint on the quark chemical potentials. We plot the mass radius ratio for stable stars for two different masses of the strange quark. Since we know that the larger mass stars would occur in the range of bag constant values between 130 - 140 MeV, we give the results for two values within this range.

We can see from the figures 7.5 and 7.6, that larger mass stars are obtained with smaller values of the strange quark mass. For a star with massive strange quarks in it's core, the compactness of the star is constrained by the strange quark mass. The plot of the gravitational redshift values for different masses of the stars in given in fig 7.7 and fig 7.8.

Here since we have constrained the strange quark value to a lower limit of 90 MeV, we do not get massive stars with masses greater than  $2M_0$ . We can get such values if we lower the strange quark values to around 75 MeV. We find that stars with masses of the order of  $1.5M_0$  would typically have surface red shift values around 0.22. This has also been seen in other models [149–153]. Thus the observational constraints given by red shift values are all satisfied with different values of strange quark mass in our model. We now discuss some observational data in support of our model.

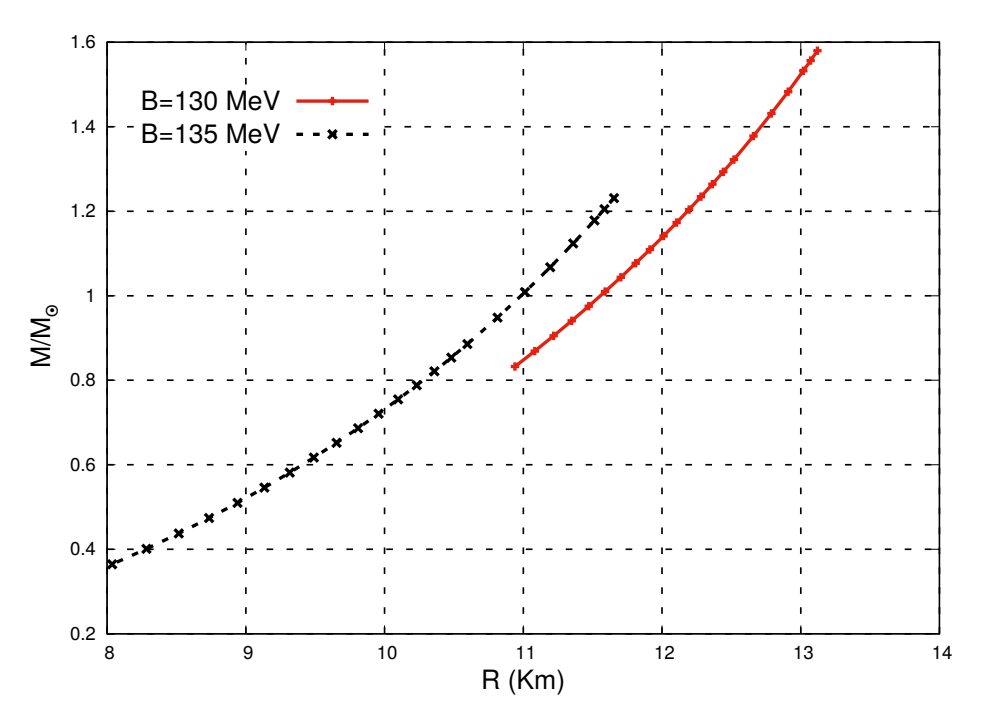


FIGURE 7.5: Graph of mass M (in solar masses) vs radius R ( in kms) of stars at different bag constants for  $m_s=100$  MeV,  $\mu_u=100$  MeV for a core with u-d-s massive plasma

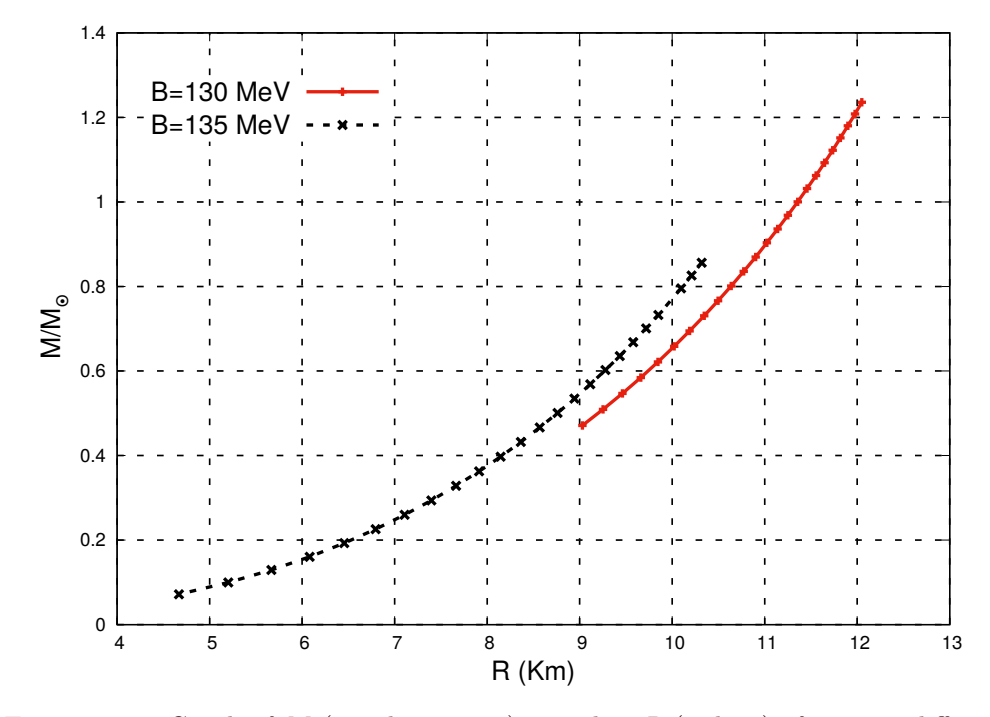


FIGURE 7.6: Graph of M (in solar masses) vs radius R (in kms) of stars at different bag constants for  $m_s = 150$  MeV,  $\mu_u = 100$  MeV for core with a u-d-s massive plasma

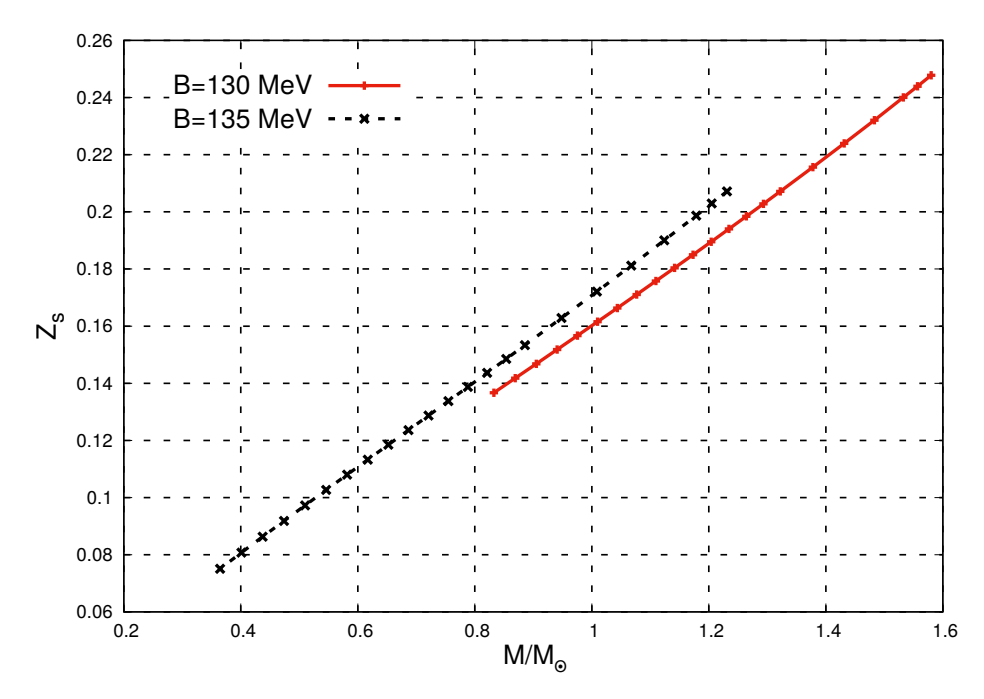


Figure 7.7: A plot of the gravitational redshift values with a core having a massive strange quark of mass  $m_s=100~{\rm MeV}$ 

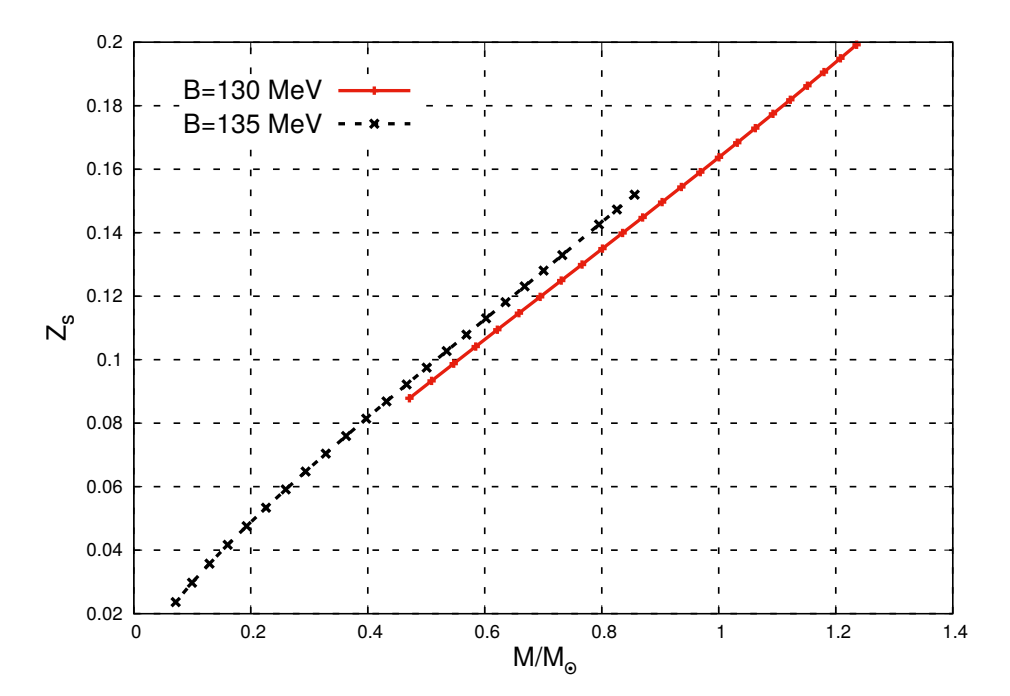


Figure 7.8: A plot of the gravitational redshift values for a core having a massive strange quark of mass  $m_s=150~{\rm MeV}$ 

There are many observational instances of stars with these kind of parameters. We discuss only some of them in this section. The XTE J1739-285 has a mass of 1.51 solar mass and a radius of 10.9 km [181]. It is sometimes referred to as a quark star and sometimes as a neutron star. Recent observational data for XTE J1739-285 has been made available by the NICER collaboration. It is rapidly spinning and has a red shift ranging from 1.8 to values of 2.4 depending on its radius. Our model for the quark star with a massive strange quark of 100 MeV and bag constants between 130 - 135 MeV gives red shifts in this range.

The low mass X-ray binary, EXO 0748-676 has a mass of 2.1 solar masses and a radius of 13.8 km [182]. It has a red shift value of 0.35. There have been speculations that this neutron star has a color flavor locked phase in its core. In our model, the EXO 0748-676 can be a quark star with a bag constant of 135 MeV. So it is possible that the EXO 0748-676 is a quark star with a very thin crust, the core having been formed due to an isentropic phase transition. This source has been monitored over a long time and there are other observations which can be used to further understand it's structure.

We have already mentioned the massive stars like PSR J1614-2230; the gravitational redshift values of these stars are in the range 0.41-0.5. From our studies we have obtained such high redshift values for the quark plasma with massless quarks. As we have mentioned before the mass - radius ratio and the red shift values depend crucially on the masses of the strange quark. The recent NICER results of PSR J0030+0451 [183, 184] is also consistent with the strange quarks masses of 100 MeV and a bag constant of 130 MeV.

All these candidates are being extensively studied by various telescopes. As we have just discussed, our model is able to accommodate quite a few of these candidates for reasonable values of the bag constant and the strange quark mass. While lower strange quark masses give more stability to the cores, a strange quark mass of 100 MeV gives us reasonable values of gravitational redshift compatible with experimental observations. The range of the bag constant is found to be between 130-140 MeV. This is a very narrow range. We can hope to narrow it down further when we consider the spinning motion of the objects. The spinning of the stars though a well known phenomenon has not been studied in this work.

### 7.5 Summary

We would like to conclude this chapter by summarizing our results on the cores of the hybrid/neutron stars. Basically we have suggested an extension of the bag model where

the bag constant is dependent on the chemical potential and the temperature. Such a model has been used previously by Leonidov et. al. for two massless flavors of quarks in the context of heavy ion collisions. As has been discussed in detail in this chapter, we have extended the Leonidov's model to three flavors of quarks by including the strange quark. In the model we propose, an isentropic phase transition takes place and this phase transition can lead to a stable quark core inside the star. The presence of the massless strange quark increases the stability of the plasma. This leads to stars of larger masses and sizes. The model we have proposed has quite a lot of parameters. Some of these parameters are already severely constrained by ongoing experiments. The best example of this is the strange quark mass. The strange quark mass is already constrained by different experiments. So though the stability of the core increases with decreasing value of the strange quark mass, we are constrained to keep the value above 90 GeV. The most stable core is obtained for a massless strange quark. There have been cases where the strange quark mass was taken as low as 80 MeV [185]. In this chapter, we have discussed the detailed systematic study we have done for all the parameters of the model. We have also found different limitations to the values of these parameters. The stability of the plasma limits our bag constant to the lowest value of 130 MeV.

The mass radius ratio determines the surface redshift of a star. The surface redshift of these stars is measured by several experimental collaborations and is a good measure of constraining different models of the stars. We have therefore determined the surface redshift of stars of various masses using our model. We found that the model is successful in reproducing the surface redshift of stars like PSR J1614-2230, PSR J0348-0432, XTE J1739-285 and EXO 0748-676. The observational values basically put a stringent constraint on the bag value of our model. The bag values are constrained to lie between 130-140 MeV. These constraints are well within the purview of the recent experimental results released by NICER. So an isentropic phase transition in the core of a neutron star or a hybrid star can lead to massive stars with a large radius already observed by several experimental groups.

In the end we would like to mention, that nowhere in our model have we taken the rotational aspects of the stars into account. As is well known in the literature, rotational effects of these stars affect various parameters of the bag model. We have not considered this in our current study. Though the rotation will bring additional constraints on the different parameters, the main results will be unaffected. We strongly believe that the mass of the strange quark will play an important role in the EoS of the core of the neutron/hybrid star. Our work also established that it is also possible to have a stable quark gluon plasma bulk phase in the core of a massive star with no other exotic phases.

## Chapter 8

# **Summary and Conclusion**

In this chapter, we will finally wrap up the discussions and conclude them with a short summary and remarks on the work done throughout the thesis. The origin and evolution of the seed magnetic field is still a fundamental question in cosmology. The current magnetic field in the universe is believed to be the magnification of the seed magnetic field of the early universe. There are density inhomogeneities which are generated in the early universe. They can help to generate the seed magnetic field in the early universe. Density inhomogeneities are one of the reasons for all the large scale structure in the universe. The diffusion of particles are also important in the early universe. Apart from these, density inhomogeneities play an important role in the nucleosynthesis calculations. In this thesis, we have talked about density inhomogeneities and phase transition and their consequences in the context of the early universe.

We have begun our discussion by discussing the background of our work. In the first chapter, we have looked at the history of the early universe. We have talked about the Big Bang model and the thermodynamic history of the universe. There we have discussed about the phase transition that took place in the plasma of the early Universe. As a consequence of these symmetry breaking phase transition, topological defects arise in the present universe. This produce density fluctuations in the plasma. Then, we briefly discuss about the primordial fluctuations and the magnetic fields.

Next, we have explored the phase transitions in the early universe. We have given a small review of the symmetry breaking phase transition from the field theoretic point of view. These phase transitions generate topological defects. We have talked about these defects. As we have mostly worked in the QCD temperature scale, so we have ended the discussion on phase transition with a discussion on quark-hadron phase transition and its consequences.

Then we have proceeded to describe the density fluctuations. We have discussed the importance of studying density inhomogeneities in the context of the early universe cosmology. These density inhomogeneities can generate large scale structure. Topological defects can also generate density inhomogeneities in the plasma. So we have given a brief review of cosmic string and how the density inhomogeneities can be generated by a cosmic string. We have talked about the generation and evolution of baryon inhomogeneities in the plasma to highlight their importance in the context of the early universe.

After this, we have moved on to study the decay of the baryon inhomogeneities in the early universe. Baryon inhomogeneities can be generated by first order phase transition. Generally early universe plasma has high electron density. But for certain scenarios, like the collapsing Z(3) domain walls we can have large strange quark density in some regions in the plasma. Those regions will have high muon density. There are other particle decay mechanisms in the plasma which decays into muon. Due to these processes we can have higher muon density than the electron density in some inhomogeneous regions in the plasma. These inhomogeneities will decay gradually due to diffusion. Here we have studied the decay of inhomogeneities in an expanding as well as the non-expanding universe to understand their effects on the subsequent evolution of the universe. If the size of the inhomogeneities is small, then the stationary universe consideration to understand the decay will not affect the nature of the decay. But for large inhomogeneities, we have to consider the expansion factor. Inhomogeneities that have a large number of strange quarks, will be rich in muon density. But, at low temperature muon density is very low. Therefore, we have analyzed the decay of these inhomogeneities for temperature up to 100 MeV. From the study of the stationary universe, we have shown that the inhomogeneities in a muon rich plasma are decaying faster than the inhomogeneities in the electron rich plasma. So, considering muon for the decay calculation is changing the nature of inhomogeneities. Hence, any process that accumulates more strange quarks than the other quarks will need to generate large baryon inhomogeneities in order to have an impact on nucleosynthesis calculations. Again inhomogeneities, which have large number of strange quarks also generate a larger number of muon neutrinos with respect to the electron neutrinos. So, we have analyzed the neutrino degeneracy parameter too and there is a possibility of having large muon neutrino degeneracy parameter. As we know, the lithium abundance problem is still not solved. The theoretically calculated abundance does not match with the observed data. We have discussed about the modification in the lithium and helium abundance in the context of the stationary universe. This large muon neutrino degeneracy results in higher lithium abundance than the observed lithium abundance.

Density inhomogeneities can be generated at any time of the universe i.e. electroweak scale, QCD scale etc. All off these inhomogeneities will not survive up to the next phase transition or up to the nucleosynthesis epoch. Here, we have analyzed the decay of inhomogeneities in an expanding universe scenario. Inhomogeneities generated in the electroweak scale may contribute to the quark hadron phase transition dynamics. The order of amplitude of these inhomogeneities have to be greater than 10<sup>5</sup> to be present at the time of the quark hadron phase transition. But most of the inhomogeneities generated in the electroweak scale has order of magnitude less than 10<sup>4</sup>. Therefore, the inhomogeneities generated due to the electroweak phase transition would be wiped out before the QCD phase transition. Next, we have looked into the decay of baryon inhomogeneities generated in quark hadron epoch. The muon density of the plasma will be less after 100 MeV temperature. We have analyzed the decay by dividing whole temperature scale into two parts. Hence up to 100 MeV temperature we have studied the decay for a muon rich plasma and below that temperature analyzed it for the electronic plasma. As the orders of magnitude of the inhomogeneities generated in the QCD epoch decay by 5-6 order, they can survive up to nucleosynthesis. Therefore, we have shown that these electroweak phase generated inhomogeneities will not survive up to the nucleosynthesis, but hadronic phase generated inhomogeneities will survive. Large scale baryon overdensities generated by the collapsing domain walls and the other topological defects during the phase transition will survive up to the nucleosynthesis epoch. We have restricted the minimum order for the amplitude of those inhomogeneities. This will also help to understand which inhomogeneities we can consider for the nucleosynthesis calculations. Thus constraints can be obtained on the various models of the inhomogeneity generation in the early universe.

The other problem that density inhomogeneities can contribute to is in the generation of primordial magnetic fields in the early universe. There can be many sources of magnetic field generation like, cosmological phase transition and topological defects (cosmic strings, domain walls etc.). Here, we have proposed a completely new method of generating the seed magnetic field in the early universe. We have investigated how density inhomogeneities generated by a moving cosmic string can give rise to a seed magnetic field in the early universe. A neutral density current indirectly generates the magnetic field. Cosmic strings once produced will always be there in the plasma and they will always move throughout the plasma. So, this model can be valid throughout the temperature scale under the proper conditions. Here, we have talked about density inhomogeneities and magnetic field generation for an Abelian Higgs string system. The motion of cosmic strings gives rise to wakes behind them. For a specific value of energy, angular momentum and linear momentum, particles have closed orbits around the Abelian Higgs cosmic string. As a result, particles will be trapped close to the string.

We have studied neutrinos in the wakes of Abelian Higgs cosmic strings. As neutrinos have mass, for definite values of angular momentum, linear momentum, and energy, they will rotate in closed orbits around the string. This rotating neutrinos will generate a neutrino current. This current acts as a cross-perturbation across the cosmic string wake. Therefore, there will be the neutrino-electron interaction in the plasma. This two fluid description of the plasma leads to the electron current, generated in the plasma. This perturbation together with the high Reynolds number of the plasma generates a seed magnetic field in the wake of the cosmic string. Particles around moving cosmic strings are subjected to generate a velocity kick towards the string. This velocity kick enhance the current in the wake region. The neutrino current density is oscillatory in nature and depends on its distance from the string. This neutral current leads to the neutrino density gradients in the plasma. Electron gradients generated by these neutrino density gradients give rise to the magnetic fields. We have done an order of magnitude estimation of this seed magnetic field using the Biermann battery mechanism. Here, we are getting a magnetic field of the order of 10<sup>13</sup> Gauss at around 200 GeV temperature scale. This order is smaller than the equipartition magnetic field at that time, which is around  $10^{26}$  Gauss. As the Reynolds number of the plasma is very high in the plasma, this magnetic field value can be magnified up to the equipartition magnetic field value.

Since we have looked into the quark hadron phase transition, we have also discussed about the phase transition in a compact object. Modelling higher massive stars is an ongoing challenge in cosmology. Here, we have successfully modeled some higher massive compact star. These compact stars have a very high baryon density. We have done our calculations for the high baryon density regime. For a high baryon dense system the bag model is one of the models that give rise to a phase transition from quarks to hadrons. It predominantly gives a first order phase transition in QCD, and has been used previously to model such compact objects. A density dependant bag model has been used extensively to model the compact stars. In our case, we have considered a bag constant dependant on temperature and chemical potential, which is an extension of the original bag model. Previously in literature, for bag constant calculation strange quark chemical potential has not been considered. But here we have taken into account the strange quark potential for bag constant derivation. We have studied how this extended bag model can lead to stable massive stars that have been observed recently. This modified bag model can lead to an isentropic phase transition in the core of the neutron star. Here, we have calculated the Maxwell construction along the phase boundary and have also taken into account the conservation of various charges. With decrease of the bag constant, the stability of the quark matter increases. We have found that the stability of the plasma and mass of the compact stars depends on both the bag constant and the mass of the strange quark. As we can calculate the surface redshift value of

the stars from the mass-radius ratio, so we have obtained the redshift values for both massless and massive strange quark stars. Next, we have matched the mass radius and the redshift data from our model to some of the experimentally observed data and it is quite consistent with our model.

In conclusion, in this thesis we have studied certain aspects of the density inhomogeneities and the phase transition in the early universe. Our main motivation is to study the consequences of density inhomogeneities and phase transitions that have occurred in the early universe and see whether they will lead to any observational consequences. We have studied the decay of density inhomogeneities in the electroweak and the QCD scale. Our studies indicate that electroweak inhomogeneities can not be constrained by observable data, but inhomogeneities generated at QCD scale can be constrained by observable data. We have also studied a unique way of generating seed magnetic field in the early universe. The seed magnetic field is generated from inhomogeneities in cosmic string wakes. Finally, we have analyzed the first order QCD phase transition in the context of compact stars, where the bag constant was dependant on the temperature and the chemical potential. Our study indicates the cosmological density fluctuations have important consequences in early universe cosmology. More detailed studies of these will yield better understanding of the history of the evolution of the universe.

- [1] A. Mégevand and F. Astorga, "Generation of baryon inhomogeneities in the electroweak phase transition," Phys. Rev. D 71 (Jan, 2005) 023502.
   https://link.aps.org/doi/10.1103/PhysRevD.71.023502.
- [2] B. Layek, A. P. Mishra, A. M. Srivastava, and V. K. Tiwari, "Baryon inhomogeneity generation in the quark-gluon plasma phase," Phys. Rev. D 73 (May, 2006) 103514. https://link.aps.org/doi/10.1103/PhysRevD.73.103514.
- [3] R. H. Brandenberger and N. Turok, "Fluctuations from cosmic strings and the microwave background," Phys. Rev. D 33 (Apr, 1986) 2182-2195. https://link.aps.org/doi/10.1103/PhysRevD.33.2182.
- [4] J. Traschen, N. Turok, and R. Brandenberger, "Microwave anisotropies from cosmic strings," Phys. Rev. D 34 (Aug, 1986) 919–930. https://link.aps.org/doi/10.1103/PhysRevD.34.919.
- [5] E. W. Kolb and M. S. Turner, The Early Universe, vol. 69. 1990.
- [6] E. Hubble, "A relation between distance and radial velocity among extra-galactic nebulae," Proceedings of the National Academy of Sciences 15 (1929) no. 3, 168–173, https://www.pnas.org/content/15/3/168.full.pdf. https://www.pnas.org/content/15/3/168.
- [7] F. Hoyle, "A New Model for the Expanding Universe," Monthly Notices of the Royal Astronomical Society 108 (10, 1948) 372-382, https://academic.oup.com/mnras/article-pdf/108/5/372/8073757/mnras108-0372.pdf. https://doi.org/10.1093/mnras/108.5.372.
- [8] H. Bondi and T. Gold, "The Steady-State Theory of the Expanding Universe," Monthly Notices of the Royal Astronomical Society 108 (06, 1948) 252-270, https://academic.oup.com/mnras/article-pdf/108/3/252/8076977/mnras108-0252.pdf. https://doi.org/10.1093/mnras/108.3.252.

[9] J. Kanipe, "The pillars of cosmology: a short history and assessment," in Plasma Astrophysics and Cosmology, pp. 109–118. Springer, 1995.

- [10] A. A. Penzias and R. W. Wilson, "A measurement of excess antenna temperature at 4080 Mc/s.," The Astrophysical Journal 142 (1965) 419–421.
- [11] P. Peebles, "Penzias & Wilson's discovery of the cosmic microwave background," The Astrophysical Journal **525** (1999) 1067.
- [12] A. H. Guth, "Inflationary universe: A possible solution to the horizon and flatness problems," Phys. Rev. D 23 (Jan, 1981) 347-356. https://link.aps.org/doi/10.1103/PhysRevD.23.347.
- [13] E. Witten, "Cosmic separation of phases," Phys. Rev. D 30 (Jul, 1984) 272-285. https://link.aps.org/doi/10.1103/PhysRevD.30.272.
- [14] E. M. Lifshitz, "On the gravitational stability of the expanding universe," Zhurnal Eksperimentalnoi i Teoreticheskoi Fiziki 16 (1946) 587–602.
- [15] J. M. Bardeen, "Gauge-invariant cosmological perturbations," Phys. Rev. D 22 (Oct, 1980) 1882-1905. https://link.aps.org/doi/10.1103/PhysRevD.22.1882.
- [16] K. Jedamzik and G. M. Fuller, "The evolution of nonlinear subhorizon-scale entropy fluctuations in the early universe," The Astrophysical Journal 423 (Mar, 1994) 33. http://dx.doi.org/10.1086/173788.
- [17] J. H. Applegate, C. J. Hogan, and R. J. Scherrer, "Cosmological baryon diffusion and nucleosynthesis," Phys. Rev. D 35 (Feb, 1987) 1151–1160. https://link.aps.org/doi/10.1103/PhysRevD.35.1151.
- [18] B. Banerjee and S. Chitre, "Diffusion coefficients of nucleons in the inhomogeneous big-bang model," Physics Letters B 258 (1991) no. 3, 247-250. https://www.sciencedirect.com/science/article/pii/037026939191078A.
- [19] D. Grasso and H. R. Rubinstein, "Magnetic fields in the early Universe," Physics Reports 348 (2001) no. 3, 163–266. https://www.sciencedirect.com/science/article/pii/S0370157300001101.
- [20] K. Subramanian, "The origin, evolution and signatures of primordial magnetic fields," Reports on Progress in Physics 79 (may, 2016) 076901. https://doi.org/10.1088/0034-4885/79/7/076901.
- [21] S. Hutschenreuter, S. Dorn, J. Jasche, F. Vazza, D. Paoletti, G. Lavaux, and T. A. Enßlin, "The primordial magnetic field in our cosmic backyard," Classical

```
and Quantum Gravity 35 (jul, 2018) 154001. https://doi.org/10.1088/1361-6382/aacde0.
```

- [22] E. R. Harrison, "Origin of Magnetic Fields in the Early Universe," Phys. Rev. Lett. 30 (Jan, 1973) 188-190. https://link.aps.org/doi/10.1103/PhysRevLett.30.188.
- [23] T. Vachaspati and A. Vilenkin, "Large-scale structure from wiggly cosmic strings," Phys. Rev. Lett. 67 (Aug, 1991) 1057–1061. https://link.aps.org/doi/10.1103/PhysRevLett.67.1057.
- [24] K. M. Schoeffler, N. F. Loureiro, R. A. Fonseca, and L. O. Silva, "The generation of magnetic fields by the Biermann battery and the interplay with the Weibel instability," Physics of Plasmas 23 (2016) no. 5, 056304, https://doi.org/10.1063/1.4946017. https://doi.org/10.1063/1.4946017.
- [25] S. Sau and S. Sanyal, "Neutrino currents in wakes of cosmic strings," The European Physical Journal C 80 (Feb, 2020). http://dx.doi.org/10.1140/epjc/s10052-020-7734-z.
- [26] J. Schaffner-Bielich, "Signals of the QCD Phase Transition in the Heavens," arXiv preprint arXiv:0709.1043 (2007).
- [27] K. Fukushima and T. Hatsuda, "The phase diagram of dense QCD," Reports on Progress in Physics **74** (2010) no. 1, 014001.
- [28] J. Goldstone, "Field Theories with Superconductor Solutions," Nuovo Cim. 19 (1961) 154–164.
- [29] J. Goldstone, A. Salam, and S. Weinberg, "Broken Symmetries," Phys. Rev. 127 (Aug, 1962) 965-970. https://link.aps.org/doi/10.1103/PhysRev.127.965.
- [30] P. W. Higgs, "Spontaneous Symmetry Breakdown without Massless Bosons," Phys. Rev. 145 (May, 1966) 1156-1163. https://link.aps.org/doi/10.1103/PhysRev.145.1156.
- [31] P. Higgs, "Broken symmetries, massless particles and gauge fields," Physics Letters 12 (1964) no. 2, 132–133.

  https://www.sciencedirect.com/science/article/pii/0031916364911369.
- [32] T. Skyrme, "A unified field theory of mesons and baryons," Nuclear Physics 31 (1962) 556-569. https://www.sciencedirect.com/science/article/pii/0029558262907757.

[33] H. Nielsen and P. Olesen, "Vortex-line models for dual strings," Nuclear Physics B 61 (1973) 45-61. https://www.sciencedirect.com/science/article/pii/0550321373903507.

- [34] A. E. Everett, "Observational consequences of a "domain" structure of the universe," Phys. Rev. D 10 (Nov, 1974) 3161-3166. https://link.aps.org/doi/10.1103/PhysRevD.10.3161.
- [35] Y. B. Zel'dovich, I. Y. Kobzarev, and L. B. Okun, "Cosmological consequences of spontaneous violation of discrete symmetry," Zh. Eksp. Teor. Fiz. 67 (1974) 3-11. https://cds.cern.ch/record/411756.
- [36] T. W. B. Kibble, "Topology of cosmic domains and strings," Journal of Physics A: Mathematical and General 9 (aug, 1976) 1387–1398. https://doi.org/10.1088/0305-4470/9/8/029.
- [37] Y. Zeldovich and M. Khlopov, "On the concentration of relic magnetic monopoles in the universe," Physics Letters B 79 (1978) no. 3, 239-241. https://www.sciencedirect.com/science/article/pii/0370269378902320.
- [38] J. P. Preskill, "Cosmological production of superheavy magnetic monopoles," Physical Review Letters 43 (1979) no. 19, 1365.
- [39] Y. B. Zeldovich, "Cosmological fluctuations produced near a singularity," Monthly Notices of the Royal Astronomical Society 192 (10, 1980) 663-667, https://academic.oup.com/mnras/article-pdf/192/4/663/4029208/mnras192-0663.pdf. https://doi.org/10.1093/mnras/192.4.663.
- [40] A. Vilenkin, "Cosmological Density Fluctuations Produced by Vacuum Strings," Phys. Rev. Lett. 46 (Apr, 1981) 1169–1172. https://link.aps.org/doi/10.1103/PhysRevLett.46.1169.
- [41] R. Brandenberger, A.-C. Davis, and M. Trodden, "Cosmic strings and electroweak baryogenesis," Physics Letters B 335 (1994) no. 2, 123-130. https://www.sciencedirect.com/science/article/pii/0370269394914028.
- [42] M. Trodden, A.-C. Davis, and R. Brandenberger, "Particle physics models, topological defects and electroweak baryogenesis," Physics Letters B 349 (1995) no. 1, 131-136. https://www.sciencedirect.com/science/article/pii/0370269395002146.
- [43] R. Brandenberger, A.-C. Davis, T. Prokopec, and M. Trodden, "Local and nonlocal defect-mediated electroweak baryogenesis," Phys. Rev. D 53 (Apr, 1996) 4257–4266. https://link.aps.org/doi/10.1103/PhysRevD.53.4257.

[44] T. Prokopec, R. Brandenberger, A. C. Davis, and M. Trodden, "Dynamical breaking of CPT symmetry in defect networks and baryogenesis," Physics Letters B 384 (1996) no. 1, 175–179. https://www.sciencedirect.com/science/article/pii/0370269396006028.

- [45] B. Layek, S. Sanyal, and A. M. Srivastava, "Cosmic string induced sheetlike baryon inhomogeneities at the quark-hadron transition," Phys. Rev. D 63 (Mar, 2001) 083512. https://link.aps.org/doi/10.1103/PhysRevD.63.083512.
- [46] A. Strumia and N. Tetradis, "Bubble-nucleation rates for cosmological phase transitions," Journal of High Energy Physics **1999** (1999) no. 11, 023.
- [47] M. S. Turner, E. J. Weinberg, and L. M. Widrow, "Bubble nucleation in first-order inflation and other cosmological phase transitions," Phys. Rev. D 46 (Sep, 1992) 2384–2403. https://link.aps.org/doi/10.1103/PhysRevD.46.2384.
- [48] L. P. Csernai and J. I. Kapusta, "Nucleation of relativistic first-order phase transitions," Physical Review D 46 (1992) no. 4, 1379.
- [49] K. Johnson, "A field theory Lagrangian for the MIT bag model," Physics Letters B 78 (1978) no. 2, 259–262. https://www.sciencedirect.com/science/article/pii/0370269378900187.
- [50] J. S. Langer, "Statistical theory of the decay of metastable states," Annals of Physics 54 (1969) no. 2, 258–275.
- [51] L. Landau and E. Lifshitz, "Statistical Physics, Course Theoretical Phys., vol. 5," 1999.
- [52] M. S. M. de Sousa and A. A. de Lima, "Applications of the Abelian Vortex Model to Cosmic Strings and the Universe Evolution," in New Ideas Concerning Black Holes and the Universe. IntechOpen, 2019.
- [53] J. R. Gott III, "Gravitational lensing effects of vacuum strings-Exact solutions," The Astrophysical Journal 288 (1985) 422–427.
- [54] W. A. Hiscock, "Exact gravitational field of a string," Phys. Rev. D 31 (Jun, 1985) 3288-3290. https://link.aps.org/doi/10.1103/PhysRevD.31.3288.
- [55] D. P. Bennett and F. R. Bouchet, "High-resolution simulations of cosmic-string evolution. I. Network evolution," Physical Review D 41 (1990) no. 8, 2408.
- [56] J. Silk and A. Vilenkin, "Cosmic Strings and Galaxy Formation," Phys. Rev. Lett. 53 (Oct, 1984) 1700-1703. https://link.aps.org/doi/10.1103/PhysRevLett.53.1700.

[57] T. Vachaspati, "Cosmic Strings and the Large-Scale Structure of the Universe," Phys. Rev. Lett. 57 (Sep, 1986) 1655-1657. https://link.aps.org/doi/10.1103/PhysRevLett.57.1655.

- [58] G. M. Fuller, G. J. Mathews, and C. R. Alcock, "Quark-hadron phase transition in the early Universe: Isothermal baryon-number fluctuations and primordial nucleosynthesis," Phys. Rev. D 37 (Mar, 1988) 1380–1400. https://link.aps.org/doi/10.1103/PhysRevD.37.1380.
- [59] B. Layek, S. Sanyal, and A. M. Srivastava, "Baryon inhomogeneity generation via cosmic strings at QCD scale and its effects on nucleosynthesis," Phys. Rev. D 67 (Apr, 2003) 083508. https://link.aps.org/doi/10.1103/PhysRevD.67.083508.
- [60] M. M. Wygas, I. M. Oldengott, D. Bödeker, and D. J. Schwarz, "Cosmic QCD Epoch at Nonvanishing Lepton Asymmetry," Phys. Rev. Lett. 121 (Nov, 2018) 201302. https://link.aps.org/doi/10.1103/PhysRevLett.121.201302.
- [61] S. Das Gupta, A. Z. Mekjian, and M. B. Tsang, Liquid-Gas Phase Transition in Nuclear Multifragmentation, pp. 89–166. Springer US, Boston, MA, 2001. https://doi.org/10.1007/0-306-47915-X\_2.
- [62] M. Fromerth, I. Kuznetsova, L. Labun, J. Letessier, and J. Rafelski Acta Physica Polonica B 43 (2012) no. 12, 2261. http://dx.doi.org/10.5506/APhysPolB.43.2261.
- [63] D. J. Schwarz and M. Stuke, "Lepton asymmetry and the cosmic QCD transition," Journal of Cosmology and Astroparticle Physics 2009 (nov, 2009) 025–025. https://doi.org/10.1088/1475-7516/2009/11/025.
- [64] D. Schwarz, "The first second of the Universe," Annalen der Physik 12 (2003) no. 4, 220-270, https://onlinelibrary.wiley.com/doi/pdf/10.1002/andp.200310010. https://onlinelibrary.wiley.com/doi/abs/10.1002/andp.200310010.
- [65] P. K. Das, S. Sau, A. Saha, and S. Sanyal, "Decay of baryon inhomogeneities in an expanding universe," arXiv e-prints (Jan., 2021) arXiv:2101.01980, arXiv:2101.01980.
- [66] T. Boeckel and J. Schaffner-Bielich, "A Little Inflation in the Early Universe at the QCD Phase Transition," Phys. Rev. Lett. 105 (Jul, 2010) 041301. https://link.aps.org/doi/10.1103/PhysRevLett.105.041301.

[67] T. Boeckel and J. Schaffner-Bielich, "Little inflation at the cosmological QCD phase transition," Phys. Rev. D 85 (May, 2012) 103506. https://link.aps.org/doi/10.1103/PhysRevD.85.103506.

- [68] C. Alcock and E. Farhi, "Evaporation of strange matter in the early Universe," Phys. Rev. D 32 (Sep, 1985) 1273–1279. https://link.aps.org/doi/10.1103/PhysRevD.32.1273.
- [69] J. Madsen, H. Heiselberg, and K. Riisager, "Does strange matter evaporate in the early Universe?," Phys. Rev. D 34 (Nov, 1986) 2947–2955. https://link.aps.org/doi/10.1103/PhysRevD.34.2947.
- [70] K. Sumiyoshi and T. Kajino, "Survival condition of primordial strange quark matter with low baryon penetrability," Nuclear Physics B - Proceedings Supplements 24 (1991) no. 2, 80-83. https://www.sciencedirect.com/science/article/pii/092056329190303V.
- [71] P. Bhattacharjee, J.-e. Alam, B. Sinha, and S. Raha, "Survivability of cosmological quark nuggets in the chromoelectric flux-tube fission model of baryon evaporation," Phys. Rev. D 48 (Nov, 1993) 4630–4638. https://link.aps.org/doi/10.1103/PhysRevD.48.4630.
- [72] I.-S. Suh and G. J. Mathews, "Finite temperature effects on cosmological baryon diffusion and inhomogeneous big-bang nucleosynthesis," Phys. Rev. D 58 (Nov, 1998) 123002. https://link.aps.org/doi/10.1103/PhysRevD.58.123002.
- [73] A. Atreya, A. Sarkar, and A. M. Srivastava, "Reviving quark nuggets as a candidate for dark matter," Phys. Rev. D 90 (Aug, 2014) 045010. https://link.aps.org/doi/10.1103/PhysRevD.90.045010.
- [74] Atreya, Abhishek and Sanyal, Soma, "Generation of magnetic fields near QCD Transition by collapsing Z(3) domains," Eur. Phys. J. C 78 (2018) no. 12, 1027. https://doi.org/10.1140/epjc/s10052-018-6501-x.
- [75] L. Husdal, "Viscosity in a lepton-photon universe," Astrophysics and Space Science **361** (2016) no. 8, 1–12.
- [76] A. Dobado, F. J. Llanes-Estrada, and D. Rodríguez Fernández, "Entropy production in the early-cosmology pionic phase," International Journal of Modern Physics A 31 (2016) no. 20n21, 1650118, https://doi.org/10.1142/S0217751X16501189. https://doi.org/10.1142/S0217751X16501189.

[77] K. A. Olive, D. N. Schramm, D. Thomas, and T. P. Walker, "Neutrino degeneracy and cosmological nucleosynthesis, revisited," Physics Letters B 265 (1991) no. 3, 239-244.
https://www.sciencedirect.com/science/article/pii/037026939190048U.

- [78] H. Kurki-Suonio and E. Sihvola, "Constraining Antimatter Domains in the Early Universe with Big Bang Nucleosynthesis," Phys. Rev. Lett. 84 (Apr., 2000) 3756-3759. https://link.aps.org/doi/10.1103/PhysRevLett.84.3756.
- [79] H. Kurki-Suonio and E. Sihvola, "Antimatter regions in the early universe and big bang nucleosynthesis," Phys. Rev. D 62 (Oct, 2000) 103508. https://link.aps.org/doi/10.1103/PhysRevD.62.103508.
- [80] R. V. Wagoner, "Big-bang nucleosynthesis revisited," The Astrophysical Journal 179 (1973) 343–360.
- [81] B. D. Fields, S. Dodelson, and M. S. Turner, "Effect of neutrino heating on primordial nucleosynthesis," Phys. Rev. D 47 (May, 1993) 4309-4314. https://link.aps.org/doi/10.1103/PhysRevD.47.4309.
- [82] R. B. Bird, "Transport phenomena," Applied Mechanics Reviews 55 (01, 2002) R1-R4, https://asmedigitalcollection.asme.org/appliedmechanicsreviews/article-pdf/55/1/R1/5438 https://doi.org/10.1115/1.1424298.
- [83] H. Kurki-Suonio and R. A. Matzner, "Effect of small-scale baryon inhomogeneity on cosmic nucleosynthesis," Phys. Rev. D 39 (Feb, 1989) 1046–1053. https://link.aps.org/doi/10.1103/PhysRevD.39.1046.
- [84] G. Steigman, "Neutrinos and Big Bang Nucleosynthesis," Advances in High Energy Physics 2012 (2012) 1–24. http://dx.doi.org/10.1155/2012/268321.
- [85] H.-S. Kang and G. Steigman, "Cosmological constraints on neutrino degeneracy," Nuclear Physics B 372 (1992) no. 1, 494-520. https://www.sciencedirect.com/science/article/pii/055032139290329A.
- [86] A. Ray and S. Sanyal, "Baryon inhomogeneities in a charged quark gluon plasma," Physics Letters B 726 (2013) no. 1, 83-87. https://www.sciencedirect.com/science/article/pii/S0370269313007247.
- [87] A. F. Heckler, "Effects of electroweak phase transition dynamics on baryogenesis and primordial nucleosynthesis," Phys. Rev. D 51 (Jan, 1995) 405–428. https://link.aps.org/doi/10.1103/PhysRevD.51.405.

[88] A. Mégevand and A. D. Sánchez, "Supercooling and phase coexistence in cosmological phase transitions," Phys. Rev. D 77 (Mar, 2008) 063519. https://link.aps.org/doi/10.1103/PhysRevD.77.063519.

- [89] H. Kurki-Suonio, "Baryon inhomogeneity from the cosmic quark-hadron phase transition," Nuclear Physics B Proceedings Supplements 24 (1991) no. 2, 67–73. https://www.sciencedirect.com/science/article/pii/092056329190301T.
- [90] A. G. Cohen, D. B. Kaplan, and A. E. Nelson, "Weak scale baryogenesis," Physics Letters B 245 (1990) no. 3, 561-564. https://www.sciencedirect.com/science/article/pii/0370269390906908.
- [91] A. G. Cohen, D. B. Kaplan, and A. E. Nelson, "Baryogenesis at the weal phase transition," Nuclear Physics B 349 (1991) no. 3, 727-742. https://www.sciencedirect.com/science/article/pii/055032139190395E.
- [92] A. Cohen, D. Kaplan, and A. Nelson, "Spontaneous baryogenesis at the weak phase transition," Physics Letters B 263 (1991) no. 1, 86-92. https://www.sciencedirect.com/science/article/pii/0370269391917114.
- [93] L. McLerran, M. Shaposhnikov, N. Turok, and M. Voloshin, "Why the baryon asymmetry of the universe is 10-10," Physics Letters B 256 (1991) no. 3-4, 477–483.
- [94] L. McLerran, "Can the observed baryon asymmetry be produced at the electroweak phase transition?," Phys. Rev. Lett. 62 (Mar, 1989) 1075–1078. https://link.aps.org/doi/10.1103/PhysRevLett.62.1075.
- [95] M. E. Shaposhnikov, "Possible appearance of the baryon asymmetry of the universe in an electroweak theory," Soviet Journal of Experimental and Theoretical Physics Letters 44 (Oct., 1986) 465.
- [96] M. Shaposhnikov, "Baryon asymmetry of the universe in standard electroweak theory," Nuclear Physics B 287 (1987) 757-775. https://www.sciencedirect.com/science/article/pii/0550321387901271.
- [97] M. Shaposhnikov, "Structure of the high temperature gauge ground state and electroweak production of the baryon asymmetry," Nuclear Physics B 299 (1988) no. 4, 797-817. https://www.sciencedirect.com/science/article/pii/0550321388903732.
- [98] N. Turok and J. Zadrozny, "Dynamical generation of baryons at the electroweak transition," Phys. Rev. Lett. 65 (Nov, 1990) 2331-2334. https://link.aps.org/doi/10.1103/PhysRevLett.65.2331.

[99] N. Turok and J. Zadrozny, "Electroweak baryogenesis in the two-doublet model," Nuclear Physics B 358 (1991) no. 2, 471-493. https://www.sciencedirect.com/science/article/pii/0550321391903563.

- [100] S. Sanyal, "Effect of pre-existing baryon inhomogeneities on the dynamics of the quark-hadron transition," Phys. Rev. D 67 (Apr., 2003) 074009. https://link.aps.org/doi/10.1103/PhysRevD.67.074009.
- [101] N. Sasaki, O. Miyamura, S. Muroya, and C. Nonaka, "Calculation of the baryon diffusion constant in hot and dense hadronic matter based on an ultrarelativistic collision event generator," Phys. Rev. C 62 (Jun, 2000) 011901. https://link.aps.org/doi/10.1103/PhysRevC.62.011901.
- [102] R. J. Scherrer and M. S. Turner, "Diffusion-limited relic particle production," Phys. Rev. D 100 (Aug, 2019) 043545. https://link.aps.org/doi/10.1103/PhysRevD.100.043545.
- [103] S. Sau, S. Bhattacharya, and S. Sanyal, "Diffusion coefficients and constraints on hadronic inhomogeneities in the early universe," The European Physical Journal C 79 (May, 2019). http://dx.doi.org/10.1140/epjc/s10052-019-6938-6.
- [104] E. LIFSHITZ and L. PITAEVSKI, "CHAPTER I KINETIC THEORY OF GASES," in Physical Kinetics, E. LIFSHITZ and L. PITAEVSKI, eds., pp. 1-88. Butterworth-Heinemann, Oxford, 1981. https: //www.sciencedirect.com/science/article/pii/B9780080570495500060.
- [105] K. McFarland, "Neutrino Interactions," Nuclear Physics B Proceedings Supplements 235-236 (2013) 143-148. https://www.sciencedirect.com/science/article/pii/S0920563213001254. The XXV International Conference on Neutrino Physics and Astrophysics.
- [106] J. Lizarraga, J. Urrestilla, D. Daverio, M. Hindmarsh, and M. Kunz, "New CMB constraints for Abelian Higgs cosmic strings," Journal of Cosmology and Astroparticle Physics 2016 (oct, 2016) 042–042. https://doi.org/10.1088/1475-7516/2016/10/042.
- [107] D. Daverio, M. Hindmarsh, M. Kunz, J. Lizarraga, and J. Urrestilla, "Energy-momentum correlations for Abelian Higgs cosmic strings," Phys. Rev. D 93 (Apr, 2016) 085014. https://link.aps.org/doi/10.1103/PhysRevD.93.085014.
- [108] V. A. Gasilov, V. I. Masliankin, and M. I. Khlopov, "Gas-dynamic effects of cosmic strings," Astrofizika 23 (July, 1985) 191–201.

[109] M. J. Rees, "Baryon concentration in string wakes at Z greater than about 200-Implications for galaxy formation and large-scale structure," Monthly Notices of the Royal Astronomical Society 222 (1986) 27P–32P.

- [110] N. Kaiser and A. Stebbins, "Microwave anisotropy due to cosmic strings," Nature 310 (1984) no. 5976, 391–393.
- [111] O. F. Hernández, Y. Wang, R. Brandenberger, and J. Fong, "Angular 21 cm power spectrum of a scaling distribution of cosmic string wakes," Journal of Cosmology and Astroparticle Physics 2011 (aug, 2011) 014–014. https://doi.org/10.1088/1475-7516/2011/08/014.
- [112] B. Hartmann and P. Sirimachan, "Geodesic motion in the space-time of a cosmic string," Journal of High Energy Physics **2010** (Aug, 2010). http://dx.doi.org/10.1007/JHEP08(2010)110.
- [113] A. Saha and S. Sanyal, "Diffusion of massive particles around an Abelian-Higgs string," Journal of Cosmology and Astroparticle Physics 2018 (mar, 2018) 022–022. https://doi.org/10.1088/1475-7516/2018/03/022.
- [114] G. Mangano, G. Miele, S. Pastor, O. Pisanti, and S. Sarikas, "Updated BBN bounds on the cosmological lepton asymmetry for non-zero  $\theta$ 13," Physics Letters B **708** (2012) no. 1-2, 1–5.
- [115] R. Buras and D. Semikoz, "Lepton asymmetry creation in the early universe," Astroparticle Physics 17 (2002) no. 2, 245-261. https://www.sciencedirect.com/science/article/pii/S0927650501001554.
- [116] R. Bingham, J. Dawson, J. Su, and H. Bethe, "Collective interactions between neutrinos and dense plasmas," Physics Letters A 193 (1994) no. 3, 279–284. https://www.sciencedirect.com/science/article/pii/0375960194905975.
- [117] R. Bingham, H. Bethe, J. Dawson, P. Shukla, and J. Su, "Nonlinear scattering of neutrinos by plasma waves: a ponderomotive force description," Physics Letters A 220 (1996) no. 1, 107–110. https://www.sciencedirect.com/science/article/pii/0375960196005038.
- [118] L. O. Silva, R. Bingham, J. M. Dawson, and W. B. Mori, "Ponderomotive force of quasiparticles in a plasma," Phys. Rev. E 59 (Feb, 1999) 2273-2280. https://link.aps.org/doi/10.1103/PhysRevE.59.2273.
- [119] P. K. Shukla, R. Bingham, J. T. Mendonça, and L. Stenflo, "Neutrinos generating inhomogeneities and magnetic fields in the early universe," Physics of

- Plasmas **5** (1998) no. 7, 2815–2817, https://doi.org/10.1063/1.872971. https://doi.org/10.1063/1.872971.
- [120] L. Bento, "Plasma wave instabilities induced by neutrinos," Phys. Rev. D 61 (Dec, 1999) 013004. https://link.aps.org/doi/10.1103/PhysRevD.61.013004.
- [121] L. Bento, "Instabilities in neutrino-plasma density waves," Phys. Rev. D 63 (Mar, 2001) 077302. https://link.aps.org/doi/10.1103/PhysRevD.63.077302.
- [122] Birrell, Jeremiah and Rafelski, Johann, "Proposal for resonant detection of relic massive neutrinos," Eur. Phys. J. C 75 (2015) no. 2, 91. https://doi.org/10.1140/epjc/s10052-015-3310-3.
- [123] A. Vilenkin, "Macroscopic parity-violating effects: Neutrino fluxes from rotating black holes and in rotating thermal radiation," Phys. Rev. D 20 (Oct, 1979) 1807–1812. https://link.aps.org/doi/10.1103/PhysRevD.20.1807.
- [124] Y. Cui and D. E. Morrissey, "Nonthermal dark matter from cosmic strings," Phys. Rev. D 79 (Apr. 2009) 083532. https://link.aps.org/doi/10.1103/PhysRevD.79.083532.
- [125] V. B. Semikoz and M. Dvornikov, "Generation of the relic neutrino asymmetry in a hot plasma of the early universe," International Journal of Modern Physics D 27 (Jan., 2018) 1841008, arXiv:1712.06565.
- [126] L. O. Silva, R. Bingham, J. M. Dawson, J. T. Mendonça, and P. K. Shukla, "Collective neutrino-plasma interactions," Physics of Plasmas 7 (2000) no. 5, 2166-2172, https://doi.org/10.1063/1.874037. https://doi.org/10.1063/1.874037.
- [127] A. Serbeto, "Fluid description of collective neutrino-plasma interaction," Physics Letters A 296 (2002) no. 4, 217-221. https://www.sciencedirect.com/science/article/pii/S0375960102001238.
- [128] B. Müller and D.-L. Yang, "Viscous leptons in the quark gluon plasma," Phys. Rev. D 91 (Jun, 2015) 125010. https://link.aps.org/doi/10.1103/PhysRevD.91.125010.
- [129] B. Layek, A. P. Mishra, and A. M. Srivastava, "Strings with a confining core in a quark-gluon plasma," Phys. Rev. D 71 (Apr. 2005) 074015. https://link.aps.org/doi/10.1103/PhysRevD.71.074015.
- [130] G. Baym, D. Bödeker, and L. McLerran, "Magnetic fields produced by phase transition bubbles in the electroweak phase transition," Phys. Rev. D 53 (Jan, 1996) 662–667. https://link.aps.org/doi/10.1103/PhysRevD.53.662.

[131] D. N. Vollick, "Cosmic string shocks, magnetic fields, and microwave anisotropies," Phys. Rev. D 48 (Oct, 1993) 3585-3591. https://link.aps.org/doi/10.1103/PhysRevD.48.3585.

- [132] P. P. Avelino and E. P. S. Shellard, "Dynamical friction on cosmic string motion and magnetic field generation," Phys. Rev. D 51 (May, 1995) 5946-5949. https://link.aps.org/doi/10.1103/PhysRevD.51.5946.
- [133] K. Dimopoulos and A.-C. Davis, "Evolution of primordial magnetic fields," Physics Letters B **390** (1997) no. 1, 87–96. https://www.sciencedirect.com/science/article/pii/S0370269396013664.
- [134] A.-C. Davis and K. Dimopoulos, "Cosmic superstrings and primordial magnetogenesis," Phys. Rev. D 72 (Aug, 2005) 043517. https://link.aps.org/doi/10.1103/PhysRevD.72.043517.
- [135] J. K. Bloomfield and D. F. Chernoff, "Cosmic string loop microlensing," Phys. Rev. D 89 (Jun, 2014) 124003. https://link.aps.org/doi/10.1103/PhysRevD.89.124003.
- [136] T. Hiramatsu, Y. Sendouda, K. Takahashi, D. Yamauchi, and C.-M. Yoo, "Type-I cosmic-string network," Phys. Rev. D 88 (Oct, 2013) 085021. https://link.aps.org/doi/10.1103/PhysRevD.88.085021.
- [137] "The Chandrasekhar limit for quark stars,".
- [138] J. C. Collins and M. J. Perry, "Superdense matter: neutrons or asymptotically free quarks," Phys. Rev. Lett., v. 34, no. 21, pp. 1353-1356. https://www.osti.gov/biblio/4182837.
- [139] G. Baym, "Confinement of quarks in nuclear matter," Physica A: Statistical Mechanics and its Applications 96 (1979) no. 1, 131-135. https://www.sciencedirect.com/science/article/pii/0378437179902000.
- [140] E. Alvarez and J. M. Ibanez, "Quark core in neutron stars. II," Astronomy and Astrophysics 98 (May, 1981) 390–396.
- [141] M. Fasano, T. Abdelsalhin, A. Maselli, and V. Ferrari, "Constraining the Neutron Star Equation of State Using Multiband Independent Measurements of Radii and Tidal Deformabilities," Physical Review Letters 123 (Sep. 2019). http://dx.doi.org/10.1103/PhysRevLett.123.141101.
- [142] G. Baym, T. Hatsuda, T. Kojo, P. D. Powell, Y. Song, and T. Takatsuka, "From hadrons to quarks in neutron stars: a review," Reports on Progress in Physics 81 (mar, 2018) 056902. https://doi.org/10.1088/1361-6633/aaae14.

[143] A. Rosenhauer, E. Staubo, L. Csernai, T. Øvergård, and E. Østgaard, "Neutron stars, hybrid stars and the equation of state," Nuclear Physics A 540 (1992) no. 3, 630-645.
https://www.sciencedirect.com/science/article/pii/037594749290177L.

- [144] M. Kutschera and A. Kotlorz, "Maximum quark core in a neutron star for realistic equations of state," The Astrophysical Journal 419 (1993) 752.
- [145] G. H. BORDBAR, M. BIGDELI, and T. YAZDIZADEH, "STRUCTURE OF NEUTRON STAR WITH A QUARK CORE," International Journal of Modern Physics A 21 (Nov, 2006) 5991–6001. http://dx.doi.org/10.1142/S0217751X06033854.
- [146] H. Li, X.-L. Luo, and H.-S. Zong, "Bag model and quark star," Phys. Rev. D 82 (Sep, 2010) 065017. https://link.aps.org/doi/10.1103/PhysRevD.82.065017.
- [147] A. Aziz, S. Ray, F. Rahaman, M. Khlopov, and B. K. Guha, "Constraining values of bag constant for strange star candidates," International Journal of Modern Physics D 28 (2019) no. 13, 1941006, https://doi.org/10.1142/S0218271819410062. https://doi.org/10.1142/S0218271819410062.
- [148] R. Mallick, "Maximum mass of a hybrid star having a mixed-phase region based on constraints set by the pulsar PSR J1614-2230," Phys. Rev. C 87 (Feb, 2013) 025804. https://link.aps.org/doi/10.1103/PhysRevC.87.025804.
- [149] F. Özel, D. Psaltis, S. Ransom, P. Demorest, and M. Alford, "THE MASSIVE PULSAR PSR J1614-2230: LINKING QUANTUM CHROMODYNAMICS, GAMMA-RAY BURSTS, AND GRAVITATIONAL WAVE ASTRONOMY,"The Astrophysical Journal 724 (Nov, 2010) L199-L202. http://dx.doi.org/10.1088/2041-8205/724/2/L199.
- [150] X.-F. Zhao, A.-J. Dong, and H.-Y. Jia, "The mass calculations for the neutron star PSR J1614-2230," Acta Physica Polonica B 43 (2012) no. 8, 1783-1789. https://www.scopus.com/inward/record.uri?eid=2-s2.0-84864590895&doi=10.5506%2fAPhysPolB.43.1783&partnerID=40&md5=56f4e0a629771a91ededaa735b75dbab. cited By 5.
- [151] X.-F. Zhao and H.-Y. Jia, "The surface gravitational redshift of the neutron star PSR B2303+ 46," Bull. Astr. Soc. India 41 (2013) 291–298.
- [152] J.-L. Huo and X.-F. Zhao, "The moment of inertia of the proto neutron star PSR J0348+0432 under neutrino trapped," Chinese Journal of Physics **56** (2018)

- no. 1, 292-299. https://www.sciencedirect.com/science/article/pii/S0577907317312509.
- [153] X.-F. Zhao, "The properties of the massive neutron star PSR J0348+0432," International Journal of Modern Physics D 24 (2015) no. 08, 1550058. https://doi.org/10.1142/S0218271815500583.
- [154] N. Prasad and R. S. Bhalerao, "Strange stars with a density-dependent bag parameter," Phys. Rev. D 69 (May, 2004) 103001. https://link.aps.org/doi/10.1103/PhysRevD.69.103001.
- [155] E. Farhi and R. L. Jaffe, "Strange matter," Phys. Rev. D 30 (Dec, 1984) 2379-2390. https://link.aps.org/doi/10.1103/PhysRevD.30.2379.
- [156] T. Harko, K. Cheng, and P. Tang, "Nucleation of quark matter in neutron star cores," The Astrophysical Journal 608 (2004) no. 2, 945.
- [157] M. Orsaria, H. Rodrigues, F. Weber, and G. A. Contrera, "Quark-hybrid matter in the cores of massive neutron stars," Phys. Rev. D 87 (Jan, 2013) 023001. https://link.aps.org/doi/10.1103/PhysRevD.87.023001.
- [158] Zdunik, J. L. and Haensel, P., "Maximum mass of neutron stars and strange neutron-star cores," A&A 551 (2013) A61. https://doi.org/10.1051/0004-6361/201220697.
- [159] V. Soni and D. Bhattacharya, "A consistent description of neutron stars with quark cores," Physics Letters B 643 (2006) no. 3, 158-164. https://www.sciencedirect.com/science/article/pii/S0370269306012536.
- [160] Mariani, M., Orsaria, M., and Vucetich, H., "Constant entropy hybrid stars: a first approximation of cooling evolution," A&A 601 (2017) A21. https://doi.org/10.1051/0004-6361/201629315.
- [161] K. Masuda, T. Hatsuda, and T. Takatsuka, "Hadron-quark crossover and hot neutron stars at birth," Progress of Theoretical and Experimental Physics 2016 (Feb, 2016) 021D01. http://dx.doi.org/10.1093/ptep/ptv187.
- [162] K. Masuda, T. Hatsuda, and T. Takatsuka, "Hyperon puzzle, hadron-quark crossover and massive neutron stars," The European Physical Journal A 52 (Mar, 2016) . http://dx.doi.org/10.1140/epja/i2016-16065-6.
- [163] A. Leonidov, K. Redlich, H. Satz, E. Suhonen, and G. Weber, "Entropy and baryon number conservation in the deconfinement phase transition," Phys. Rev. D 50 (Oct, 1994) 4657–4662. https://link.aps.org/doi/10.1103/PhysRevD.50.4657.

[164] B. Patra and C. Singh, "Temperature and baryon-chemical-potential-dependent bag pressure for a deconfining phase transition," Physical Review D - Particles, Fields, Gravitation and Cosmology 54 (1996) no. 5, 3551-3555.

https://www.scopus.com/inward/record.uri?eid=2-s2.0-0001470608&doi=10.1103%2fPhysRevD.54.3551&partnerID=40&md5=72be2e060dc623ae19f2ff3b5d4e1a7e. cited By 19.

- [165] B. Patra and C. Singh, "EOS for a QGP with a temperature and baryon chemical potential dependent bag pressure," Zeitschrift fur Physik C-Particles and Fields 74 (1997) no. 4, 699-703. https://www.scopus.com/inward/record.uri?eid=2-s2.0-0001128850&doi=10.1007%2fs002880050433&partnerID=40&md5=d5a3f3ba20f232dcc8a53894007bc7c3. cited By 5.
- [166] K. Schertler, C. Greiner, and M. Thoma, "Medium effects in strange quark matter and strange stars," Nuclear Physics A 616 (1997) no. 3, 659-679. https://www.sciencedirect.com/science/article/pii/S0375947497000146.
- [167] Zdunik, J. L., Fortin, M., and Haensel, P., "Neutron star properties and the equation of state for the core," A&A 599 (2017) A119. https://doi.org/10.1051/0004-6361/201629975.
- [168] X. Wu, S. Du, and R. Xu, "What if the neutron star maximum mass is beyond 2.3M?," Monthly Notices of the Royal Astronomical Society 499 (2020) no. 3, 4526–4533.
- [169] M. I. Gorenstein and S. N. Yang, "Gluon plasma with a medium-dependent dispersion relation," Physical Review, D 52 (11, 1995) . https://www.osti.gov/biblio/118556.
- [170] Z. Xiaoping, Y. Shuhua, L. Jiarong, and C. Xu Phys. Lett. B 548 (2002) 29–34. cited By 1.
- [171] X.-P. Zheng, X. Zhou, and S.-H. Yang, "Novel non-equilibrium phase transition caused by non-linear hadronic-quark phase structure," Physics Letters B 729 (2014) 79-84. https://www.sciencedirect.com/science/article/pii/S0370269314000069.
- [172] J. Madsen, "Physics and astrophysics of strange quark matter," in Hadrons in Dense Matter and Hadrosynthesis, J. Cleymans, H. B. Geyer, and F. G. Scholtz, eds., pp. 162–203. Springer Berlin Heidelberg, Berlin, Heidelberg, 1999.
- [173] A. V. Olinto, "The physics of strange matter,". https://www.osti.gov/biblio/5508236.

[174] J. Buitrago and E. Mediavilla, "The limit of mass for gravitational collapse and nuclear forces at short distance," Astrophysics and space science 109 (1985) no. 2, 407–409.

- [175] C. J. Horowitz and J. Piekarewicz, "The Neutron radii of Pb-208 and neutron stars," Phys. Rev. C 64 (2001) 062802, arXiv:nucl-th/0108036.
- [176] C. Alcock, E. Farhi, and A. Olinto, "Strange stars," The Astrophysical Journal **310** (1986) 261–272.
- [177] K. Olive, "Review of Particle Physics," Chinese Physics C 38 (aug, 2014) 090001. https://doi.org/10.1088/1674-1137/38/9/090001.
- [178] R. C. Tolman, "Static Solutions of Einstein's Field Equations for Spheres of Fluid," Phys. Rev. 55 (Feb, 1939) 364-373. https://link.aps.org/doi/10.1103/PhysRev.55.364.
- [179] J. R. Oppenheimer and G. M. Volkoff, "On Massive Neutron Cores," Phys. Rev. 55 (Feb, 1939) 374–381. https://link.aps.org/doi/10.1103/PhysRev.55.374.
- [180] H. T. Cromartie, E. Fonseca, S. M. Ransom, P. B. Demorest, Z. Arzoumanian, H. Blumer, P. R. Brook, M. E. DeCesar, T. Dolch, J. A. Ellis, and et al., "Relativistic Shapiro delay measurements of an extremely massive millisecond pulsar," Nature Astronomy 4 (Sep. 2019) 72–76. http://dx.doi.org/10.1038/s41550-019-0880-2.
- [181] C. M. Zhang, H. X. Yin, Y. H. Zhao, Y. C. Wei, and X. D. Li, "Does Submillisecond Pulsar XTE J1739-285 Contain a Weak Magnetic Neutron Star or Quark Star?," Publications of the Astronomical Society of the Pacific 119 (oct, 2007) 1108-1113. https://doi.org/10.1086/522796.
- [182] G. Zhang, M. Méndez, P. Jonker, and B. Hiemstra, "The distance and internal composition of the neutron star in EXO 0748- 676 with XMM-Newton," Monthly Notices of the Royal Astronomical Society 414 (2011) no. 2, 1077-1081.
- [183] T. E. Riley, A. L. Watts, S. Bogdanov, P. S. Ray, R. M. Ludlam, S. Guillot, Z. Arzoumanian, C. L. Baker, A. V. Bilous, D. Chakrabarty, et al., "A NICER view of PSR J0030+ 0451: Millisecond pulsar parameter estimation," The Astrophysical Journal Letters 887 (2019) no. 1, L21.
- [184] M. C. Miller, F. K. Lamb, A. J. Dittmann, S. Bogdanov, Z. Arzoumanian, K. C. Gendreau, S. Guillot, A. K. Harding, W. C. G. Ho, J. M. Lattimer, and et al., "PSR J0030+0451 Mass and Radius from NICER Data and Implications for the

Properties of Neutron Star Matter,"The Astrophysical Journal 887 (Dec, 2019) L24. http://dx.doi.org/10.3847/2041-8213/ab50c5.

[185] N.-N. Pan and X.-P. Zheng, "Observational Constraints on Quark Matter in Neutron Stars," Chinese Journal of Astronomy and Astrophysics 7 (oct, 2007) 675–684. https://doi.org/10.1088/1009-9271/7/5/08.

### List of Publications

#### Thesis Publications

- "Diffusion coefficients and constraints on hadronic inhomogeneities in the early universe", Sovan Sau, Sayantan Bhattacharya and Soma Sanyal, Eur. Phys. J. C 79, 439 (2019).
- 2. "Neutrino currents in wakes of cosmic strings", Sovan Sau and Soma Sanyal, Eur. Phys. J. C 80, 152 (2020).
- 3. "Quark cores in extensions of the MIT Bag model", Salil Joshi, Sovan Sau and Soma Sanyal, J. High Energy Astrophys. 30, 16-23 (2021).
- 4. "Decay of baryon inhomogeneities in an expanding universe", Pratik K. Das, Sovan Sau, Abhisek Saha, Soma Sanyal, Eur. Phys. J. C 81, 816 (2021).

#### Conference Proceedings

- 1. "Diffusion coefficients and constraints on hadronic inhomogeneities in the early universe", Sovan Sau and Soma Sanyal, Springer Proc. Phys. 248, 87-91 (2020).
- 2. "Generation of magnetic fields in cosmic string wakes", Sovan Sau and Soma Sanyal, Proceedings of Science, 390, 607 (2021)

# Cosmological Density Fluctuations and Their Effects in the Early Universe

by Sovan Sau

Submission date: 04-Oct-2021 12:42PM (UTC+0530)

**Submission ID:** 1664753825 **File name:** Sovan\_Sau.pdf (1.65M)

Word count: 38230 Character count: 188508

## Cosmological Density Fluctuations and Their Effects in the Early Universe

51% IMILARITY INDEX	35% INTERNET SOURCES	50% PUBLICATIONS	1% STUDENT PAPERS
RIMARY SOURCES			
Sanyal an exp	K. Das, Sovan Sau "Decay of baryo anding universe" al Journal C, 2021	n inhomogen	eities in
2 export Internet Sou	arxiv.org		11%
3 arxiv.o			8%
4 link.spi	ringer.com		7%
cores i	shi, Sovan Sau, Son extensions of the large	he MIT bag m	odel",
in wak	Sau, Soma Sanya es of cosmic strin al Journal C, 2020	igs", The Euro	pean #%
			Dr. SOMA SANY Asst. Professor School of Phys School of Hyd University of Hyd Hyderabad-500

7	Salil Joshi, Sovan Sau, Soma Sanyal. "Quark cores in extensions of the MIT Bag model", Journal of High Energy Astrophysics, 2021	<b>1</b> %
8	Sovan Sau, Sayantan Bhattacharya, Soma Sanyal. "Diffusion coefficients and constraints on hadronic inhomogeneities in the early universe", The European Physical Journal C, 2019 Publication	<1 %
9	Submitted to SASTRA University Student Paper	<1%
10	NATO Science Series II Mathematics Physics and Chemistry, 2006. Publication	<1%
11	Arun Kumar Pandey, Sampurn Anand. " Generating a seed magnetic field the chiral Biermann battery ", Physical Review D, 2021 Publication	<1%
12	"Workshop on Frontiers in High Energy Physics 2019", Springer Science and Business Media LLC, 2020 Publication	<1%
13	NATO ASI Series, 1994. Publication	SOM Professor School of Hyderales
14	G. M. Fuller, G. J. Mathews, C. R. Alcock. "Quark-hadron phase transition in the early	<1%

Universe: Isothermal baryon-number fluctuations and primordial nucleosynthesis", Physical Review D, 1988

Publication

15	"Magnetic Fields in Diffuse Media", Springer Science and Business Media LLC, 2015 Publication	<1%
16	Astronomy and Astrophysics Abstracts, 1992.  Publication	<1%
17	en.wikipedia.org Internet Source	<1%
18	Abhishek Atreya, Soma Sanyal. "Generation of magnetic fields near QCD Transition by collapsing Z(3) domains", The European Physical Journal C, 2018 Publication	<1%
19	K. ATAZADEH, A. M. GHEZELBASH, H. R. SEPANGI. "QCD PHASE TRANSITION IN DGP BRANE COSMOLOGY", International Journal of Modern Physics D, 2012 Publication	<1%
20	Ruth Durrer, Andrii Neronov. "Cosmological magnetic fields: their generation, evolution and observation", The Astronomy and Astrophysics Review, 2013 Publication	<1%

Springer Handbook of Spacetime, 2014.

Yang Bai, Andrew J. Long. "Six flavor quark matter", Journal of High Energy Physics, 2018

Publication

<1%

George Rhee. "Cosmic Dawn", Springer Science and Business Media LLC, 2013
Publication

<1%

Soma Sanyal. "Effect of pre-existing baryon inhomogeneities on the dynamics of the quark-hadron transition", Physical Review D, 2003

<1%

- Publication
- Silvio A. Bonometto, Ornella Pantano.
  "Physics of the cosmological quark-hadron transition", Physics Reports, 1993

  Publication

<1%

Donoghue, John F.. "CP Violation and the Limits of the Standard Model: Proceedings of the 1994 Theoretical Advanced Study Institute in Elementary Particle Physics", CP Violation and the Limits of the Standard Model, 1995.

Publication

<1%

Submitted to Queen Mary and Westfield College

<1%

Student Paper

28	Nakamura, K "Second-Order Gauge Invariant Cosmological Perturbation Theory: Einstein Equations in Terms of Gauge Invariant Variables", Progress of Theoretical Physics, 2007. Publication	<1%
29	worldwidescience.org Internet Source	<1%
30	Oswaldo D. Miranda. "Seed magnetic Fields Generated by Primordial Supernova Explosions", Monthly Notices of the Royal Astronomical Society, 12/1998 Publication	<1%
31	Submitted to Universidade do Porto Student Paper	<1%
32	cds.cern.ch Internet Source	<1%
33	pure.uva.nl Internet Source	<1%
34	Biswanath Layek, Ananta P. Mishra, Ajit M. Srivastava, Vivek K. Tiwari. "Baryon inhomogeneity generation in the quark-gluon plasma phase", Physical Review D, 2006	<1%
35	Giovannini, . "From CMB to the Standard Cosmological Model", A Primer on the Physics	<1%

of the Cosmic	Microwave	Background	, 2008.
---------------	-----------	------------	---------

Publication

36	Lawrence M. Widrow, Dongsu Ryu, Dominik R. G. Schleicher, Kandaswamy Subramanian, Christos G. Tsagas, Rudolf A. Treumann. "The First Magnetic Fields", Space Science Reviews, 2011 Publication	<1%
37	Abhijit Bhattacharyya, Jan-e Alam, Sourav Sarkar, Pradip Roy, Bikash Sinha, Sibaji Raha, Pijushpani Bhattacharjee. "Relics of the cosmological QCD phase transition", Physical Review D, 2000 Publication	<1%
38	Astronomy and Astrophysics Abstracts, 1990.  Publication	<1%
39	eprints.nottingham.ac.uk Internet Source	<1%
40	etheses.dur.ac.uk Internet Source	<1%
41	Robert H. Brandenberger. "Chapter 5 Lectures on the Theory of Cosmological Perturbations", Springer Science and Business Media LLC, 2004 Publication	<1%
42	physics.comu.edu.tr Internet Source	<1%

43	www.nat.vu.nl Internet Source	<1%
44	Biswanath Layek, Soma Sanyal, Ajit M. Srivastava. "Cosmic string induced sheetlike baryon inhomogeneities at the quark-hadron transition", Physical Review D, 2001 Publication	<1%
45	Mattias Christensson. "Magnetic fields in the early universe in the string approach to MHD", Physical Review D, 08/1999 Publication	<1%
46	doaj.org Internet Source	<1%
47	www.docme.ru Internet Source	<1%
48	Debashish Chowdhury, Dietrich Stauffer. "Principles of Equilibrium Statistical Mechanics", Wiley, 2000 Publication	<1%
49	R P Malik. "Superfield approach to (non-)local symmetries for 1-form Abelian gauge theory", Journal of Physics A: Mathematical and General, 2004 Publication	<1%
50	ivanik3.narod.ru Internet Source	<1%



57	Submitted to University of Nottingham  Student Paper	<1%
58	Vladimir S. Netchitailo. "World-Universe Model—Alternative to Big Bang Model", Journal of High Energy Physics, Gravitation and Cosmology, 2020 Publication	<1%
59	www.wiese.itp.unibe.ch Internet Source	<1%
60	"Plasma Astrophysics And Space Physics", Springer Science and Business Media LLC, 1999	<1%
61	Alexandre Obertelli, Hiroyuki Sagawa. "Modern Nuclear Physics", Springer Science and Business Media LLC, 2021 Publication	<1%
62	Bhaskar Dutta, Yukihiro Mimura, R.N. Mohapatra. "Neutrino masses and mixings in a predictive SO(10) model with CKM CP violation", Physics Letters B, 2004 Publication	<1%
63	Love, . "Phase transitions in the early universe", Graduate Student Series in Physics, 2004.  Publication	<1%

64	Sarira Sahu. "Neutrino propagation in a random magnetic field", Physical Review D, 1997 Publication	<1%
65	Ying, S "The Quantum Aspects of Relativistic Fermion Systems with Particle Condensation", Annals of Physics, 19980701	<1%
66	hdl.handle.net Internet Source	<1%
67	Buballa, M "NJL-model analysis of dense quark matter", Physics Reports, 200502	<1%
68	De Risi, G "Quark-hadron phase transitions in brane-world cosmologies", Nuclear Physics, Section B, 20081211 Publication	<1%
69	M. D. Glinchuk, A. N. Morozovska, V. A. Stephanovich, L. Jastrabik. "Surface Tension and Mismatch Effects in Ferroelectric Thin Film Properties", Ferroelectrics, 2004	<1%
70	V. B. SEMIKOZ, D. D. SOKOLOFF. "LARGE- SCALE COSMOLOGICAL MAGNETIC FIELDS AND MAGNETIC HELICITY", International Journal of Modern Physics D, 2012 Publication	<1%

71	pure.royalholloway.ac.uk Internet Source	<1%
72	www.haverford.edu Internet Source	<1%
73	John ELLIS. "Particle Physics and Cosmology", Annals of the New York Academy of Sciences, 9/1995 Publication	<1%
74	Majumdar, . "Particle Physics Basics", Dark Matter, 2014.	<1%
75	Submitted to University of Oklahoma Student Paper	<1%
76	Zhi-Zhong Xing, Shun Zhou. "Neutrinos in Particle Physics, Astronomy and Cosmology", Springer Science and Business Media LLC, 2011	<1%
77	innsida.ntnu.no Internet Source	<1%
Name of the last o		

Exclude quotes

On

Exclude bibliography On

Exclude matches

Dr. SOMA SANYAL

Dr. SOMA SANYAL

Asst. Professor

School of Hyderabad

School of Hyderabad

University of 500 046.

University of Hyderabad



Dr. Soma Sanyal School of Physics University of Hyderabad

This is to certify that the thesis entitled "Cosmological density fluctuations and their effects in the early universe" has been screened by the Turnitin software at the library of University of Hyderabad. The software shows 51% similarity index, out of which 27% comes from the candidates own research articles related to this thesis. The candidate has four published papers related to this thesis, all the journal versions of which are available on the Springer website of European Journal C and Journal of High Energy Astrophysics. All these papers are also available on the Physics ArXiv (www.arxiv.org) which is responsible for 19% of the similarity index. Therefore out of the total 51%, 46% of the similarity index is accounted for by the candidates own work in this thesis. Removing these websites, the similarity index will be below 10%. The rest of the similarity index comes from scientific terms and equations found in similar contexts in the vast literature present on the internet. Therefore, the thesis is free from plagiarism.

Dr. Soma Sanyal School of Physics

University of Hyderabad

(Thesis supervisor)

Dr. SOMA SANYAL
Asst. Professor
School of Physics
University of Hyderabad
Hyderabad-500 046.